GEOMATICS
ENGINEERING

UCGE Reports

Number 20299

Department of Geomatics Engineering

Doppler Measurements and Velocity Estimation:

Comparison of Standard and High Sensitivity Receivers

(URL: http://www.geomatics.ucalgary.ca/graduatetheses)

by

Nadezda Sokolova

December 2009

SCHULICH
School of Engineering
UNIVERSITY OF
CALGARY

UNIVERSITY OF CALGARY

Doppler Measurements and Velocity Estimation:
Comparison of Standard and High Sensitivity Receivers

by

Nadezda Sokolova

A THESIS
SUBMITTED TO THE FACULTY OF GRADUATE STUDIES
IN PARTIAL FULFILMENT OF THE REQUIREMENTS FOR THE
DEGREE OF MASTER OF SCIENCE

DEPARTMENT OF GEOMATICS ENGINEERING
CALGARY, ALBERTA
December, 2009

Abstract

The use of a Global Positioning System (GPS) receiver as a velocity and acceleration sensor has gained an increasing research interest due to the potential applications in navigation and control, as well as being used as an aiding source in GPS/INS integration. In all the above mentioned applications the accuracy of the provided velocity and therefore Doppler measurements is very important. Moreover, it is desirable not only to have accurate velocity and Doppler information, but also a figure of merit to provide a bounding estimate of the uncertainty of this information.

Previous studies on Doppler and velocity estimation using Global Navigation Satellite System (GNSS) have been essentially limited to hardware receivers. In this way, only the relationship between measurement quality and velocity estimation and its relevance to variation in Carrier to Noise Ratio (C/N_0) has been investigated. Doppler measurements are obtained by processing Phase Lock Loop (PLL) outputs and parameters such as the integration time, loop order and bandwidth strongly impact their quality. Given control over the PLL parameters by the flexibility of the Software Defined Radio (SDR) receiver, a complete theoretical framework has been developed in order to study the Doppler and velocity accuracy, relating the variance and biases of the Doppler estimates to C/N_0, user dynamics and PLL parameters, and translating them to the errors in the final velocity estimates.

The developed theoretical model has been verified by performing a number of static and dynamic pedestrian-based field tests and simulations with the major focus on the environments with strong signal attenuation and multipath.

To be able to operate in signal degraded environments and obtain higher Doppler and velocity measurement quality a novel High Sensitivity GPS (HSGPS) architecture based on memory discriminators providing increased noise rejection capabilities has been characterized and used together with a number of commercial hardware receivers. A good agreement between empirical and theoretical results has been found, showing the validity of the proposed theoretical framework.

Acknowledgements

I owe the completion of this thesis to many and would like to express my gratitude to those that devoted their ideas, time and patience to its completion.

- My supervisor, Dr. Gérard Lachapelle, for his unwavering support of my research and academic endeavours.
- Dr. Daniele Borio who has been an infinite source of ideas for discussion that led to so many research opportunities.
- Research in Motion for funding this work.
- The support of my friends and colleagues at the Geomatics department cannot be over appreciated. Particular thanks to Aiden Morrison, Florence Macchi, Cyrille Gernot, Aleks Knezevic, James Curran and Jared Bancroft for their precious suggestions and discussions on my work and for simply being good friends.

Lastly, I would like to thank everybody who was important to the successful realization of thesis, as well as expressing my apology that I could not mention everyone.

Table of Contents

List of Tables

List of Figures

Acronyms and Abbreviations

Abbreviation	**Definition**
A-GPS	Assisted GPS
C/N_0	Carrier-to-Noise density ratio
DOP	Dilution Of Precision
E911	Enhanced 911
FCC	Federal Communications Commission
FFT	Fast Fourier Transform
FIR	Finite Impulse Response
GNSS	Global Navigation Satellite System
GPS	Global Positioning System
HS-GPS	High Sensitivity GPS
IF	intermediate frequency
INS	Inertial Navigation System
KF	Kalman Filter
LOS	Line-Of-Sight
MA	moving average
ML	ML – maximum likelihood
MMSE	minimum mean square error
MSE	mean square error
NCO	numerically controlled oscillator
PLL	Phase Lock Loop
PRN	Pseudo Random Noise
PSD	power spectral density
SDR	Software Defined Radio
SNR	signal-to-noise ratio
WLS	weighted least squares

List of Symbols

Symbol	**Definition**
A	signal amplitude
A_c	signal amplitude at the correlator output
B_d	Doppler bandwidth
B_n	loop bandwidth
G_d	discriminator gain
$I(z)$	transfer function of an integrator
K	number of complex correlator outputs
L	order of the loop
$N_d[k]$	equivalent phase noise
$N_f[k]$	equivalent frequency noise
P	prompt complex correlator output
R	covariance matrix of observations
R_v	variance-covariance matrix of the unknowns
S_L	squaring loss
T_c	coherent integration time
T_{eff}	effective integration time
T_s	sampling interval
W	analysis window length
$\hat{f}$	final Doppler frequency estimate
f_s	sampling frequency
f_{cp}	carrier phase derived Doppler measurement
f_d	true Doppler frequency

f_{raw}	raw Doppler measurement
$h^{(k)}$	user-to-satellite LOS unit vector
$\mathbf{v}$	user velocity vector
$\mathbf{v}^{(k)}$	k^{th} satellite velocity vector
$\Delta(z)$	transfer function of a differentiator
α	forgetting factor
$\delta[\cdot]$	Kronecker delta
ε_f	systematic errors in Doppler measurements
ε_ϕ	residual phase error
ϕ	average phase at the correlator output
$\overline{\phi}$	phase estimate
$\dot{\overline{\phi}}$	phase rate at the input of the NCO
$\hat{\phi}$	phase estimated by the discriminator
λ_{L1}	L1 wavelength
τ_0	delay experienced by the received signal

CHAPTER 1: INTRODUCTION

The increasing demand for Location Based Services (LBS) in signal degraded environments and increasing requirements from the Federal Communications Commission for the provision of Enhanced 911 (E-911) services have been driving the development of positioning technologies. Applications meant for emergency situations and many commercial services are in continuous development. Some of them are aimed at reaching a large user base with mass-markets such as vehicular and personal navigation. Others focus on specific applications such as fleet management, e-tourism, and personnel tracking.

Several techniques can be used to achieve positioning of the user in various environments. Among them, GPS-based techniques that have become very attractive due to the great effort made by the industry to miniaturize front-ends and processing cores into one single chipset while increasing both acquisition and tracking sensitivity. Those developments have substantially increased the availability of the position solution especially in urban environments. Software-based solutions are also gaining more and more importance since they offer more flexibility and cost effective means to enable GPS in handsets (Pany et al 2006).

However, GPS-based positioning techniques still encounter issues in urban canyon and indoor areas where LBS users are very likely to be. In such environments, already attenuated GPS signals are further affected by strong multipath and fading, making it a real challenge for positioning systems. To enhance the sensitivity and thus the availability of the position solution using GPS in these adverse environments, High Sensitivity (HS) techniques based on the use of long integration times have been developed (Petterson et al 1997, Van Diggelen 2001).

Alternatively, performance can be achieved by telecommunication network assistance (Turunen 2007), or integrating different technologies such as standard or HSGPS with dead-reckoning sensors such as Inertial Navigation Systems (INS) (Mezentsev 2005, Bancroft et al 2008). Recent development of the Micro-ElectroMechanical System (MEMS) technology and quick reduction of the MEMS sensor cost made the approach of GPS and MEMS based INS integration more attractive and affordable for cost sensitive applications such as car navigation and LBS.

Traditionally, a GPS/INS integrated system employs GPS derived pseudorange measurements to aid the INS system, whereas indoors and in urban areas pseudorange measurements suffer significant errors deriving from multipath and non-line of sight signals (Lachapelle 2008). Moreover, the position solution, where still possible, is degraded by limited satellite geometry (Lachapelle 2008).

To circumvent this problem velocity information derived from the GPS Doppler measurements (Moafipoor et al 2004), raw Doppler measurements (Petovello et al 2003) or time-differenced carrier phase measurements (Wendel et al 2006) can be used as alternative aiding sources. But for successful implementation of an integrated system, the accuracy of aiding information is critical. Moreover, it is desirable not only to have accurate aiding information, but also a figure of merit providing an estimate of the uncertainty of this information.

1.1 Limitations of the Previous Research

Previous studies on Doppler and velocity estimation using GNSS have been essentially limited to hardware receivers (Ryan et al 1997, Van Graas & Soloviev 2003, Serrano et al 2004). In this way, only the relationship between measurement quality and velocity estimation as a function of the Carrier-to-Noise density ratio (C/N_0) (Petovello et al 2003) has been investigated.

Hardware receivers with proprietary algorithms and software do not provide any insight on how the Doppler measurements are formed and do not allow any analysis at the tracking loop level. Doppler measurements are obtained by processing Phase Lock Loop (PLL) outputs and parameters such as the integration time, loop order and bandwidth strongly impact their quality. Therefore, a Software Defined Radio (SDR) GPS receiver with access to algorithms and source code is a fundamental tool for the analysis of the process of Doppler measurement and velocity estimation. The flexibility of the SDR receiver allows processing of the same dataset several times with different parameters. In this way, it is possible to analyze the impact of several parameters such as the PLL bandwidth integration time and loop order. Given control over the PLL parameters, the variance in the Doppler measurements can be related to the C/N_0, the user dynamics and the PLL parameters. Furthermore, the noise propagation from the Doppler measurements to the velocity estimates can be studied and quantified.

Given the benefits provided by the use of a SDR GPS receiver, further insight on the velocity analysis can be achieved. An approximated model for Doppler and velocity errors, accounting for the C/N_0, the user dynamics and the PLL parameters can be derived and used to provide bounds on the velocity accuracy.

Finally, most of the previous studies on the velocity estimation (Ryan et al 1997, Van Graas & Soloviev 2003, Serrano et al 2004) were focused on Line Of Sight (LOS) conditions only, which are in the absence of multipath and for high to moderate values of C/N_0. The impact of strong signal attenuation and biases introduced by multipath has been rarely addressed.

Signal tracking in degraded environments can be achieved using HSGPS technology at the expense of measurement quality. The assessment of the quality of measurements produced by HSGPS is still lacking in the literature. Moreover, a new HSGPS receiver architecture based on memory discriminators has been recently proposed by Borio et al (2009). Although this novel architecture provides increased noise rejection capabilities, its performance in terms of measurement quality has not been assessed yet. These deficiencies in the current literature motivate the analysis developed in this research.

1.2 Objectives and Contributions

The overall objective of this thesis is to develop, test and verify a comprehensive theoretical framework for the analysis of the process of velocity estimation. This framework includes the impact of tracking loop parameters such as bandwidth, integration time and loop order as well as the C/N_0 and user dynamics on the accuracy of Doppler and velocity measurements.

The major contributions of this thesis reported in the following chapters can be summarised as follows:

1. **Study of different Doppler/velocity estimation methodologies.** The major focus here is on the different methods for Doppler determination including raw Doppler measurements, directly from the output of the PLL filter, and the use of indirect Doppler calculation methods employing GPS carrier phase measurements. The following approaches for improving the quality of Doppler measurements have been identified:
    - implementation of a Savitsky-Golay filter for derivation of the Doppler from the carrier phase measurements.
    - design of a smoothing filter for reducing the variance of raw Doppler measurements to show the equivalence between time-differenced carrier-phase measurements and filtered raw Doppler measurements .

2. **Noise propagation analysis and theoretical framework development**. All Doppler measurements are obtained by processing PLL outputs and therefore parameters such as the integration time, loop order and bandwidth, strongly impact their quality. To be able to quantify GPS receivers as velocity sensors it is necessary to perform a complete and cohesive analysis of the noise propagation through the entire velocity estimation process from the PLL input to the final velocity estimate. Therefore, a general linear model is developed for the analysis of the Doppler measurements and the variance and bias of Doppler estimates related to the C/N_0, the user dynamics and

the loop parameters. Moreover, the concept of Doppler bandwidth is introduced for quantifying the amount of input noise transferred to the final Doppler estimates. To get a comprehensive model the following types of Doppler measurements have to be considered:

- raw Doppler measurements
- filtered raw Doppler measurements
- Doppler measurements derived from the carrier phase using Savitsky-Golay filter.

3. **Characterization of a memory discriminator based tracking loop architecture.** In order to characterise the performance of the new memory discriminator based HS tracking loops, a thorough study involving theoretical and experimental approaches is required. Moreover, the theoretical model developed for the analysis of Doppler measurements and velocity estimates has to be expanded to include the effect of memory discriminators.

4. **Verification of the developed theory.** To demonstrate the validity of the theoretical model developed in this research, a number of simulations were performed as well as extensive data collections in various GPS operating environments. Real GPS data was used to investigate the effectiveness of the developed model and, at the same time, to evaluate the performance of the memory discriminator based architecture.

5. **Development and verification of an approach for the characterisation of hardware GPS receivers based on the proposed theoretical model.** The developed theoretical model allows one to estimate the value of the Doppler bandwidth and an approximate value of the coherent integration time of a hardware receiver. This allows the application of the analytical model to hardware receivers using a standard tracking loop architecture.

1.3 Thesis Outline

In order to provide a comprehensive view of the research performed, the subsequent chapters are structured in the following way.

Chapter 2 reviews the theoretical background of standard and High Sensitivity GPS receivers. In particular, existing methods for the extension of coherent and non-coherent integration periods are discussed together with massive parallel correlation techniques where emphasis is given to the use of massive parallel correlation for tracking enhancement.

This chapter additionally recalls the basic theory behind velocity estimation using GPS, and GNSS in general and gives a review of methods for Doppler measurement determination from the output of digital tracking loops. Discussion on different differentiation methods for extraction of Doppler measurements from the carrier phase observations is also provided.

Chapter 3 introduces the concept of a novel HSGPS memory discriminator with enhanced tracking sensitivity and extended noise reduction capabilities. A new type of phase discriminator designed for the non-coherent extension of the integration time is described. This type of discriminator operates by first removing the bit dependence from the correlator outputs, and subsequently filtering the output prior to extracting the phase information. Phase estimates are then extracted using a memory-less nonlinear function. Aspects of the loop filter design and the use of an exponential filtering are then discussed and a detailed characterization of the HS receiver architecture using memory discriminators is provided.

Chapter 4 concentrates on the derivation of an approximated theoretical model relating input C/N_0, user dynamics and PLL parameters to the quality of Doppler measurements and velocity estimates. To quantify the amount of input noise transferred to the Doppler measurements the concept of Doppler bandwidth is introduced and a theoretical analysis of Doppler jitter and Doppler bias is provided. Relationship between raw and carrier-phase derived Doppler measurement types is also discussed in this chapter. The fact that carrier-phase derived Doppler measurements are a filtered version of the raw Doppler measurements is highlighted and equivalence between filtered raw Doppler and carrier phase derived Doppler measurements is shown. The same approach is then considered for use with memory discriminator based PLLs. Finally, the concept of Dilution of Precision (DOP) is used to model the error propagation from the Doppler frequency measurements to the velocity estimates. The theory developed is the basic tool extensively used in the rest of the thesis.

Chapters 5 and **6** describe the methodology adopted for the data analysis and experimental setup used for the evaluation of the theoretical framework developed in **Chapter 4**. A number of static and dynamic pedestrian-based field tests in various GPS operating environments were carried out for verification of the developed theory. Moreover, several simulations have been performed in order to evaluate the proposed theoretical model under higher levels of dynamics. **Chapters 5** and **6** introduce and discuss the results obtained using the developed theoretical model comparing them to the results obtained empirically. Effects of using different tracking loop parameters and methods for the Doppler derivation are also analyzed. An approach for characterization and comparison of different hardware receivers based on the proposed theoretical model is also introduced and illustrated using a NovAtel OEMV-1 hardware receiver.

The primary equipment used in this research includes two versions of the University of Calgary's GNSS Software Navigation Receiver (GSNRx^{TM}): standard (Petovello et al 2008) and memory discriminator based architecture.

Finally, in **Chapter 7**, conclusions are drawn from the performed investigations and directions for further research suggested.

The structure and the logical dependencies between the different chapters are depicted in Figure 1-1.

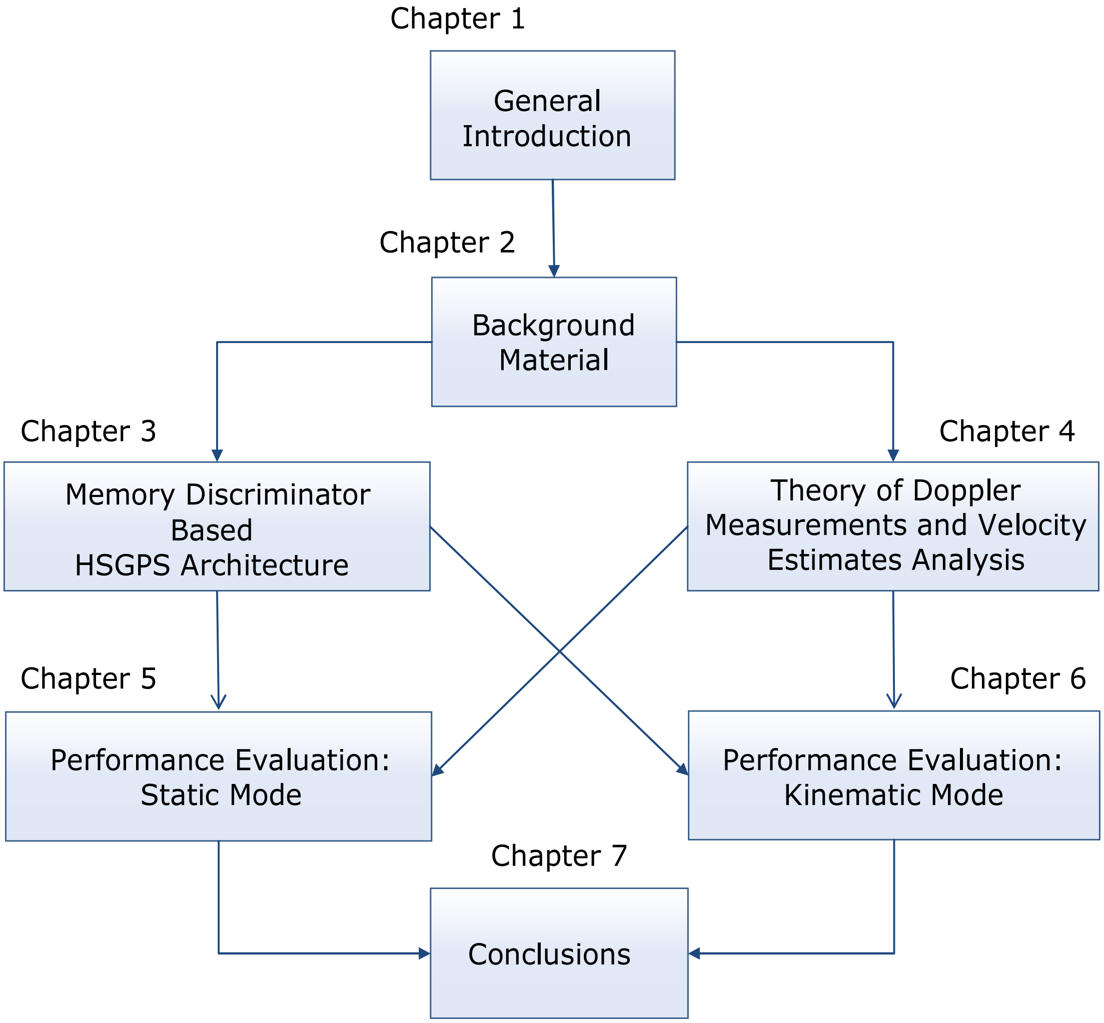

Figure 1-1: Structure of the thesis and chapter interdependence

CHAPTER 2: HIGH SENSITIVITY GPS PRINCIPLES AND VELOCITY ESTIMATION OVERVIEW

This chapter gives an overview of High-Sensitivity (HS) techniques for improving the ability of a GPS receiver to acquire and track weak signals. The basis of the velocity estimation process, as it pertains to this study, is provided as well.

First, the signal and system model is given for establishing the basic notation used in the thesis. Following this, a discussion of HSGPS techniques, with particular attention on the existing methods for extension of the coherent and non-coherent integration time, is provided together with a review of massive parallel correlation techniques for weak signal tracking.

In the second part of the chapter, different differentiation methods for extracting Doppler measurements from the carrier phase observations are reviewed. Doppler estimates are the basic measurements from which velocity is estimated, and specific focus is therefore given to the different methods for their determination from the output of digital tracking loops. Finally, the process of velocity determination from the Doppler measurements is discussed.

2.1 Signal and System Model

The complex baseband signal at the input of a digital tracking loop can be expressed as the sum of a useful signal and a noise term (Borio et al 2009a):

$$s[n] = y[n] + w[n] = Ad[n - \tau_0 / T_s]c[n - \tau_0 / T_s]\exp\{j\theta[n]\} + w[n] \tag{2.1}$$

where

- $s[n]$ is the discrete time process obtained by sampling the continuous time signal $s(t)$ at the sampling frequency $f_s = \frac{1}{T_s}$
- $y[n]$ is the useful signal components
- $w[n]$ is a zero mean complex Gaussian process
- A is the useful signal amplitude
- $d[n]$ is the bit sequence modeling the transmitted navigation message
- τ_0 is the delay experienced by the received signal
- $c[n]$ is the signal spreading sequence
- $\theta[n]$ is a time varying process modeling phase and frequency errors.

Under the assumption of perfect code synchronization and after code wipe-off, the input signal (2.1) becomes

$$r[n] = A\,d[n-\tau_0/T_s]\exp\{j\theta[n]\} + w'[n], \tag{2.2}$$

where the code dependence has been removed from the useful signal and $w'[n] = w[n]\,c[n-\tau_0/T_s]$ is a complex Gaussian process characterized by the same mean and variance of $w[n]$. Figure 2-1 shows a block diagram of a standard PLL. The signal $r[n]$ is correlated with a local carrier replica and the correlator output is then used to evaluate an estimate of the residual phase through a non-linear discriminator.

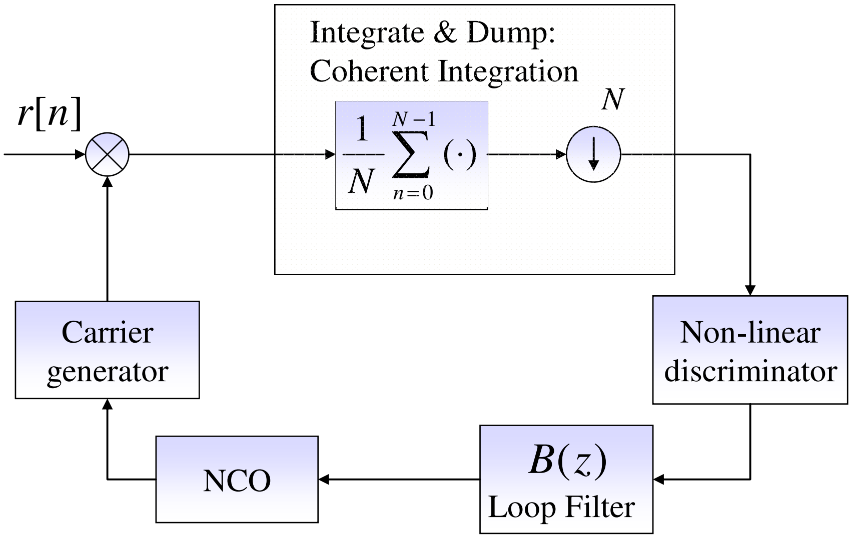

Figure 2-1: Block diagram of a standard PLL.

The discriminator output is filtered and used to drive the Numerically Controlled Oscillator (NCO) for the local carrier generation. *N* here denotes the number of samples used for evaluating the correlation between the local and received signal and $T_c = NT_s$ determines the coherent integration time. The complex correlator output can be modeled as suggested by Van Dierendonck et al, (1996):

$$P = P_I + jP_Q = dA_c \exp\{j\phi\} + \eta_P \tag{2.3}$$

where d models the effect of the navigation message, A_c is the amplitude of the correlator output, ϕ is a residual phase error that will be extracted by the non-linear discriminator and η_P is a complex Gaussian random variable derived by processing the noise term $w'[n]$. PLLs extract the phase information, ϕ, from the input correlator output, P.

The portion of input noise variance transferred from the input samples to the final estimate, ϕ, is determined by the loop filter bandwidth (Stephens & Thomas 1995). Hereafter, the loop filter bandwidth is denoted by the symbol B_n.

When considering PLL with extended integration time, several correlator outputs, obtained from subsequent portions of the input signal, are evaluated and used for producing an improved phase estimate. For this reason, the index $k = 0, 1, ..., K - 1$ is introduced and the above mentioned different correlator outputs are denoted as

$$P_k = P_{I,k} + jP_{Q,k} = d_k A_c \exp\{j\phi\} + \eta_{P,k}, \tag{2.4}$$

where the quantities $\{d_k\}_{k=0}^{K-1}$ are modeled as independent random variables assuming values from the set $\{-1, \ 1\}$ with equal probability. Eq. (2.4) represents the basic signal model used in this thesis. It is noted that in Eq. (2.4) the signal phase, ϕ, is assumed constant during the total integration time and thus does not depend on *K*.

2.2 HSGPS

To deal with weak GPS signals, new techniques have been developed during the past several years, with particular emphasis on methods for increasing the length of the integration period beyond classical limits at both acquisition and tracking. For a given integration duration and in the absence of residual frequency/phase errors, the higher the coherent integration time, the better the reduction of the noise power at the output of the correlators with respect to signal power, i.e. the higher the probability of detection (Julien 2008), or of maintaining lock in a receiver which is already in tracking mode.

To enhance acquisition and tracking thresholds and thus the availability of the position solution using GPS, High Sensitivity techniques based on the use of long integration times have been developed (Petterson et al 1997; Van Diggelen 2001). For weak signal acquisition and tracking coherent integration and non-coherent accumulation are performed in conjunction to increase the total signal dwell time. Coherent integration provides increased performance in terms of noise reduction, but at the cost of vulnerability to frequency errors and bit transitions in the navigation message. Non-coherent processing consists of applying a non-linear transformation to the input signal, removing the effects of data transitions and reducing the impact of frequency errors. This non-linear transformation generally amplifies the noise impact by incurring a squaring loss (Strässle et al 2007). Despite the gains in acquisition and tracking sensitivity that can be gained through extended coherent integrations, and the utilization of multiple correlators simultaneously, the increase in processing burden created by these approaches require massive parallel correlation architectures when taken to their full extent.

2.2.1 Coherent processing

In standard receivers the coherent integration time is typically limited to 20 ms because of the presence of the navigation data, and even where the navigation data is known a-priori, integration is limited by residual frequency errors due to the receiver motion and the receiver oscillator error inducing an additional reduction in the signal to noise ratio (SNR) that increases with the integration time (Watson 2006).

Extension of the integration time beyond the navigation data bit period can be accomplished by detecting, estimating and removing possible bit transitions. Several techniques for estimation of the received navigation message and removal of the effect of bit transitions have been considered (Soloviev et al 2004, Petovello et al 2008, Borio & Lachapelle 2009).

The basic diagram of a PLL with extended coherent integration is illustrated in Fig. 2-2. In general, an initial synchronization is assumed and the bit boundaries are supposed to be known. Thus 20 ms coherent integration can be safely performed within a given data bit. Assuming K consecutive correlator outputs integrated over 20 ms, the Maximum Likelihood (ML) estimate (Borio & Lachapelle 2009) of the data sequence is the bit combination that maximizes the accumulated energy in the in-phase (I) and quadrature (Q) channels as described in (Soloviev et al 2008).

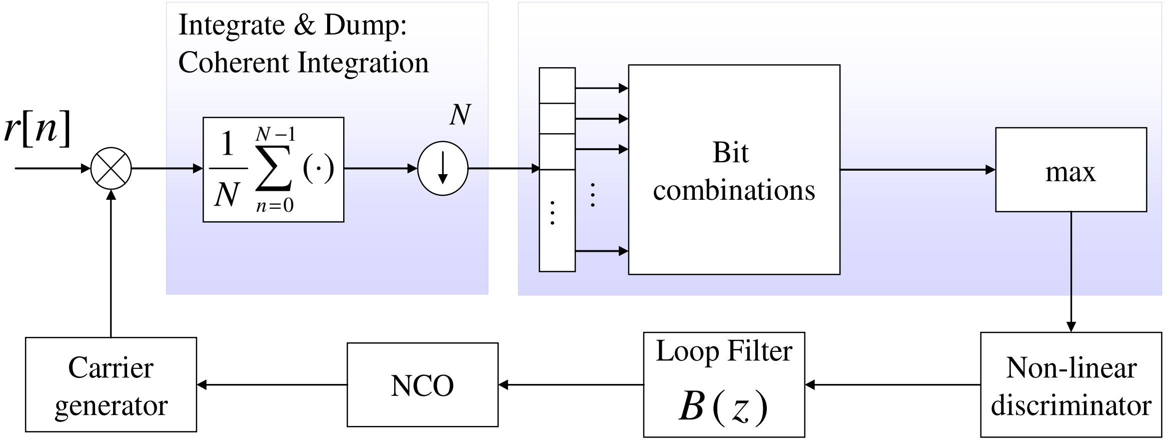

Figure 2-2: PLL with extended coherent integration (Borio & Lachapelle 2009).

This bit sequence is an estimate of the received navigation message which can then be used to remove the effect of the transmitted bits and further increase the coherent integration time. Let

$$\mathbf{P}_k = [P_k \; P_{k-1} \cdots P_{k-K+1}] \tag{2.5}$$

be the vector of the last K complex prompt correlator outputs and $\mathbf{M}_i$ the vector corresponding to the i^{th} bit combination as introduced in Borio (2008). The bit sequence is estimated by the vector $\mathbf{M}_i$, whose index can be obtained as (Borio & Lachapelle 2009)

$$i = \arg\max_l \left\{ \left| S_l \right|^2 \right\} = \arg\max_l \left\{ \left| \mathbf{P}_k \mathbf{M}_l^T \right|^2 \right\}, \tag{2.6}$$

where $(\cdot)^T$ denotes transposition. Since sign combinations differing only for the absolute sign would lead to the same energy, only $H = 2^{K-1}$ combinations are considered. $\mathbf{M}_i$ is then used to extend the integration time producing the accumulated correlator outputs that will be fed into the discriminators.

It should be noted that this approach does not determine the data bits, but instead determines the bit *transitions*.

According to analysis performed by Petovello et al (2008), for low C/N$_0$ a bit estimation approach becomes unreliable, reducing the gain provided by extended coherent integration. Moreover, as this technique requires testing of all possible bit combinations it leads to a computational load growing exponentially with the added number of integrations. For these reasons, to be able to effectively track the signals in degraded environments, other methods such as non-coherent processing have to be considered for the extension of the integration period in tracking loops.

Feasibility of extremely long coherent integration of up to several tens of seconds for positioning indoors has been thoroughly investigated by Watson et al (2006) and Gaggero & Borio, (2008). In both cases data bits have been removed using reference data in a manner similar to AGPS techniques, and ultra-stable reference oscillators were used to avoid losses due to the stability of the local frequency source.

Although signal acquisition indoors has been successfully demonstrated, the achieved position solution accuracy was rather poor, in the best case with relative error of 20 m in the horizontal plane and 100 m in the vertical plane. In addition to the relative inaccuracy of the above, the position calculations provided in the latter study referenced above required significant external aiding information, and the overall thrust of the work was not directed towards creating a receiver which could operate autonomously within degraded environments. In this work, significant attention is given to approaches that will not only allow receiver operation in degraded signal conditions, but will do so independently of external aiding information.

2.2.2 Non-coherent processing

Non-coherent integration, obtained by applying a non-linear function to the correlator outputs for removing the impact of data bits, can be much longer than coherent integration, but since this procedure involves squaring or other non-linear operations, it also implies squaring losses relative to pure coherent integration of the same net duration (Lachapelle et al 2004). This approach is mostly used for acquiring weak signals (O’Driscoll 2007). Extending the non-coherent integration period at the tracking level has been recently proposed by Borio & Lachapelle (2009). Figure 2-3 shows the basic scheme of a PLL with non-coherent integrations.

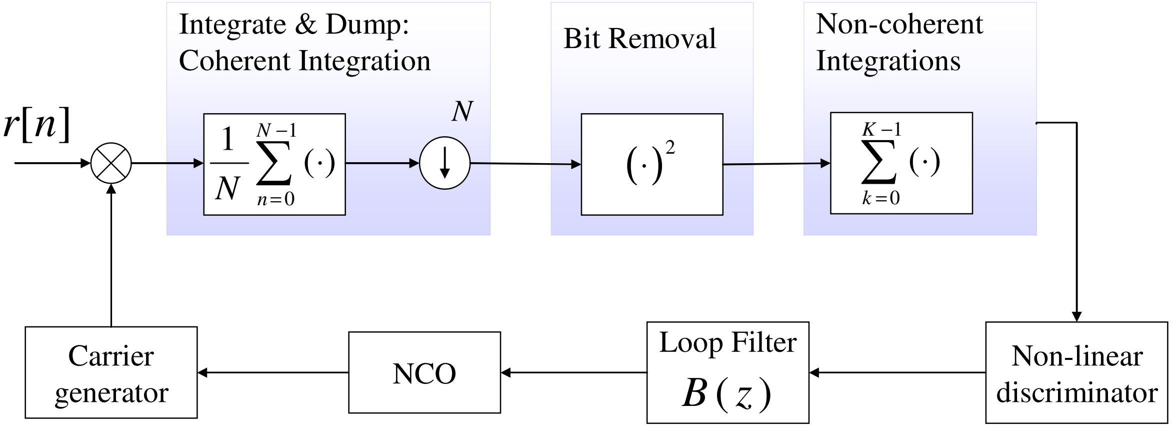

Figure 2-3: PLL with non-coherent integrations (Borio & Lachapelle 2009).

In general, a solution for non-coherently extending the integration time at the tracking level can be represented by the use of non-linear operations for removing the signal dependence on the data bit (Borio & Lachapelle 2009). Assuming a random distribution of data bits the ML estimator for the signal phase can be derived. Navigation data can then be considered as nuisance parameters that do not need to be estimated and therefore can be removed through squaring.

According to the analysis performed by Borio & Lachapelle (2009), which gives an evaluation of the non-coherent tracking loop architecture compared to the existing methodologies, the non-coherent architecture results in an effective alternative to coherent integrations enabling less noisy measurements than the ones obtained by means of standard loops.

2.2.3 Massive Parallel Correlation

To facilitate the complex task of searching for weak GPS signals while using long coherent and non-coherent processing to extend the total integration period, another technique based on massive parallel correlation has been developed. This particular method is based on simultaneous evaluation of GPS signal correlation over the entire range of possible code delays/carrier frequencies (Van Diggelen 2001). In signal degraded environments with significant signal fading, a receiver experiences frequent losses of lock, but computing all possible correlations simultaneously ensures that the correlation peak will always be detected. Thus, by providing more coverage over the probable noise/dynamics influenced code/carrier space, the tracking threshold limits of the receiver can be enhanced.

2.3 Velocity Estimation in a Digital Tracking Loop

The loop filter output of a PLL provides an indication of the observed frequency shift on the received signal. This observed frequency differs from the nominal L1 frequency because of the Doppler shift produced by the satellite and the user motion as well as the frequency error or the drift of the satellite and user clocks (Van Graas & Soloviev 2004). The Doppler shift caused by the satellite and user motion can be defined as a projection of the relative velocity onto the Line of Sight (LOS). Given the satellite velocity, the Doppler measurements can be used to estimate the velocity of the receiver.

The Doppler measurements that are used to extract velocity information can be obtained in two different ways. The first option is the use of raw Doppler measurements that are the direct output of the PLL filter. The second method uses time-differenced GPS carrier phase measurements.

In the literature, the second approach has been considered advantageous, mainly because of the achievable accuracy and the noise reduction obtained in the process of computing carrier phase measurements. Differentiating the observables for velocity estimation over a short time interval brings some advantageous effects, namely removal of the residual effects of the tropospheric and ionospheric delays and the provision of an ambiguity free solution.

Several methods of differentiation have been investigated for this purpose. Fenton & Townsend (1994) demonstrated the use of parabolic functions. Both Cannon et al (1997) and Hebert (1997) approached the task using simulated GPS data by applying low-order Taylor series approximations of the derivative (i.e. central difference equations) and by differentiating cubic spline approximations of the carrier phase data. A Kalman filtering approach was also proposed and applied by Hebert (1997). Bruton (2000) gave a comprehensive review and characterization in the frequency domain of several possible methods of carrying out the differentiation process with specific focus on higher order central difference approximations and their use in high dynamics applications.

2.3.1 GPS Carrier Phase Measurements Differentiation

According to Antoniou (1993), the frequency response, $H(e^{j\omega T})$ of an ideal uniformly-sampled discrete-time differentiator can be written in the following form:

$$H(e^{j\omega T}) = j\omega \text{ for}, 0 \leq |\omega| < \frac{\omega_S}{2} \tag{2.7}$$

where ω is the frequency of the spectrum of the signal, $\omega_S = 2\pi / T$ is the sampling frequency in radians per seconds, and T is the corresponding sampling period.

To differentiate a discrete time signal, such as GPS data, one can use a discrete time convolution, or in other words, the differentiator can be considered as a nonrecursive or finite impulse response (FIR) filter. Practically, a FIR filter can be applied to a discrete data set, such as the carrier-phase time series $\phi(t)$, using convolution as follows:

$$\dot{\phi}(t) = \sum_{k=0}^{N-1} h(t)\,\phi(t-k)\,, \tag{2.8}$$

where, $\dot{\phi}(t)$ is the derivative of the input sequence, $\phi(t)$, and $h(t)$ is the impulse response of the system, having length *N*. Theoretically, the relationship between the discrete time unit impulse response, $h(t)$ and the frequency response of the discrete-time differentiator, $H(e^{j\omega T})$ is given by the Inverse Discrete Time Fourier Transform. Practically, then, the design of a digital differentiator depends on the choice of the impulse response $h(t)$ and the order of the filter, *N*. Ideally, the order should be chosen in a way that the filter frequency response should approximate Eq.(2.7).

The following discussion on the use of the FIR filters has been limited, excluding several approaches. For example, it is well known that a Kalman filter smoother results in a smooth, band-limited solution. This result was confirmed in Hebert (1997). However, the Kalman filter approach has shown to offer little or no improvement over the low order Taylor series approximations, and therefore was not considered in this thesis. Moreover, this research is focused on pedestrian dynamics, therefore the differentiation methods proposed for high dynamics are not considered.

Because they have been used extensively in the GPS literature, low-order Taylor series approximations of the derivative are treated first.

2.3.2 Central Difference Approximation

The central difference approximations are based on a Taylor Series expansion and yield an estimate of the derivative. Derivation of the formulae for this method can be found in (Cheney & Kincaid, 1985). Given a function $f(x)$ and a step length h, the Taylor Series at $(x+h)$ expanded about x is defined as:

$$f(x+h)=f(x)+hf^{'}(x)+\frac{h^2 f^{''}(x)}{2!}+\frac{h^3 f^{'''}(x)}{3!}+\ldots \tag{2.9}$$

In a similar way, the Taylor Series for the function $f(x)$ at $(x-h)$ expanded about x is given by:

$$f(x-h)=f(x)-hf^{'}(x)+\frac{h^2 f^{''}(x)}{2!}-\frac{h^3 f^{'''}(x)}{3!}+\ldots \tag{2.10}$$

By combining Eqs. (2.9) and (2.10), and truncating to first order, the first-order central difference approximation to the derivative is obtained:

$$f^{'}(x)\approx\frac{f(x+h)-f(x-h)}{2h}\,. \tag{2.11}$$

The use of the first order central difference approximation of the carrier-phase measurements to generate the Doppler observations, as was demonstrated by Szarmes et al (1997) and Cannon et al (1997) is easy to implement and provides the most appropriate velocity estimates in static and low dynamics modes.

Higher order central difference approximations are often presented in the literature as an alternative to this simple first-order approximation (this is justified by the intuition that using more data provides a better estimate of the derivative). These higher order differentiation techniques are also based on the Taylor series expansion, and can simply be obtained by including more data points about the central point of expansion.

Neglecting the higher-order terms, the second order central difference approximation is obtained as follows:

$$f^{'}(x) \approx 8\frac{f(x+h)-f(x-h)}{12h}-\frac{f(x+2h)-f(x-2h)}{12h}. \tag{2.12}$$

These basic equations can be then implemented as FIR filters. The impulse response corresponding to the first and the second-order differentiators given above is usually represented as a vector as follows:

$$h=\frac{1}{2}\begin{bmatrix}1 & 0 & -1\end{bmatrix}^{T} \tag{2.13}$$

$$h=\frac{1}{12}\begin{bmatrix}1 & -8 & 0 & 8 & -1\end{bmatrix}^{T}. \tag{2.14}$$

As this work focuses on low (pedestrian) dynamics, only the first and the second -order central difference approximations will be considered.

2.3.3 Smoothing and Differentiation by Savitsky-Golay Filter

Essentially, the Savitzky-Golay smoothing and differentiation filter optimally fits a set of data points to a polynomial in the least-squares sense. It should be noted that in some previous works including Hebert et al (1997), Cannon et al (1997) and Serrano et al (2004) this technique is referred to as curve fitting.

This filter can be described as follows: a set of points needs to be fitted to some curve; in this case the points are carrier phase measurements to be fit by the third order polynomial

$S_p(t) = a + b(t-\overline{t}) + c(t-\overline{t})^2 + d(t-\overline{t})^3$,

where $\overline{t}$ is the time instant corresponding to the centre of the analysis window.

In matrix form, a general expression for $S_p(t)$ can be written as

$$S_p = \underbrace{\begin{bmatrix} 1 & (t_0-\overline{t}) & (t_0-\overline{t})^2 & (t_0-\overline{t})^3 \\ 1 & (t_1-\overline{t}) & (t_1-\overline{t})^2 & (t_1-\overline{t})^3 \\ \dots & \dots & \dots & \dots \\ 1 & (t_{L-2}-\overline{t}) & (t_{L-2}-\overline{t})^2 & (t_{L-2}-\overline{t})^3 \\ 1 & (t_{L-1}-\overline{t}) & (t_{L-1}-\overline{t})^2 & (t_{L-1}-\overline{t})^3 \end{bmatrix}}_{V} \underbrace{\begin{bmatrix} a \\ b \\ c \\ d \end{bmatrix}}_{P}. \tag{2.15}$$

For time instant *t*, a fixed number of data points centered around *t* and varying from $-W/2$ to $W/2$ is used for determining the coefficients of the polynomial $S_p(t)$. $W+1$ is the total number of observations used for the interpolation process. The coefficients, *a, b, c* and *d,* are then selected such that the Mean Square Error

$$\left\| S_p(t) - y \right\|^2 \tag{2.16}$$

is minimized. y is the vector containing the observed carrier phase measurements corresponding to the different time instants used for the interpolation.

The procedure has to be repeated over the entire data set, by gradually moving analysis window used to specify the $W+1$ points for the interpolation around *t*. There is one important detail to be noted, in order to reduce discontinuities, an overlap in between consecutive analysis windows needs to be adopted (Hebert 1997). Taking the first derivative of $S_p(t)$ gives the relation:

$$\frac{dS_p(t)}{dt} = b + 2c(t-\overline{t}) + 3d(t-\overline{t})^2 . \tag{2.17}$$

When (2.17) is evaluated for the central point of the interval $t=\overline{t}$,

$$\left.\frac{dS_p(t)}{dt}\right|_{t=\overline{t}} = b \tag{2.18}$$

The MMSE problem (2.16) is solved by:

$$\begin{bmatrix} a \\ b \\ c \\ d \end{bmatrix} = H\,y = \left(V^H V\right)^H y \tag{2.19}$$

where matrix *V* is the Vandermonde matrix from Eq.(2.15). Additionally, *H* can be written in terms of its rows:

$$H = (V^H V)^{-1} V^H = \begin{bmatrix} h_1 \\ h_2 \\ h_3 \\ h_4 \end{bmatrix} \tag{2.20}$$

Each row of *H* can be then interpreted as the impulse response of a FIR filter. Moreover, the second coefficient, *b*, can be written as

$$b = h_2 y = \sum_{i=0}^{L-1} h_{2,i} y_i \ . \tag{2.21}$$

According to (2.18), b is the carrier phase derived Doppler at the central instant $\bar{t}$ and it is given by a filtered version of the carrier phase measurements y. Equation (2.20) defines the impulse response of the Savitzky-Golay smoothing and differentiation filter.

As it can be seen from Eq.(2.21), this procedure produces both smoothing and differentiation, and therefore can be represented as a smoothing filter. For a given time instant, t_k, Eq. (2.21) can be written as

$$b_k = \sum_{i=-W/2}^{W/2} h_{2,i} y_{k+i} \ . \tag{2.22}$$

This type of filter smoothes the input data and provides an estimate of its derivative. The level of smoothing provided is a function of both the order of the polynomial, in this case 3, and the size of the analysis window $W+1$. The Savitsky-Golay approach is suitable for band-limited low-frequency signals and it will approximate the ideal differentiator only up to a certain frequency. This means that such a filter can only be used for static or low dynamic conditions. This has been confirmed in the research reported in several publications. For example, Fenton & Townsend (1994) used a parabolic fit within the receiver to estimate the derivative. They found that velocity results were improved in static cases. Both Cannon et al (1997) and Hebert (1997) approached this task in post mission using simulated GPS data by employing cubic spline fits for differentiation. In each of these cases, good results were observed in static and low dynamic cases, but errors increased with higher dynamics.

2.3.4 Velocity Estimation

Having obtained raw or carrier phase derived Doppler measurements and given the satellite velocity, velocity of the receiver can be finally estimated. The Doppler measurement $\dot{\phi}$ can be written as a projection of the relative velocity vector on the satellite LOS vector (Enge & Misra 2001). The observation equation for velocity determination can be written as follows (Lachapelle 2008):

$$\dot{\phi}^{(k)} = \dot{\rho}^{(k)} + c(\dot{dt}^{(k)} - \dot{dT}) - \dot{d}_{ion}^{(k)} + \dot{d}_{trop}^{(k)} + \varepsilon_{\dot{\phi}}^{(k)} \tag{2.23}$$

where $\dot{\rho}^{(k)}$ stands for the geometric range rate between the receiver and the satellite; $\dot{dt}^{(k)}$ for the bias rate of the satellite clock; $\dot{d}_{ion}^{(k)}$ for the ionospheric delay rate; $\dot{d}_{trop}^{(k)}$ for the tropospheric delay rate and $\varepsilon_{\dot{\phi}}^{(k)}$ for the receiver system noise, assigned for satellite k, while $\dot{dT}$ stands for the bias rate of the receiver clock. A thorough review of the behavior and magnitude of each error source can be found in Raquet (1998) or Bruton (2000). After modeling the measurements according to Parkinson et al (1996), the observation equation for velocity determination can be stated as follows:

$$\dot{\phi} = (\mathbf{v}^{(k)} - \mathbf{v}) \cdot \mathbf{h}^{(k)} + \dot{dT} + \varepsilon_{\dot{\phi}}^{(k)}, \tag{2.24}$$

where $\mathbf{v}^{(k)}$ stands for the satellite velocity vector; $\mathbf{v}$ for the receiver velocity vector, to be estimated, and $\mathbf{h}^{(k)}$ is a user-to-satellite LOS unit vector that can be determined from an estimate of the user position; $\dot{dT}$ is the bias rate of the receiver clock, and $\varepsilon_{\dot{\phi}}^{(k)}$ is the combined error due to changes during the measurement interval in the satellite clock, ionosphere and troposphere. Equation (2.24) is linear in user velocity components, so that it can be rewritten as

$$(\dot{\phi}^{(k)} - \mathbf{v}^{(k)} \cdot \mathbf{h}^{(k)}) = -\mathbf{h}^{(k)} \cdot \mathbf{v} + d\dot{T} + \varepsilon_{\dot{\phi}}^{(k)} \tag{2.25}$$

Denoting $(\dot{\phi}^{(k)} - \mathbf{v}^{(k)} \cdot \mathbf{h}^{(k)})$ as $\dot{\phi}'^{(k)}$, the combined set of measurements from k satellites, (2.25) can be finally written as a set of equations in matrix form as:

$$\dot{\phi}' = \mathbf{A} \begin{bmatrix} \mathbf{v} \\ d\dot{T} \end{bmatrix} + \varepsilon_{\dot{\phi}}, \tag{2.26}$$

where

$$\mathbf{A} = \begin{bmatrix} h_x^{(1)} & h_y^{(1)} & h_z^{(1)} & 1 \\ h_x^{(2)} & h_y^{(2)} & h_z^{(2)} & 1 \\ \cdots & \cdots & \cdots & \cdots \\ h_x^{(k)} & h_y^{(k)} & h_z^{(k)} & 1 \end{bmatrix} \tag{2.27}$$

is an $(k \times 4)$ matrix characterizing the receiver-satellite geometry consisting of unit vectors between the receiver and satellites $h_{x,y,z}^{(k)}$. The receiver velocity can then be estimated by implementing epoch by epoch least squares solution or Kalman Filter (KF) approach. In order to simplify the analysis, and to decouple any filtering effects for the velocity solution, only the LS solution is considered in this work.

CHAPTER 3: MEMORY DISCRIMINATORS IN GPS TRACKING LOOPS

Extending the integration time is one of the alternative solutions for a GNSS receiver to be able to operate in signal degraded areas such as indoors and urban canyons.

As it has been described in **Chapter 2**, integration time can be extended by detecting, estimating and removing possible bit transitions or, alternatively, using nonlinear operations for removing the signal dependence on the data bit. This chapter focuses mainly on the concept of PLL discriminators employing non-coherent integrations for extending the total integration time.

First, a brief discussion of the Maximum Likelihood (ML) discriminator is given followed by the introduction of the concept of memory discriminators. Use of low-pass filters implementing exponential smoothing for the non-coherent extension of the integration time is then discussed with specific focus on the procedure for the loop filter design. The definition of effective integration time for non-coherent tracking loops is also given.

Lastly in this chapter, an overview of the performance of the memory discriminator based tracking loop architecture is provided.

3.1 Memory Discriminators: General Formulation

The concept of the memory discriminator was previously introduced by Borio & Lachapelle (2009) and directly derives from the ML phase estimator in the presence of sign transitions. The ML phase estimator is derived assuming that the navigation data bits are randomly distributed. When making this assumption the navigation data is considered as nuisance parameters which do not need to be estimated, and therefore can be removed through squaring. This non-coherent ML phase estimator is used as a discriminator for a new type of tracking loop that allows extended non-coherent integrations.

In (Borio & Lachapelle 2009) the ML phase discriminator in the presence of bit transitions is derived as:

$$S(\phi_k) = \frac{1}{2}\arctan_2\left[2\sum_{i=0}^{K-1} P_{I,k-i}P_{Q,k-i}, \sum_{i=0}^{K-1}(P_{I,k-i}^2 - P_{Q,k-i}^2)\right] = \frac{1}{2}\arg\left\{\sum_{i=0}^{K-1} P_{k-i}^2\right\}, \tag{3.1}$$

where P_k is the complex correlator output, as defined in Eq.(2.4), and $k = 0,1, ..., K -1$ is the index denoting the number of correlator outputs when considering PLL with extended integration time. It should be noted that for only one complex correlator output, $K = 1$, $S(\phi_k)$ equals to the standard *arctan* discriminator

$$S(\phi_k) = \arctan\left(\frac{P_{Q,k}}{P_{I,k}}\right). \tag{3.2}$$

The discriminator type represented by Eq. (3.1) performs bit removal by squaring the complex correlator outputs, P_k, and non-coherent integration by further summing the squared correlator outputs. Finally, the phase is extracted using the *arctan₂* operators.

The process of non-coherent integration is equivalent to low-pass filtering the squared correlator P_k^2 with a moving average filter of length K (Borio & Lachapelle 2009).

By updating the filter at correlator rate, $T_c = NT_s$, a first type of memory discriminator is obtained. In this case, T_c is the coherent integration time and T_s is the sampling interval.

In this way, longer integration time can be achieved without reduction of the loop's update rate. Substituting the moving average filter with a general low pass filtering stage results in a new class of memory discriminators. Thus, the expression for the ML phase discriminator given in Eq. (3.1) can be generalised to

$$S(\phi_k)=\frac{1}{2}\arg\left\{\sum_{i=0}^{+\infty} f_i P_{k-i}^2\right\}, \tag{3.3}$$

where $\{f_i\}_{i=0}^{+\infty}$ define the low-pass filter impulse response

$$f[n]=\sum_{i=0}^{+\infty} f_i \cdot \delta[n-i]. \tag{3.4}$$

The ML discriminator given in Eq. (3.1) has been derived assuming that the phase is constant during the integration interval. In this case, a uniform filtering is performed and all the input samples are weighted equally.

Including a more general low-pass filtering into the discriminator allows to progressively de-weight the input observations, so that the older samples, P_k, will have less impact on the current phase estimate with respect to more recent ones.

Figure 3-1 illustrates the general structure of a PLL with memory discriminator.

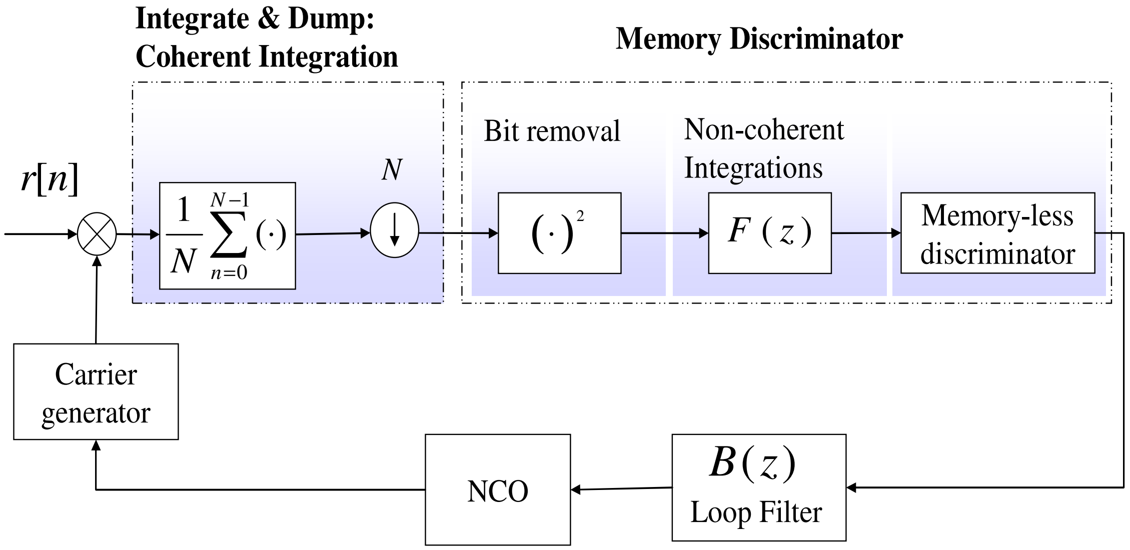

Figure 3-1: PLL with non-coherent integrations (Borio et al 2009a). The integration time is extended non-coherently by the additional filter after the squaring block.

As shown on Fig. 3-1, this type of discriminator operates by first removing the bit dependence from the correlator outputs by squaring. A low-pass filtering stage responsible for the discriminator memory is then applied to further extend the integration time. A memory-less discriminator finally extracts the phase information.

Similarly, the same method can be applied for frequency and delay estimation as well, as shown by Borio et al (2009a).

3.2 Loop Linear Model: Discriminator as a Filter

To be able to evaluate the transfer function of the tracking loop and define the design criteria for the loop filter, it is necessary to derive the loop linear model. Only the case with the PLL is considered in this section, though, the model is general and can therefore be applied to other tracking loops (Borio & Lachapelle 2009).

The loop linear model is obtained by approximating the loop discriminator with its linear filter. The PLL linear model is shown in Fig. 3-2, where

– $\phi[k]$ is the average phase at the correlator output that the loop is trying to track;

– $\bar{\phi}[k]$ is the phase estimated from the loop;

– $\dot{\bar{\phi}}[k]$ is the phase rate at input of the NCO;

–$\hat{\phi}[k]$ is the phase estimated by the discriminator;

– $N_d[k]$ is a white random process accounting for the noise at the input of the loop and the distortions introduced by the non-linearities in the discriminator.

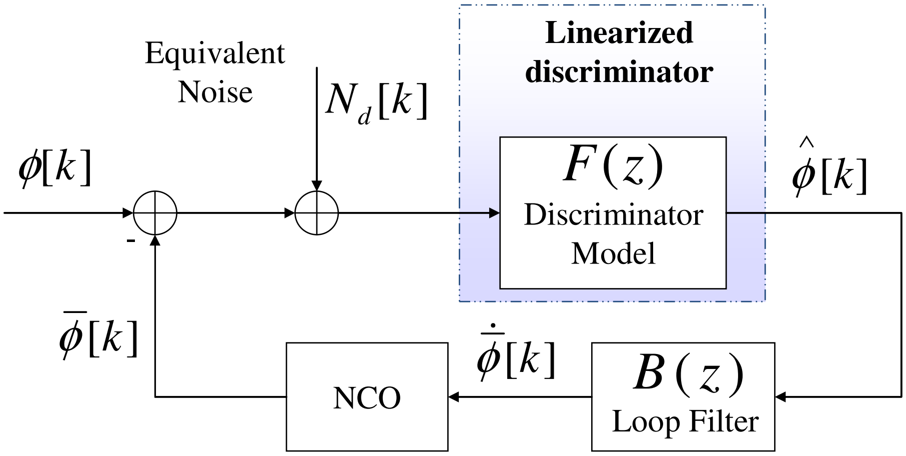

Figure 3-2: Linear model for a PLL with discriminator with memory (Borio & Lachapelle 2009).

In traditional tracking loops, the discriminator is approximated by a constant gain (Gardner 2005). Due to the fact that a memory discriminator introduces memory into the system, as well as the constraint that only a finite number of correlator outputs is used for the evaluation of the discriminator output a FIR filter has been found to be a more appropriate linear approximation (Borio & Lachapelle 2009). Therefore, the ML phase discriminator can be approximated by a moving average filter with transfer function

$$F(z) = \frac{1}{K}\sum_{i=0}^{K-1} z^{-i}. \qquad (3.5)$$

In the case where only one complex correlator output is used ($K = 1$), the linear model adopted for the tracking loops with extended non-coherent integration becomes a constant gain. Extending the discriminator to include a more general low-pass filtering stage by introducing the coefficients $\{f_i\}_{i=0}^{+\infty}$ as in Eq. (3.3) gives the linear transfer function defined in (Borio et al, 2009a):

$$F(z) = \frac{1}{\sum_{i=0}^{+\infty} f_i}\sum_{i=0}^{+\infty} f_i z^{-i}. \qquad (3.6)$$

The use of approximations (3.5) and (3.6) allows to remove the non-linearities present in the PLL and the tracking loop is approximated by a linear device that computes phase estimates as a linear combination of filtered noise and input signal. In this respect a PLL is characterized by a noise transfer function, $H(z)$, that determines the amount of noise transferred from the input signal to the final phase estimate. When considering a rate-only feedback NCO (Stephens & Thomas 1995), it is possible to show that the PLL noise transfer function assume the following expression (Borio et al 2009a):

$$H(z)=\frac{\frac{1}{2}(z+1)T_cB(z)F(z)}{z(z-1)+\frac{1}{2}(z+1)T_cB(z)F(z)} \tag{3.7}$$

where $B(z)$ is the loop filter transfer function defined as

$$B(z)=\frac{1}{T_c}\sum_{i=0}^{L-1}K_i\frac{1}{(1-z^{-1})^i}=\frac{1}{T_c}\sum_{i=0}^{L-1}K_i\left[\frac{z}{z-1}\right]^i. \tag{3.8}$$

In (3.8), $\{K_i\}_{i=0}^{L-1}$ are the integrator gains to be determined according to the procedure described in Section 3.4. The noise bandwidth is then defined as

$$B_n=\frac{1}{2}\int_{-1/2T}^{1/2T}\left|H(e^{j2\pi fT})\right|^2 df=\frac{1}{2}\frac{1}{2\pi j}\oint H(z)H(z^{-1})z^{-1}dz.$$

3.3 Exponential Discriminator

This section discusses the use of a special class of low-pass filters implementing exponential smoothing (Borio et al 2009a). To be more specific, an exponential filter can be used to extend the integration time before extracting the phase/ frequency/delay information. Exponential filtering has been chosen for its reduced computational load and for the possibility of progressively de-weighting the squared correlator outputs, according to the filter forgetting factor, α. The transfer function of an exponential filter can be expressed as follows:

$$F(z) = (1-\alpha)\sum_{i=0}^{+\infty} \alpha^i \cdot z^{-i} = (1-\alpha)\frac{1}{1-\alpha z^{-1}}, \tag{3.9}$$

where $0 \le \alpha < 1$ is the filter forgetting factor. From (3.9) it is possible to determine the filter impulse response that is given by

$$f[n] = (1-\alpha)\sum_{i=0}^{+\infty} \alpha^i \delta[n-i]. \tag{3.10}$$

Figure 3-3 shows an example of the exponential filter impulse responses for different values of α.

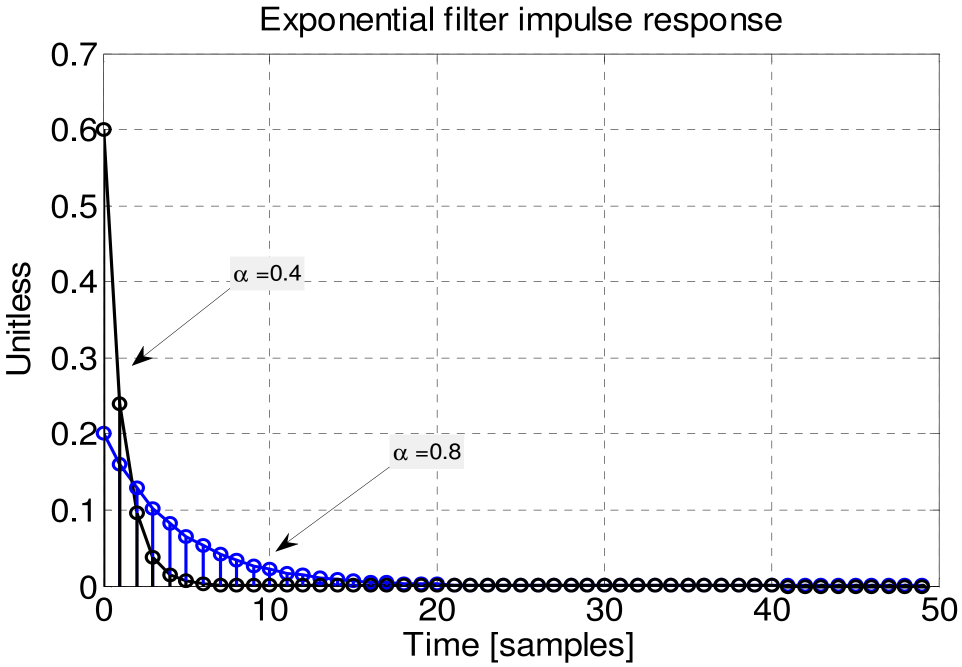

Figure 3-3: Exponential filter impulse response.

Setting $\alpha = 0$ makes the memory discriminator degenerate into a standard memory-less discriminator.

Following the methodology suggested by Borio et al (2009) and described in the previous section, the loop transfer function in the case of exponential filter can be expressed as follows:

$$H(z)=\frac{\frac{1-\alpha}{2}(z+1)\sum_{i=0}^{L-1}K_i z^i (z-1)^{L-1-i}}{(z-1)^L(z-\alpha)+\frac{1-\alpha}{2}(z+1)\sum_{i=0}^{L-1}K_i z^i (z-1)^{L-1-i}}=$$

$$=\frac{D_\alpha(z)-(z-1)^L(z-\alpha)}{D_\alpha(z)}, \tag{3.11}$$

where

$$D_\alpha(z)=(z-1)^L(z-\alpha)+\frac{1-\alpha}{2}(z+1)\sum_{i=0}^{L-1}K_i z^i (z-1)^{L-1-i} \tag{3.12}$$

is the denominator of $H(z)$ that determines the poles of the system.

3.4 Loop Filter Design

Memory discriminators introduce additional poles and zeros in the linear transfer function of the loop and a new procedure for the design of the loop filter is required to ensure the stability of the loop.

Since standard techniques derived from the transformation of analog filters cannot be directly applied, the controlled-root formulation proposed by Stephens & Thomas (1995) can be modified to account for the effect of the addition poles introduced by the new discriminators (Borio & Lachapelle 2009). In this way, stable loops able to work under strongly attenuated conditions can be obtained. According to the controlled-root formulation (Stephens & Thomas 1995), L poles of the loop transfer function are constrained to lie on a geometric locus parameterized with respect to a control parameter β. This parameter determines the decay rate of the loop impulse response and has to be adjusted to meet the bandwidth requirements. However, the transfer function given in Eq. (3.11) can have more than L poles. The controlled-root formulation allows constraining only L poles corresponding to the available L free parameters, the integrator gains. The position of the remaining poles is determined by the type of NCO (Stephens & Thomas 1995) and the type of memory discriminator (Borio et al 2009).

The procedure for determining the control parameter, β, has been addressed in detail in (Borio & Lachapelle 2009) and is summarized in Fig. 3-4, where the control parameter, β, is progressively adjusted in order to meet the bandwidth requirements and used for fixing the position of L poles.

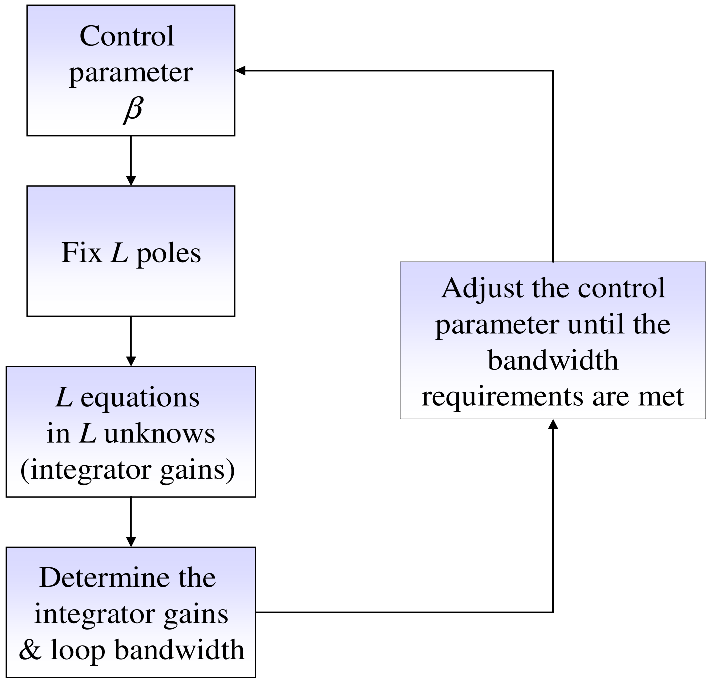

Figure 3-4: Iterative algorithm for filter design according to the controlled-root formulation (Borio & Lachapelle 2009).

As it can be seen from Fig. 3-4, first *L* poles are fixed according to an initial value of the design parameter. By substituting the values of these *L* poles into Eq.(3.12), a system of *L* equations with *L* unknowns is defined. By solving this system of equations, the integrator gains $\{K_i\}_{i=0}^{L-1}$ that define the transfer function of the system, from which the loop bandwidth can be evaluated, are obtained. The design parameters are then iteratively adjusted until the required bandwidth is obtained.

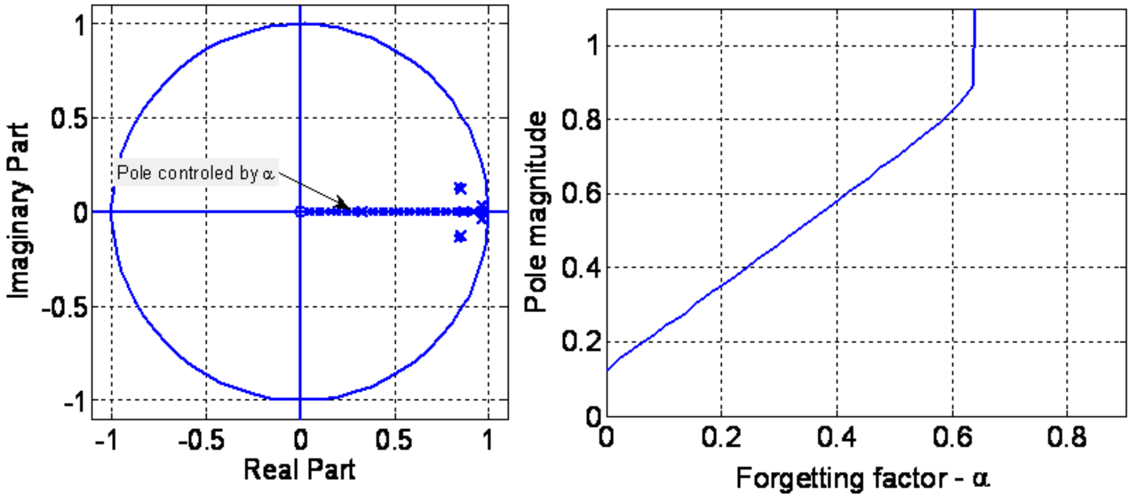

Figure 3-5: Pole placement as a function of the forgetting factor, α, for a third order loop with B_n = 2 Hz and T_c = 20 ms.

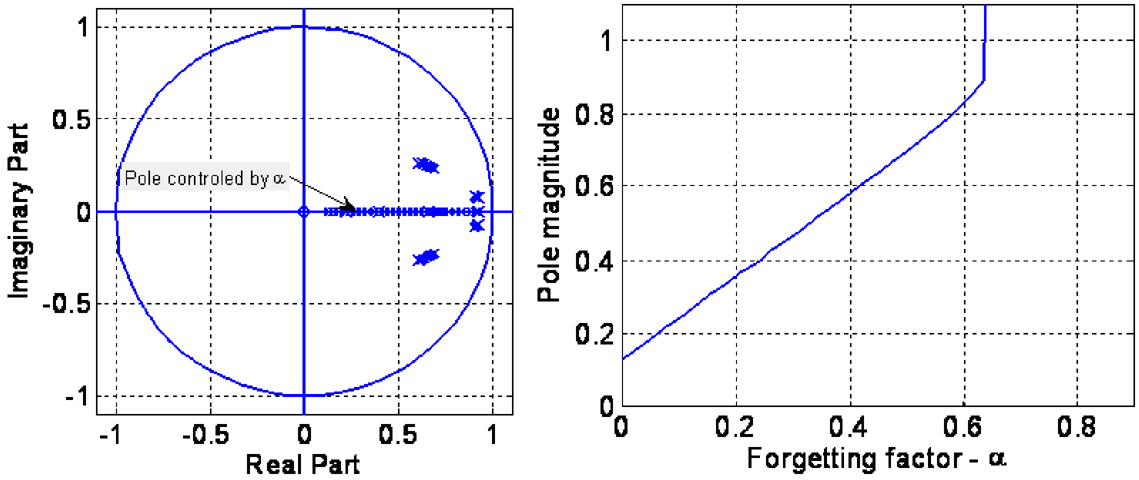

Figure 3-6: Pole placement as a function of the forgetting factor, α, for a third order loop with B_n = 5 Hz and T_c = 20 ms.

In Figures 3-5 and 3-6 the pole placement is shown as a function of α for a third order loop with 5 and 2 Hz bandwidth. A third order loop is characterized by four poles, three of which are fixed according to the controlled-root formulation. The position of the fourth pole essentially depends on α and it is progressively pushed to the limits of the unit circle as α increases.

One should note that the pole determined by the exponential discriminator is always real and the positions of the poles fixed according to controlled-root formulation are not significantly affected by the forgetting factor value (Borio et al 2009a). The first property directly derives from the way the other poles are fixed and from the fact that the denominator given by Eq. (3.12) has real coefficients. The second property has been thoroughly studied in (Borio et al 2009a) and can be accordingly described by the following relationship:

$$D_\alpha(z) = (1-\alpha)D_0(z) + \alpha(z-1)^{L+1}, \tag{3.13}$$

where $D_\alpha(z)$ is the denominator given by Eq. (3.12) and $D_0(z) = D_\alpha(z)\big|_{\alpha=0}$. In this particular case, for the considered bandwidths, 2 and 5 Hz, the poles placed according to the controlled-root formulation assume values close to unity, making the term $\alpha(z-1)^{L+1}$ negligible. Therefore, Eq. (3.13) can be simplified as

$$D(z_i) = D_\alpha(z_i) \approx (1-\alpha)D_0(z_i) = 0, \tag{3.14}$$

showing that the L poles placed according to the controlled-formulation are not significantly influenced by the forgetting factor α. As it has been shown in (Borio et al 2009a) the loop becomes unstable for α greater than a threshold value $\alpha \cdot T_c$. This fact is illustrated in Fig. 3-7, where the magnitude of the pole controlled by α is shown as a function of the forgetting factor and several bandwidths are considered.

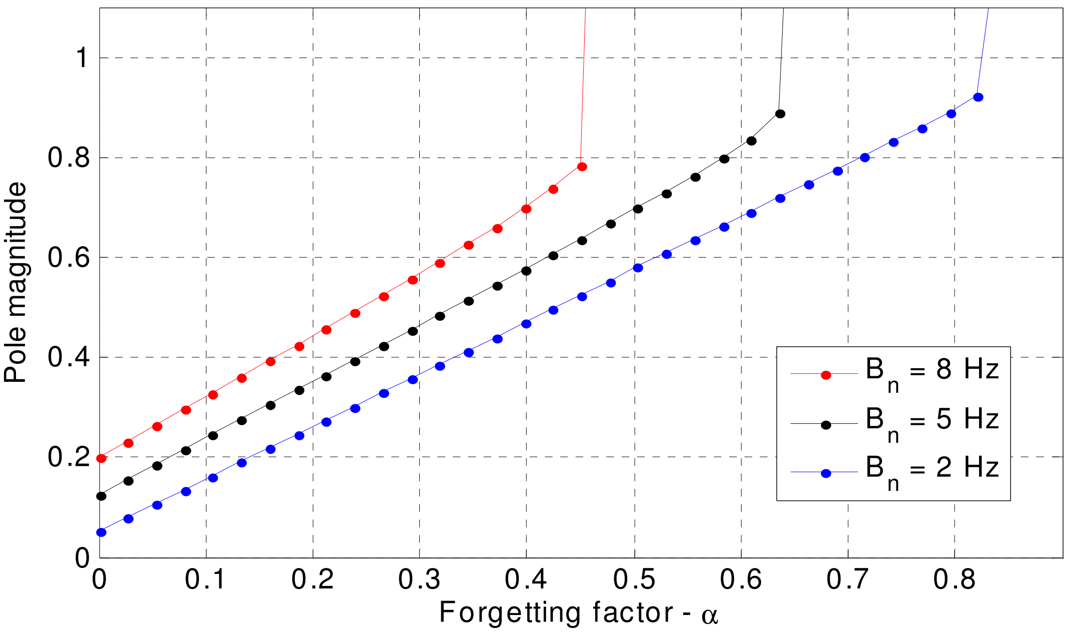

Figure 3-7: Pole magnitude as a function of the forgetting factor, α, and the equivalent bandwidth B_n.

The pole magnitude increases almost linearly as a function of α until the threshold value, $\alpha \cdot T_c$, is reached. This threshold is different for each bandwidth.

3.5 Non-coherent Discriminators and Effective Integration Time

In the previous sections the theoretical background of the concept of memory discriminators has been given. This section focuses on the quantification of the effective integration time achieved by non-coherent tracking loops.

Thus far only the coherent integration time has been specified as NT_s. To determine the non-coherent integration time the approach suggested in (Proakis et al 1963) for defining the effective measurement time can be adopted, and the tracking loop's effective integration time can be obtained using the following relationship:

$$T_{eff} = \frac{\left(\sum_{i=0}^{+\infty} f_i\right)^2}{\sum_{i=0}^{+\infty} f_i^2} \cdot T_c \, , \tag{3.15}$$

where T_c is the coherent integration time and $\{f_i\}_{i=0}^{+\infty}$ are the memory discriminator filter coefficients. Having specified the transfer function of a memory discriminator with extended non-coherent integration as given by Eq.(3.5), and substituting this transfer function into Eq.(3.15), the following relation is obtained:

$$T_{eff} = \frac{\left(\sum_{i=0}^{K-1} \frac{1}{K}\right)^2}{\sum_{i=0}^{+\infty} \frac{1}{K^2}} \cdot T_c = K \cdot T_c \, , \tag{3.16}$$

indicating that in this case, the total effective integration time is a product of the coherent integration time and the number of non-coherent integrations *K*. In the special case of exponential filtering, as discussed in (Borio 2009), substituting the expression for the coefficients of an exponential filter as given in Eq. (3.9) into Eq. (3.15) leads to the following expression for the integration time:

$$T_{eff} = \frac{\left(\sum_{i=0}^{+\infty} \alpha_i\right)^2}{\sum_{i=0}^{+\infty} \alpha_i^2} \cdot T_c = \frac{1+\alpha}{1-\alpha} \cdot T_c \, . \tag{3.17}$$

The above shows that in the case of exponential filtering, the effective integration time depends on the choice of the forgetting factor value. Assuming for example $\alpha = 0.5$, and setting the coherent integration time to be 1 ms, the effective integration time according to the Eq. (3.17) becomes 3 ms.

3.6 Overview and Comparative Performance

The concept of memory discriminators is quite new. It has been first proposed by Borio & Lachapelle (2009) and then further studied in (Borio et al 2009a). The major objective of memory discriminators is to introduce extended integration times, without requiring the estimation of the navigation message. This gives origin to tracking loops capable to track strongly attenuated signals in the presence of additional impairments such as fading and multipath.

For practical verification the memory discriminators described in the previous sections have been integrated into the University of Calgary's GNSS Software Navigation Receiver GSNRx^{TM} (Petovello et al, 2008) that now represents a fully operational platform. Performance of this memory discriminator based architecture has been studied in a number of different GPS operating environments with the main focus on degraded signal areas.

Performance of the memory discriminator based architecture, using different values of the forgetting factor parameter, can be illustrated by using a dataset with progressively attenuated LOS GPS signals. In this experiment the antenna was mounted on the roof of the building so that the data was collected in an open sky environment with a few nearby multipath sources. The signals have been collected using one of the National Instruments (NI) *NI PXI-5661* system front-ends characteristics of which are reported in Table 3-1.

Table 3-1: Characteristics of the GPS signals collected using the NI system front-end.

Parameter	**Value**
Sampling frequency	$f_s = 10\ MHz$
Intermediate frequency	$f_{IF} = 3.42\ MHz$
Sampling	Real

In this test, the signal was progressively attenuated with a step of 1 dB each 30 s after a minute without attenuation. One should consider the fact that the decrease in C/N$_0$ is not directly proportional to the provided attenuation since both signal and noise components were attenuated at the same time. The decrease in C/N$_0$ is caused by both the signal attenuation and additional noise introduced by the attenuator.

The attenuated data has been then processed using the GSNRx^{TM} software for different forgetting factor and different bandwidth values. The Doppler has been estimated for different configurations and the quality of the measurements determined by estimating their standard deviation using a moving average window. Figures 3-8 and 3-9 show the results of this test for B_n = 2 Hz and B_n = 5 Hz, indicating that memory discriminators improve the quality of Doppler estimates by reducing the variance of the measurements.

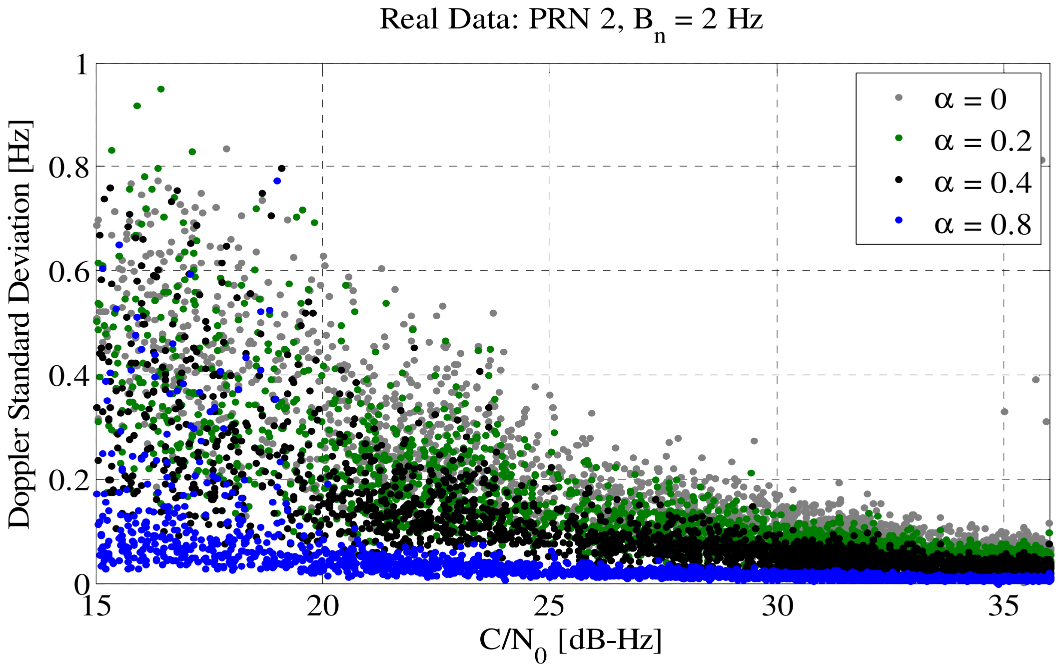

Figure 3-8. Standard deviation of the discriminator outputs as a function of the C/N_0 and the forgetting parameter, α. B_n = 2 Hz.

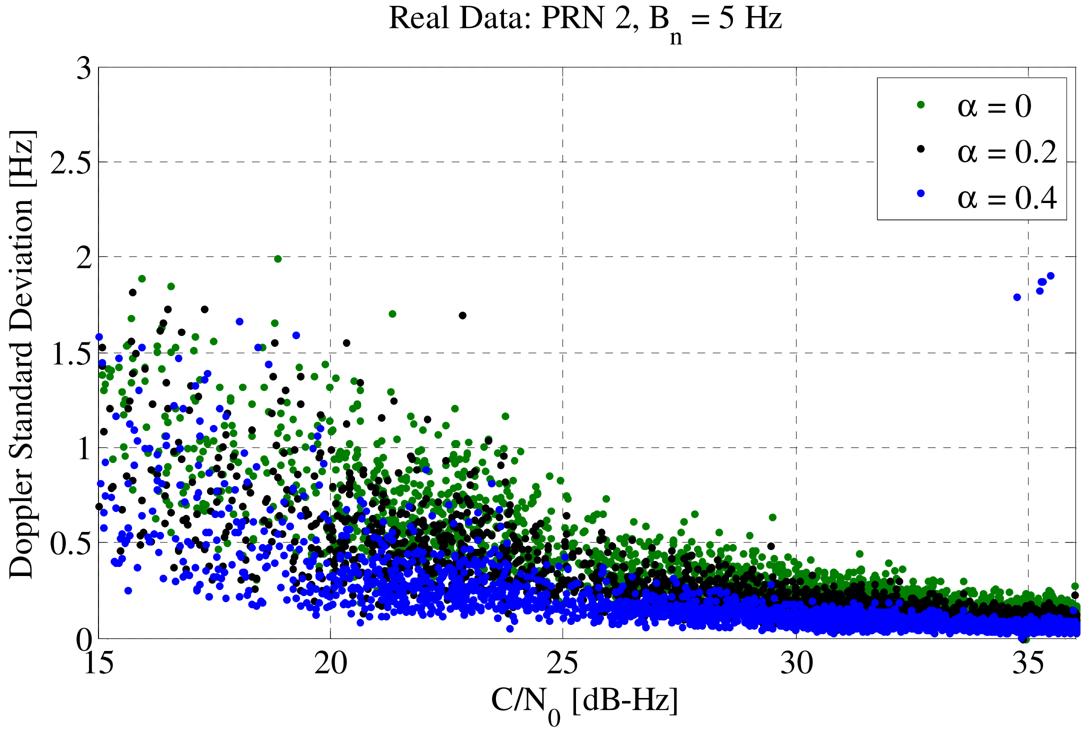

Figure 3-9. Standard deviation of the discriminator outputs as a function of the C/N_0 and the forgetting parameter, α. B_n = 5 Hz.

The impact of the forgetting factor was further analyzed in more challenging environments. The results of the next test shown here were obtained indoors, in a corridor where the GPS signals were blocked from two sides by heavy walls and strongly attenuated by silvered glass windows (about 20 dB attenuation) in the other directions.

This scenario was chosen for testing memory discriminators under realistic conditions where strong multipath and fading affect the already attenuated GPS signals.

For this test an 8 Hz bandwidth was selected for the processing. This bandwidth was chosen because it was considered large enough for effectively responding to the signal amplitude fluctuations caused by multipath reflections. But in this very harsh environment, with C/N_0 going down to 27 dB-Hz, the receiver was not able to determine bit synchronization and the integration time had to be reduced from 20 ms to 1 ms. For this reason the product B_nT_c was decreased, allowing higher values of α.

The correlator outputs obtained using the memory discriminator based architecture using different values of α are shown on Fig. 3-10. The signal amplitude fluctuates because of the strong fading in the indoor environment. Figure 3-10 illustrates as well the improvement provided by memory discriminators in a shorter time period for signal frequency and phase recovery in comparison to standard loops $(\alpha = 0)$. Sample Doppler measurements obtained using memory discriminators with forgetting factor $\alpha = 0$ (standard loops), $\alpha = 0.5$ and $\alpha = 0.8$ for the same satellite (PRN 16, 33 dB-Hz C/N_0) are shown in Figure 3-11.

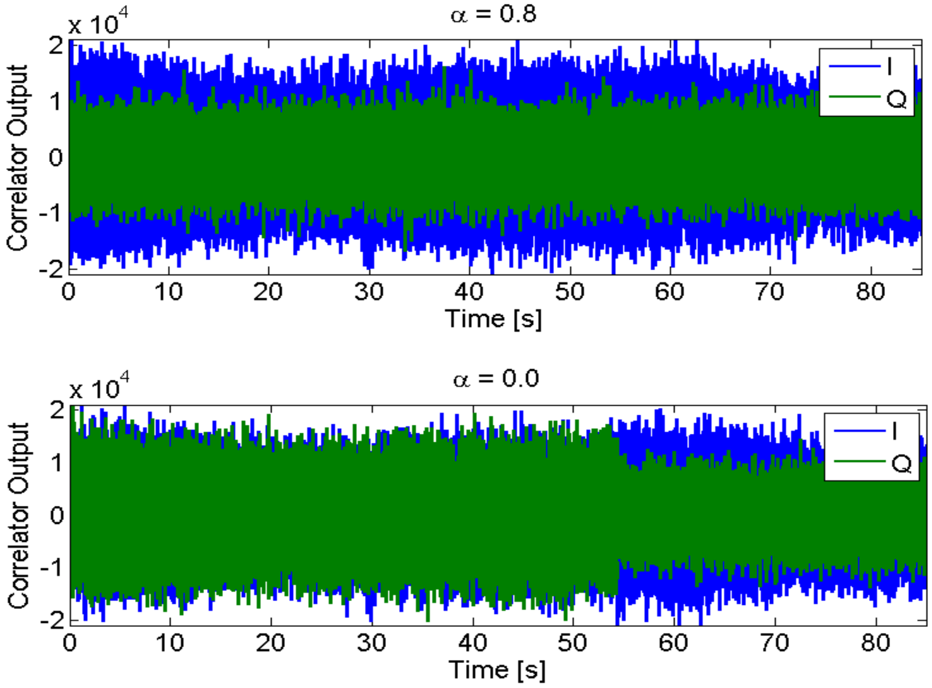

Figure 3-10: Correlator outputs obtained using standard and memory discriminators, 1 ms coherent integration.

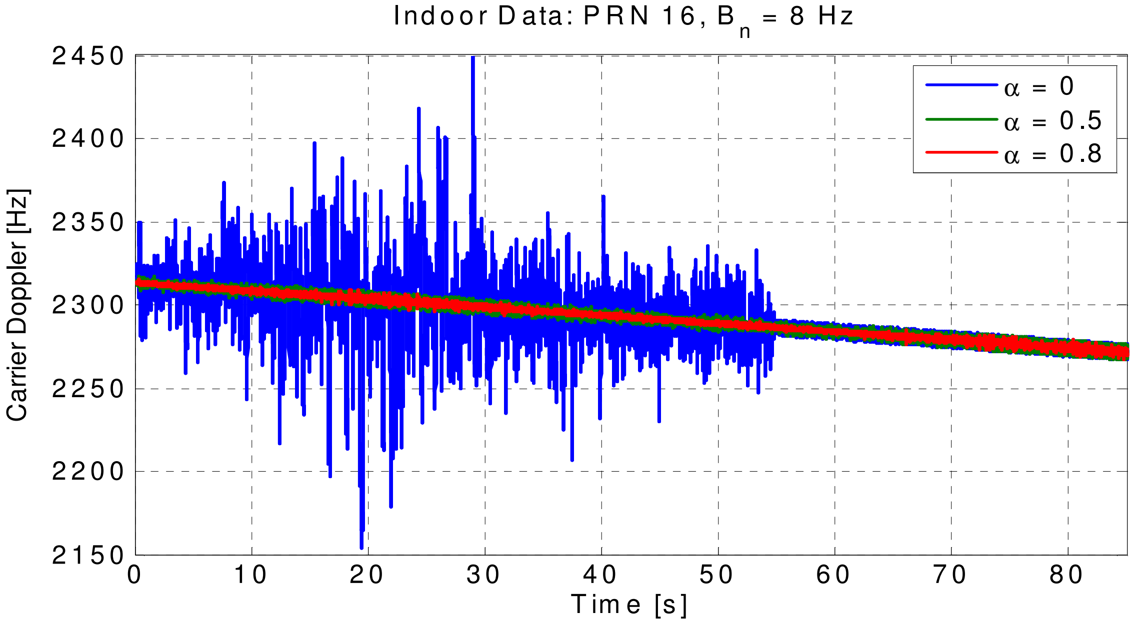

Figure 3-11. Carrier Doppler estimated using standard and memory discriminators for the indoor data.

As a conclusion for this test it can be stated that memory discriminator based tracking loop architecture provides a faster lock-in time and less noisy frequency estimation. In this particular case, the memory discriminator compensates as well for the short coherent integration time, providing better Doppler estimates.

Finally, a case with a weaker signal is considered where the signal received from PRN 1 was characterized by a nearly constant 27 dB-Hz C/N_0. The same initial parameters have been used both for the case with $\alpha = 0$ (standard loop) and higher values of the forgetting factor, α.

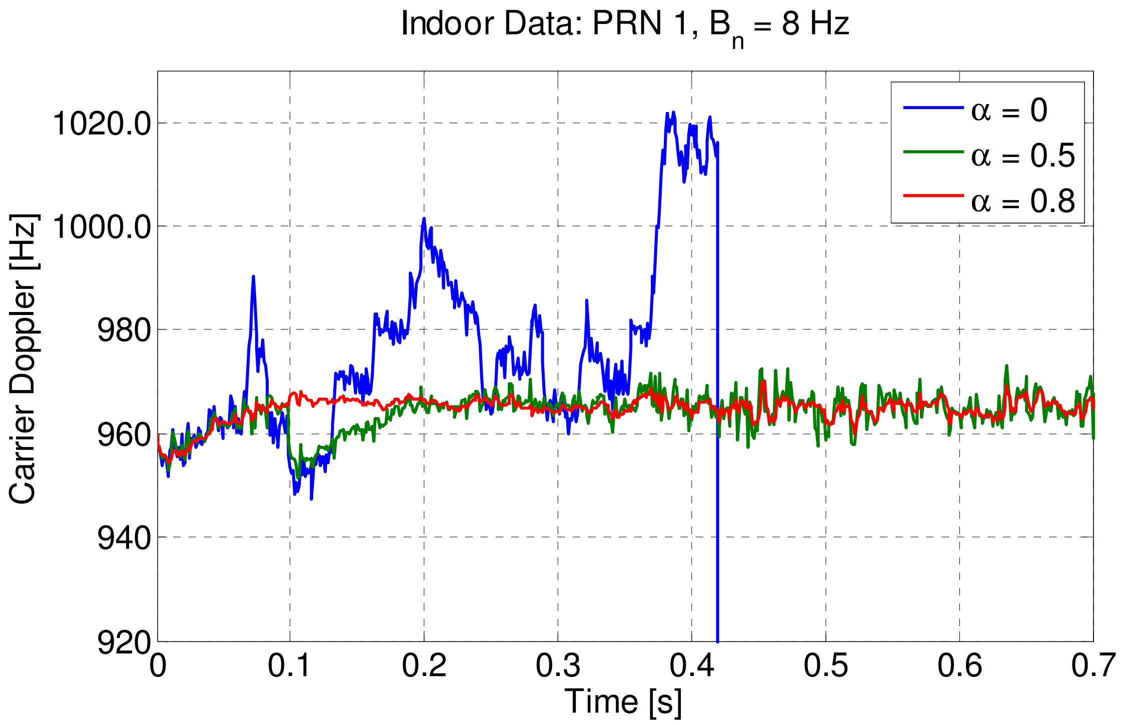

Figure 3-12. Carrier Doppler estimated using standard and memory discriminators for the indoor data, weak signal.

As it can be seen in Figure 3-12, the standard loop loses lock after a few seconds, while the memory discriminator is able to continue tracking the recovered signal. Test results shown here indicate the effectiveness of the memory discriminator based tracking loop architecture in degraded signal environments, making them a good alternative to coherent integration.

CHAPTER 4: THEORETICAL FRAMEWORK FOR DOPPLER MEASUREMENTS AND VELOCITY ESTIMATION

Because of the limitations of the previous work due to use of hardware receivers and the consequent lack of insight into the tracking loop parameters, it is desirable to develop a comprehensive theoretical model allowing the evaluation of the Doppler and velocity accuracy. This chapter introduces a theoretical framework developed in order to study the Doppler and velocity accuracy, relating the variance and biases of the Doppler estimates to C/N_0, the user dynamics and the PLL parameters, and translating them to the errors in the final velocity estimates. First, the relationship between raw Doppler and time-differenced carrier phase measurements is discussed and the equivalence between the two methods is shown. Then, the quality of Doppler measurements is theoretically evaluated by extending the PLL linear analysis and characterizing the noise propagation process from the input signal to the Doppler estimate. To quantify the amount of input noise transferred to the Doppler measurements, the concept of Doppler bandwidth is introduced and theoretical formulas for the Doppler variance and Doppler jitter are provided for the cases with both the raw and the carrier-phase derived Doppler. The same approach is then considered for use with memory discriminator based PLLs.

And finally, a concept of Dilution of Precision is used to model the error propagation from the Doppler frequency measurements to the velocity estimates.

4.1 Analysis of Doppler Estimation Process in Digital Tracking Loops

As it has been previously mentioned in **Chapter 2**, the Doppler frequency can be estimated in two different ways, either directly from the output of the loop filter, or by differentiating the carrier phase measurements. To be more specific, the loop filter output is a measure produced over a short interval of time, namely the coherent integration time, T_c, whereas carrier phase-derived Doppler is computed over a longer time period that can be several coherent integration periods long, leading to smoother observations. Denoting the raw Doppler measurements at the output of the loop filter as

$$f_{raw}[k], \tag{4.1}$$

and assuming that a new Doppler observation is produced at every loop update, the carrier phase observations can be obtained by integrating the raw Doppler measurements with the expression

$$\phi_{ob}[k] = f_{raw}[k] * i[k] \tag{4.2}$$

where $i[k]$ is the impulse response of a digital integrator. Although different types of integrators can be applied, the following model will be used in this thesis:

$$I(z) = ZT\{\, i[n] \,\} = \frac{T_c}{1 - z^{-1}}, \tag{4.3}$$

where $I(z)$ is the Z-transform of $i[n]$. In this way, the carrier phase observations can be described by the following equation:

$$\phi_{ob}[k] = \phi_{ob}[k-1] + f_{raw}[k]T_c. \tag{4.4}$$

Finally, by differentiating the carrier phase observations given by Eq.(4.4), the phase rate (carrier phase derived Doppler) measurements can be obtained. The differentiation is performed by using a digital filter with impulse response $\Delta[k]$:

$$f_{cp}[k] = \phi_{ob}[k] * \Delta[k] \tag{4.5}$$

The problem of differentiator design for the Doppler derivation from the carrier phase measurements has been frequently addressed and investigated (Hebert 1997, Bruton 2000, Zhang et al 2005) and a number of techniques has been proposed. The ones that apply to this particular research are described in detail in **Chapter 2**.

The theory presented in this chapter is general and can be applied to different filters, $\Delta[k]$. But, as it has been mentioned previously, the major focus of this work is on pedestrian /low dynamics applications. Therefore only the cases of the first order central difference approximation and the Savitsky-Golay filters will be considered further in this chapter.

4.1.1. PLL Linear Model: Doppler Filter

The same approach for the PLL analysis as described in **Chapter 3** can be applied here.

As it was noted in **Section 3.2**, the analysis of a traditional PLL is based on the approximation of the non-linear discriminator by a constant gain. In this particular case it has been assumed that the non-linear discriminator has a unit gain, where the discriminator gain is defined as

$$G_d = \left.\frac{\partial E[g(\phi)]}{\partial \phi}\right|_{\phi=0}, \tag{4.6}$$

where $g(\cdot)$ is the discriminator function and $E[\cdot]$ denotes ensemble average. This approximation leads to the PLL linear theory where the tracking loop is approximated by a linear filter, providing a linear equivalent model in the parameters domain, i.e., in the frequency and phase domain. The standard PLL linear model considered in **Chapter 3.2** is extended here to include the effect of the integrator and differentiator filters used for generating carrier phase derived Doppler measurements. The PLL linear model is illustrated in Fig. 4-1.

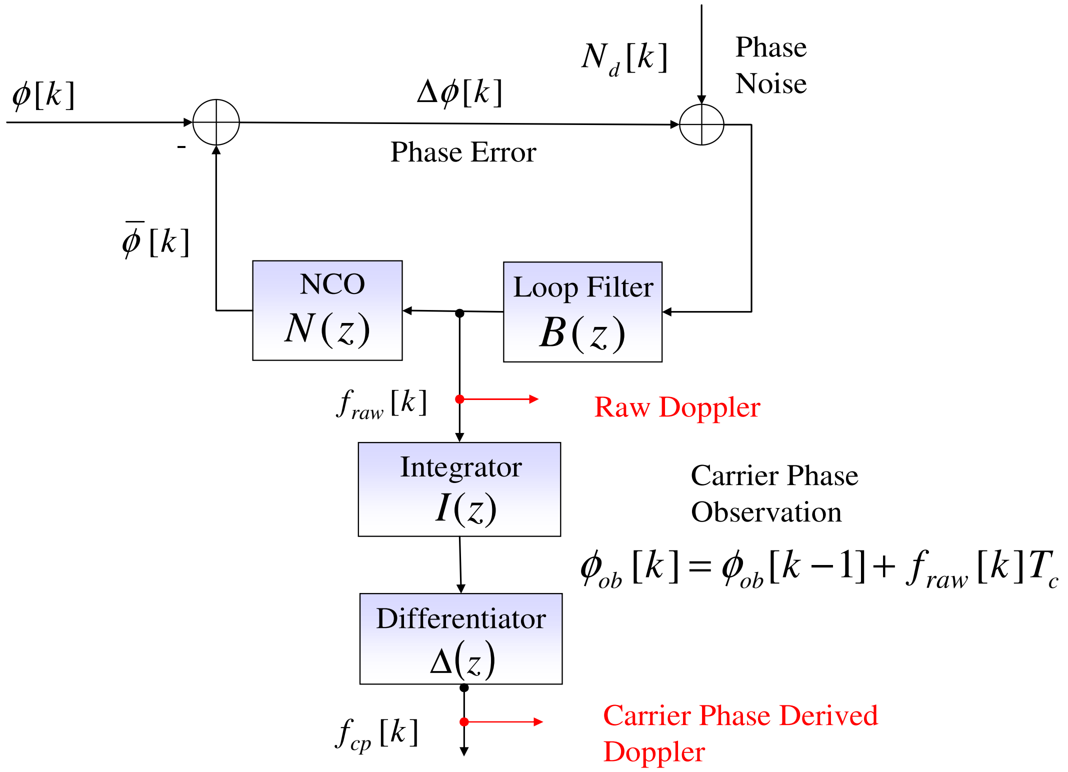

Figure 4-1: Equivalent linear model relating the carrier-phase-derived Doppler to the phase signal and noise at the input of a PLL (Borio et al 2009b).

As shown in Fig. 4-1, the phase error $\Delta\phi[k]$ is evaluated as the difference of the incoming and estimated phases:

$$\Delta\phi[k] = \phi[k] - \bar{\phi}[k] . \tag{4.7}$$

It should be considered that the effect of the noise present in the input signal is modeled by $N_d[k]$ which also accounts for the effect of the non-linear discriminator that amplifies the impact of the input noise. Denoting the loop filter impulse response as $b[k]$, raw Doppler measurements can be expressed as:

$$f_{raw}[k] = b[k] * (\Delta\phi[k] + N_d[k]) . \tag{4.8}$$

Finally, the raw Doppler is integrated by the NCO that produces a new phase estimate $\bar{\phi}[k]$.

4.1.2 Doppler Variance and Doppler Jitter Analysis

The use of the PLL linear model allows one to show that the phase error, $\Delta\phi[k]$, can be expressed as a linear combination of the filtered input signal and filtered noise:

$$\Delta\phi[k] = \left(\delta[k] - h_\phi[k]\right) * \phi[k] + h_n[k] * N_d[k], \tag{4.9}$$

where $h_\phi[k]$ and $h_n[k]$ are the signal and noise impulse responses, respectively. $N_d[k]$ is the noise term, caused by the thermal noise and the other errors at the input of the tracking loop and $\delta[\cdot]$ is the Kronecker delta. Transforming Eq.(4.9) into the Z-domain leads to the following expression:

$$\Delta\phi(z) = \left(1 - H_\phi(z)\right)\phi(z) + H_n(z)N_d(z), \tag{4.10}$$

where $H_{\phi}(z)$ and $H_n(z)$ are the signal and noise transfer functions. Assuming that the signal term $\left(\delta[k]-h_{\phi}[k]\right) * \phi[k]$ in Eq. (4.9) introduces only a deterministic bias in $\phi(z)$, according to Borio et al (2009b), the variance of $\phi(z)$ is given as

$$\begin{aligned} Var\{\phi[k]\} &= \int_{-0.5}^{0.5} \left|H_n(e^{j2\pi f})\right|^2 df\, Var\{N_d[k]\} \\ &= T_c \int_{-0.5/T_c}^{0.5/T_c} \left|H_n(e^{j2\pi f T_c})\right|^2 df\, Var\{N_d[k]\} \end{aligned} \tag{4.11}$$

where $N_d[k]$ has been assumed to be a white sequence. In Eq. (4.11) the term

$$B_n = \frac{1}{2}\int_{-0.5/T_c}^{0.5/T_c} \left|H_n(e^{j2\pi f T_c})\right|^2 df \tag{4.12}$$

quantifies the amount of noise transferred from the input equivalent noise to the tracking error, $\Delta\phi$, and defines the loop filter bandwidth. As introduced in Ward et al (2005), the variance of $N_d[k]$ is approximately given by

$$Var\{N_d[k]\} = \sigma_n^2 = \frac{1}{2T_c C/N_0}\left(1+\frac{1}{2T_c C/N_0}\right) \quad [rad^2], \tag{4.13}$$

and by using Eq.s. (4.11), (4.12) and (4.13) it is possible to obtain the standard formula for the phase tracking jitter. The PLL linear theory can be extended for quantifying the amount of noise that is transferred from the input signal to the final frequency estimate (Borio et al 2009b).

Similar to the description given above, the PLL can be approximated by a linear device that forms frequency estimates as linear combination of the filtered version of the true

Doppler frequency $f_d[k]$ and filtered noise $N_d[k]$. This relation is illustrated in Fig. 4-2, representing the PLL as a frequency filter.

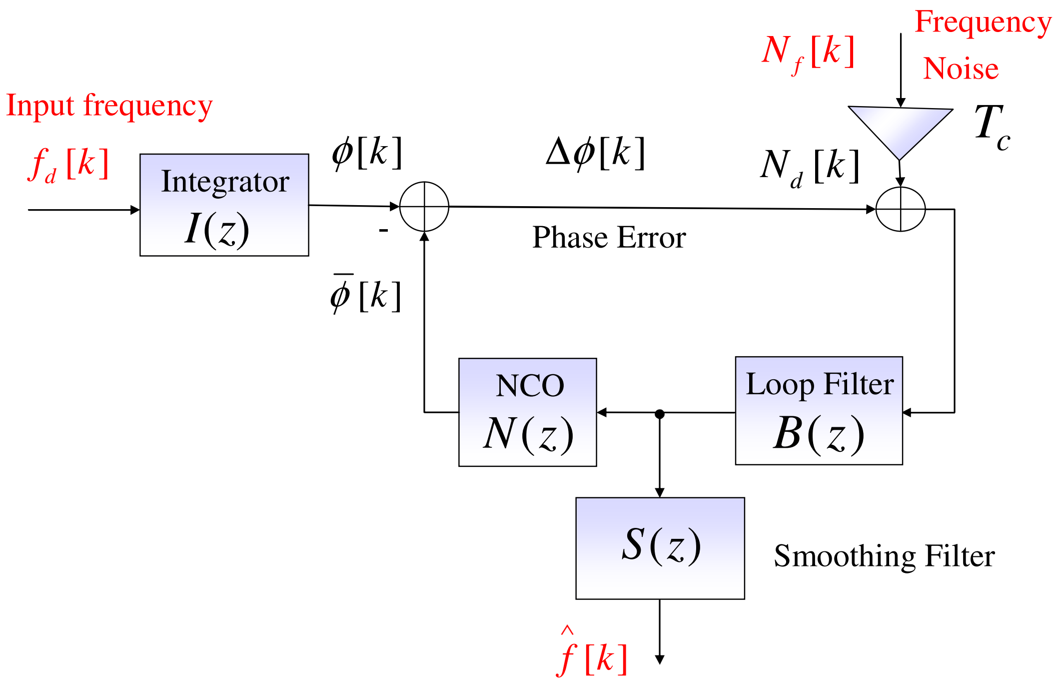

Figure 4-2: PLL as a frequency filter (Borio et al 2009b).

In this case, as shown in Fig. 4-2, the input driving frequency $f_d[k]$ has been added to the model and the phase, $\phi[k]$, is obtained by integrating $f_d[k]$. As suggested in Borio et al (2009b), the integrator modeling the relation between the frequency and the phase is characterized by the same transfer function of the NCO since both local and incoming signals are processed in the same way through the Integrate and Dump (I&D) component of the PLL.

By normalizing $N_d[k]$ by the coherent integration time T_c, a frequency noise term $N_f[k]$ is introduced as

$$N_f[k] = \frac{1}{T_c} N_d[k]. \tag{4.14}$$

The normalization needs to be performed in order to get all quantities at the inputs and the output of the PLL model in the same units of radians per second. An additional functional bock representing a smoothing filter with transfer function $S(z)$ has been added as well to incorporate both the raw and the carrier phase derived Doppler measurements. In the case with the raw Doppler measurements

$$S(z) = 1, \tag{4.15}$$

while for the case with the carrier phase derived Doppler measurements the following relationship applies:

$$S(z) = I(z)\Delta(z), \tag{4.16}$$

where $S(z)$ acts as a low pass smoothing filter. The expression for the impulse response of a first order differentiator is given in **Chapter 2**, Eq. (2.13), can also be written in the following form:

$$\Delta[k] = \frac{\delta[k+H] - \delta[k-H]}{2HT_c}, \tag{4.17}$$

where HT_c is the interval between consecutive carrier phase measurements. Because of the fact that a GNSS receiver outputs carrier phase observations at a rate that is lower than the loop update rate, the signal given by Eq.(4.4) can be considered down-sampled by a factor H.

The transfer function of this differentiator is given by

$$\Delta(z) = z^{-H} \frac{z^{H} - z^{-H}}{2HT_c}, \tag{4.18}$$

where an additional delay term z^{H} is included to account for the latency introduced by the receiver for computing the difference in Eq. (4.18). In this case the smoothing filter $S(z)$ can be expressed as follows:

$$S(z) = \frac{T_c}{1 - z^{-1}} \frac{1 - z^{-2H}}{2HT_c} = \frac{1}{2H} \sum_{i=0}^{2H-1} z^{-i}. \tag{4.19}$$

It is important to consider that Eq. (4.19) represents the transfer function of a simple moving average (MA) filter with the analysis window length equal to $2H$. This indicates that by filtering the raw Doppler measurements equivalence with the carrier phase derived Doppler measurements can be achieved. This fact is illustrated in Fig. 4-3, where the standard deviation of the raw Doppler measurements is plotted as a function of C/N_0 and is compared to the standard deviation of the Doppler obtained from the carrier phase measurements using a Savitsky-Golay filter and raw Doppler measurements filtered by a MA filter. For this particular case the same length of the analysis window (10 ms) was used in both the Savitsky-Golay and MA filters.

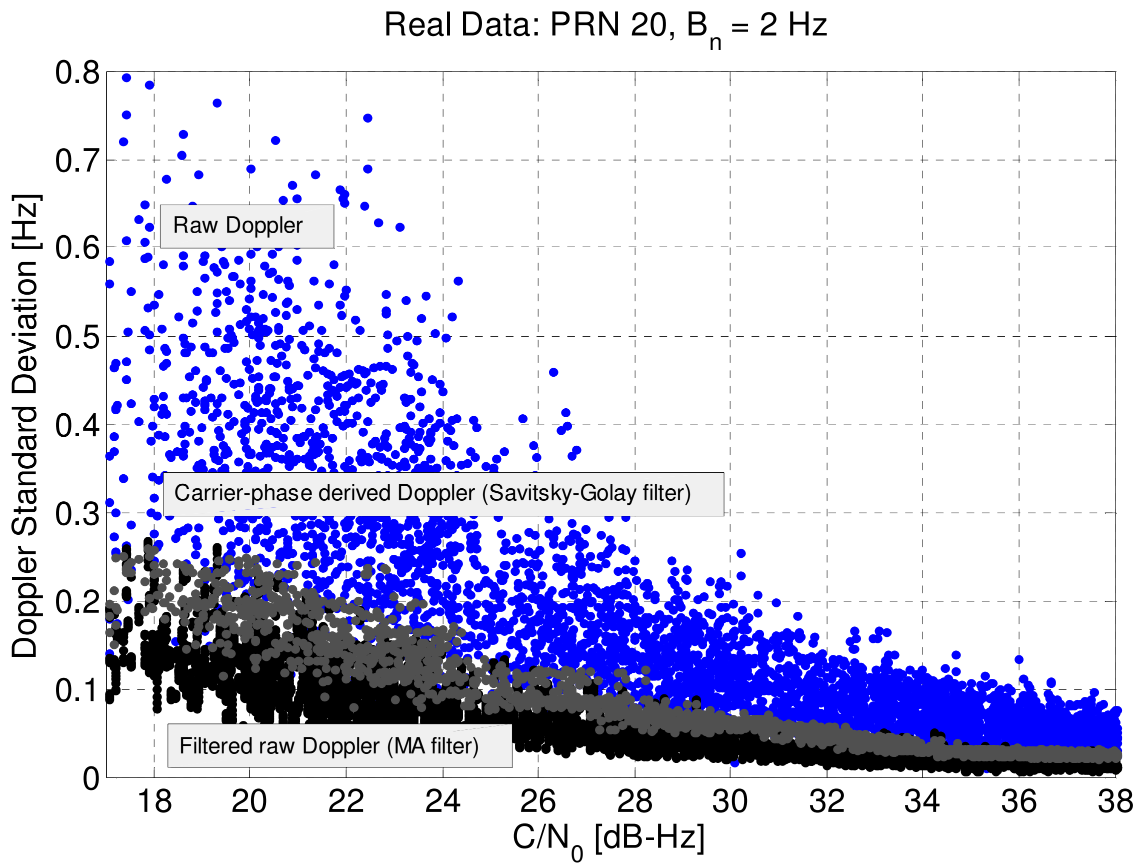

Figure 4-3: Standard deviation of the raw Doppler measurements compared to filtered raw Doppler measurements using a MA filter and carrier phase derived Doppler measurements obtained using a Savitsky-Golay filter.

Considering the model introduced above and illustrated in Fig.4-2, it is possible to show that the final frequency estimate is obtained as

$$\hat{f}[k] = h_f[k] * f_d[k] + h_{nf}[k] * N_f[k], \tag{4.20}$$

where $h_f[k]$ and $h_{nf}[k]$ are the frequency and frequency noise impulse responses. As introduced in Borio et al (2009b), the transfer functions associated with $h_f[k]$ and $h_{nf}[k]$ are given by

$$H_f(z) = \frac{S(z)B(z)N(z)}{1+B(z)N(z)}, \tag{4.21}$$

$$H_{nf}(z) = \frac{T_c S(z)B(z)}{1+B(z)N(z)}, \tag{4.22}$$

where $N(z)$ and $B(z)$ are the NCO and loop filter transfer functions. It is noted that expressions given by Eqs. (4.21) and (4.22) are general and no assumption on the loop filter and the NCO model is made. In this case, the model described in **Chapter 3.2**, for a rate-only feedback NCO (Stephens & Thomas 1995) is used. The transfer function of this type of NCO is given as

$$N(z) = \frac{T_c}{2}\frac{z^{-1}(1+z^{-1})}{(1-z^{-1})}. \tag{4.23}$$

For the loop filters, the following integrator-based model is considered:

$$B(z) = \frac{1}{T_c}\sum_{i=0}^{L-1} K_i \frac{1}{(1-z^{-1})^i} = \frac{1}{T_c}\sum_{i=0}^{L-1} K_i \left[\frac{z}{z-1}\right]^i, \tag{4.24}$$

where L is the order of the loop and $\{K_i\}_{i=0}^{L-1}$ are the filter integrator gains. Since the frequency noise, $N_f[k]$, is a normalized version of the input phase noise, Eq.(4.14), $N_f[k]$ is a white sequence with variance

$$\begin{aligned} Var\{N_f[k]\} &= \frac{1}{T_c^2}\sigma_n^2 \\ &= \frac{1}{T_c^2}\frac{1}{2T_cC/N_0}\left(1+\frac{1}{2T_cC/N_0}\right) \quad \left[\left(\frac{rad}{s}\right)^2\right]. \end{aligned} \tag{4.25}$$

Following the same approach as in the case for the phase variance, it is assumed that the term $h_f[k] * f_d[k]$ from Eq. (4.20) does not contribute to the variance of the final frequency estimates. Considering this fact the following relation is found:

$$Var\left\{\hat{f}[k]\right\} = T_c \int_{-0.5/T_c}^{0.5/T_c} \left|H_{nf}\left(e^{j2\pi f T_c}\right)\right|^2 df \, Var\left\{N_f[k]\right\}. \tag{4.26}$$

Moreover, as a counterpart of the loop bandwidth given in Eq.(4.12), the concept of **Doppler bandwidth** can then be introduced for frequency estimation:

$$B_d = \frac{1}{2} \int_{-0.5/T_c}^{0.5/T_c} \left|H_{nf}\left(e^{j2\pi f T_c}\right)\right|^2 df \, . \tag{4.27}$$

The Doppler bandwidth, B_d, summarizes in a single parameter the ability of the tracking loop to produce smooth frequency estimates. This fact makes it an effective metric for comparing different receivers. Finally, using Eqs. (4.26) and (4.27), the variance of the frequency estimate, $\hat{f}[k]$, can be found as

$$\begin{aligned} Var\left\{\hat{f}[k]\right\} &= 2T_c B_d Var\left\{N_f[k]\right\} \\ &= \frac{B_d}{T_c^2 C/N_0}\left(1+\frac{1}{2T_c C/N_0}\right) \qquad \left[\left(\frac{rad}{s}\right)^2\right]. \end{aligned} \tag{4.28}$$

The Doppler jitter can be defined as

$$\sigma_f = \frac{1}{T_c}\sqrt{\frac{B_d}{C/N_0} S_L} \quad = \quad \frac{1}{T_c}\sqrt{\frac{B_d}{C/N_0}\left(1+\frac{1}{2T_c C/N_0}\right)} \qquad \left[\frac{rad}{s}\right], \tag{4.29}$$

where S_L represents the squaring loss (Lindsey & Chie 1981).

All Doppler measurements are obtained by processing PLL outputs and therefore parameters of the loop strongly impact their quality. Expressions for the frequency estimate variance and the Doppler jitter introduced above can be effectively used for assessment of the Doppler measurements quality as a function of the input C/N$_0$, the coherent integration time and the Doppler bandwidth, B_d.

4.1.3 Doppler Bias Analysis

In a similar way to the variance analysis derivation, biases introduced by the loop can be determined starting from the frequency transfer function, $H_f(z)$. Biases in the Doppler estimates are induced by the transient response of the loop to changes in the input frequency as well as to latencies introduced by the smoothing filter, $S(z)$. The ability of the loop to recover from the changes in the input Doppler without steady-state errors depends on its order. Systematic errors in the Doppler measurements can be defined as

$$\varepsilon_f = E\left[f_d[k] - \hat{f}[k] \right]. \tag{4.30}$$

Using the relationship from Eq.(4.20), and considering the fact that $N_f[k]$ is zero mean, the Doppler systematic error, Eq.(4.30) can be formed as:

$$\begin{aligned}\varepsilon_f[k] &= f_d[k] - h_f[k] * f_d[k] = \left(\delta[k] - h_f[k]\right) * f_d[k] \\ &= h_\varepsilon[k] * f_d[k]\end{aligned}, \tag{4.31}$$

where

$$h_{\varepsilon}[k] = \delta[k] - h_f[k] \tag{4.32}$$

is the bias impulse response. Using the model given by Eq.(4.31), analysis of the bias introduced by the loop due to the variations in the input Doppler can be performed. However, one should note that for this type of analysis a reference for Doppler measurements is required.

4.2 Doppler estimation analysis in the case of memory discriminator based tracking loops

The same approach as introduced in the previous section can be applied for the analysis of the memory discriminator based PLL. The linear model for a PLL with memory discriminator is illustrated in Fig. 3-2 in **Chapter 3** and is used here for Doppler analysis. While in traditional tracking loops, the discriminator is approximated by a constant gain, in the case of memory discriminators, the additional memory introduced by this type of algorithms has to be accounted for. More specifically, the discriminator is approximated by a filter with transfer function $F(z)$. The transfer function associated with the frequency noise impulse response, $h_{nf}[k]$, introduced in Eq.(4.20) can then be written as

$$H_{nf}(z) = \frac{T_c S(z) F(z) B(z)}{1 + F(z) B(z) N(z)}. \tag{4.33}$$

In the case of exponential discriminator, the following expression for the transfer function is applied:

$$F(z) = (1-\alpha)\sum_{i=0}^{+\infty} \alpha^i \cdot z^{-i} = (1-\alpha)\frac{1}{1-\alpha z^{-1}} . \tag{4.34}$$

And the same models for the NCO and the loop filter as given in Eqs. (4.23) and (4.24) are considered. Having the expression for the transfer function of the frequency noise given by Eq.(4.33), the Doppler bandwidth and the Doppler jitter given by Eq.s. (4.27) and (4.29) can be analysed.

4.3 Variance Propagation: From Doppler to Velocity

The model for the Doppler jitter introduced above can be further used for the analysis of the variance of the estimated user velocity. The process of the velocity estimation is given in **Chapter 2**, where the final relation between the Doppler measurements and the estimates of the user velocity was given as:

$$\dot{\phi}' = \mathbf{A}\begin{bmatrix} \mathbf{v}^T & d\dot{T} \end{bmatrix} + \varepsilon_{\dot{\phi}} , \tag{4.35}$$

where $\dot{\phi}'^{(k)}$ represents $(\dot{\phi}^{(k)} - \mathbf{v}^{(k)} \cdot \mathbf{h}^{(k)})$, $\mathbf{v}$ is the user velocity estimate, $d\dot{T}$ is the receiver clock drift and $\varepsilon_{\dot{\phi}}$ the combined error due to changes during the measurement interval in the satellite clock, ionosphere and troposphere. And matrix $\mathbf{A}$ is the same as defined in Eq. (2.27), reflecting the receiver-satellite geometry and consisting of unit vectors between the receiver and satellites $\mathbf{h}^{(k)}$. A single unit vector is given by

$$\mathbf{h}^{(k)} = \frac{\mathbf{u}^{(k)} - \mathbf{u}}{\left\| \mathbf{u}^{(k)} - \mathbf{u} \right\|} , \tag{4.36}$$

where $\mathbf{u}^{(k)}$ and $\mathbf{u}$ are the position of the k^{th} satellite and user, respectively. Aside from the variance of the frequency estimates that can be quantified using the approach developed above, additional errors such as uncertainty in the user position and the correct knowledge of the satellite ephemeris and satellite velocity contribute to the final velocity. However, only the case of propagation of the frequency estimate variance will be considered further. The effect of the errors in the satellite ephemeris is beyond the scope of this discussion. User position errors will be assumed to be small and slowly varying relative to the loop update period, and therefore their contribution will not be considered.

When estimating the user position, the concept of Dilution of Precision (DOP) is often employed to study the effect of geometry on the error propagation process. DOPs are commonly treated as multipliers that convert range error into various forms of positional error through simple multiplication.

The same approach can be applied to the process of velocity estimation. Since the description of DOP is found in numerous references (e.g., Lachapelle 2008), only a brief sketch is needed. Doppler frequency observations are generally solved for velocity using Weighted Least Squares (WLS) approach:

$$\left(\mathbf{A}^T\mathbf{C}_l^{-1}\mathbf{A}\right)\left[\mathbf{v}^T \quad d\dot{T}\right] = \mathbf{A}^T\mathbf{C}_l^{-1}\dot{\phi}' \tag{4.37}$$

with k observations and four unknown parameters, where matrix $\mathbf{A}$, vector $\mathbf{v}$, and parameters $d\dot{T}$ and $\dot{\phi}'$ are as defined for Eq.(4.35), while the matrix $\mathbf{C}_l$ is the covariance matrix of the observations. Following the derivations and assumptions in (Lachapelle 2008), and using the relationship

$$\mathbf{C}_l = \sigma^2_{\hat{f}} \, \mathbf{I}, \tag{4.38}$$

where $\sigma^2_{\hat{f}}$ is the mean variance of the Doppler frequency estimate, the variance-covariance matrix of the unknowns is given by

$$\mathbf{C}_{\hat{x}} = \left(\mathbf{A}^T \mathbf{C}_l^{-1} \mathbf{A}\right)^{-1} = \begin{bmatrix} \sigma_x^2 & \sigma_{xy}^2 & \sigma_{xz}^2 & \sigma_{xt}^2 \\ \sigma_{xy}^2 & \sigma_y^2 & \sigma_{yz}^2 & \sigma_{yt}^2 \\ \sigma_{xz}^2 & \sigma_{yz}^2 & \sigma_z^2 & \sigma_{zt}^2 \\ \sigma_{xt}^2 & \sigma_{yt}^2 & \sigma_{zt}^2 & \sigma_t^2 \end{bmatrix}, \tag{4.39}$$

and describes random error propagation of noise in Doppler frequency measurements into the noise of the unknown parameters. Following the derivations and assumptions in (Lachapelle 2008), the DOPs are then derived as traces of various sub-matrices of $\mathbf{C}_{\hat{x}}$.

Thus,

Geometric DOP GDOP $= \sqrt{\left(\sigma_x^2 + \sigma_y^2 + \sigma_z^2 + \sigma_t^2\right)}$,

Horizontal DOP HDOP $= \sqrt{\left(\sigma_x^2 + \sigma_y^2\right)}$,

Vertical DOP VDOP $= \sigma_z^2$. (4.40)

Using the DOP to model the relationship between the statistics of the estimated Doppler frequency and the statistics of the velocity estimates in combination with the developed model for the analysis of the Doppler frequency variance and bias provides a complete framework that can be employed to perform cohesive analysis of the noise propagation through the entire velocity estimation process from the PLL input to the final velocity estimate.

CHAPTER 5: EXPERIMENTAL ANALYSIS: STATIC MODE

In order to evaluate the theoretical model developed in **Chapter 4**, a number of simulations and tests in various GPS operating environments have been conducted.

This chapter introduces the test methodology and equipment setup for the tests performed in static mode.

First, the Doppler jitter analysis is discussed detailing the procedure for the determination of the empirical Doppler jitter values. Then the results obtained comparing empirical and theoretical Doppler jitter in various GPS operating environments are analyzed and discussed. Different tracking loop parameters and methods for the Doppler derivation are used for the analysis.

In order to perform characterization and comparison of different hardware receivers, Doppler bandwidth and approximate coherent integration time can be estimated using the theoretical model proposed in **Chapter 4.** This approach is described and test results analysis is shown in the second part of this chapter.

5.1 Doppler Jitter Analysis

As it has been shown in **Chapter 4**, the Doppler jitter is a measure of the variability or dispersion around the mean of the Doppler measurements (see Eq. (4.29)). For this reason, no reference solution for the Doppler frequency is required for the analysis of this parameter. The following section concentrates on the tests performed in order to evaluate the developed model for the Doppler jitter, detailing the test setup and methodology for data evaluation.

5.1.1 Attenuated LOS Data

In the first experiment, data sets were collected in an open sky environment with a few nearby multipath sources. The received signal power was gradually decreased by means of a variable attenuator inserted prior to the front-end, which, in this case, was a National Instruments (NI) *NI PXI-5661* system, outputting real samples at a sampling frequency, f_s = 10 MHz. Figure 5-1 provides a detailed view of the adopted experimental setup.

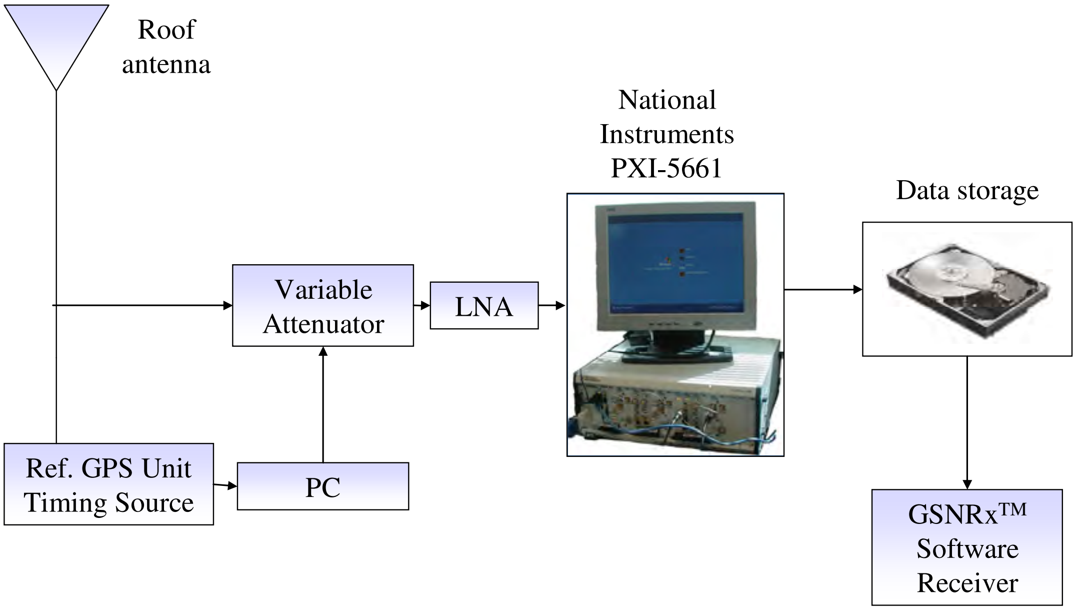

Figure 5-1: Experimental setup used to collect attenuated LOS GPS data.

After a minute without attenuation the signal was progressively attenuated with a step of 1 dB each 30 s. The collected data was stored in an external hard drive and processed in post mission using two versions of the University of Calgary's GNSS Software Navigation Receiver (GSNRx^{TM}), namely standard version (Petovello et al 2008) and a memory discriminator based architecture described in detail in **Chapter 3**.

The data set was processed several times using different values of the loop bandwidth and coherent integration time in order to analyze the impact of these parameters on the quality of the Doppler estimates. The procedure adopted for the estimation of Doppler jitter from the empirical data is illustrated in Fig. 5-2.

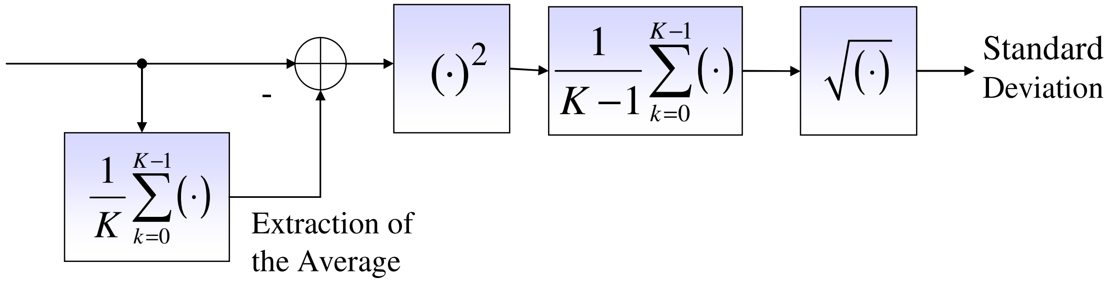

Figure 5-2: Doppler tracking jitter estimation procedure.

Following this procedure, the mean of the Doppler estimates provided by the GSNRx^{TM} receiver was obtained by implementing a moving average (MA) filter. The mean was then subtracted from the measurements which were further squared and filtered giving the final estimate of the empirical Doppler jitter (Borio et al 2009b):

$$\hat{\sigma}_f[n] = \sqrt{\frac{1}{K-1}\left[\sum_{k=0}^{K-1}\hat{f}[k-n] - \frac{1}{K}\sum_{j=0}^{K-1}\hat{f}[j-n]\right]^2} \; . \tag{5.1}$$

The use of a moving analysis window for the determination of the empirical Doppler jitter provides estimates as a function of time. As GSNRx^{TM} provides C/N$_0$ estimates as a function of time, it was possible to associate a C/N$_0$ value to each empirical Doppler tracking jitter estimate obtained using Eq.(5.1). In this way, it was possible to determine the empirical Doppler jitter as a function of the input C/N_0. Figure 5-3 shows the Doppler jitter obtained using a fixed coherent integration time of 20 ms, but different loop bandwidth values in the case of raw Doppler measurements. Empirical data are compared to the theoretical Doppler jitter Eq. (4.29) showing a good agreement between theoretical and empirical results.

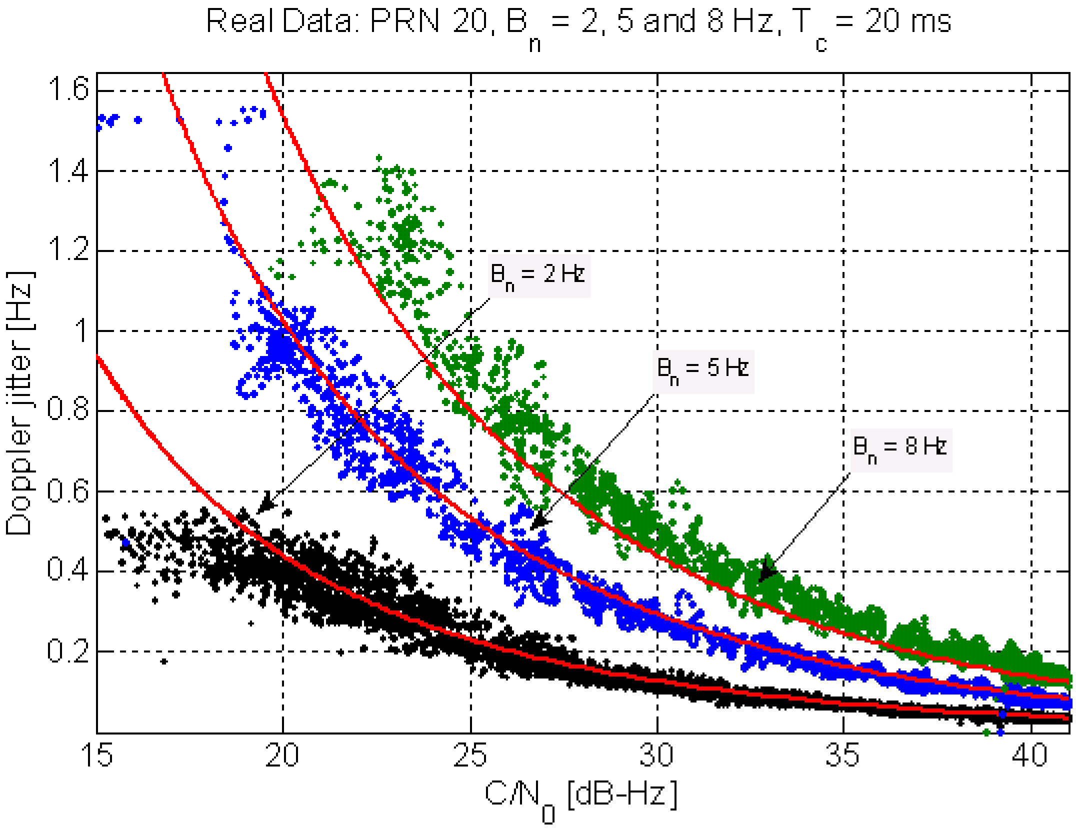

Figure 5-3: Empirical and theoretical Doppler jitter of the raw Doppler measurements as a function of C/N_0 and loop bandwidth.

Figure 5-3 also illustrates the fact that narrow bandwidths shield the tracking loop from excessive noise power, and give better Doppler estimates with lower variance in the measurements. In this context, it is important to consider that the relationship between loop and Doppler bandwidth is not simple, and these two parameters usually differ. Table 5-1 compares the values of the loop and Doppler bandwidths for the cases considered in Fig. 5-3 highlighting the difference between the two parameters.

Table 5-1: Loop and Doppler bandwidth for raw Doppler estimation; T_c = 20 ms.

Parameter	Value		
Loop bandwidth B_n [Hz]	2.00	5.00	8.00
Doppler bandwidth B_d [Hz]	0.25	1.34	2.99

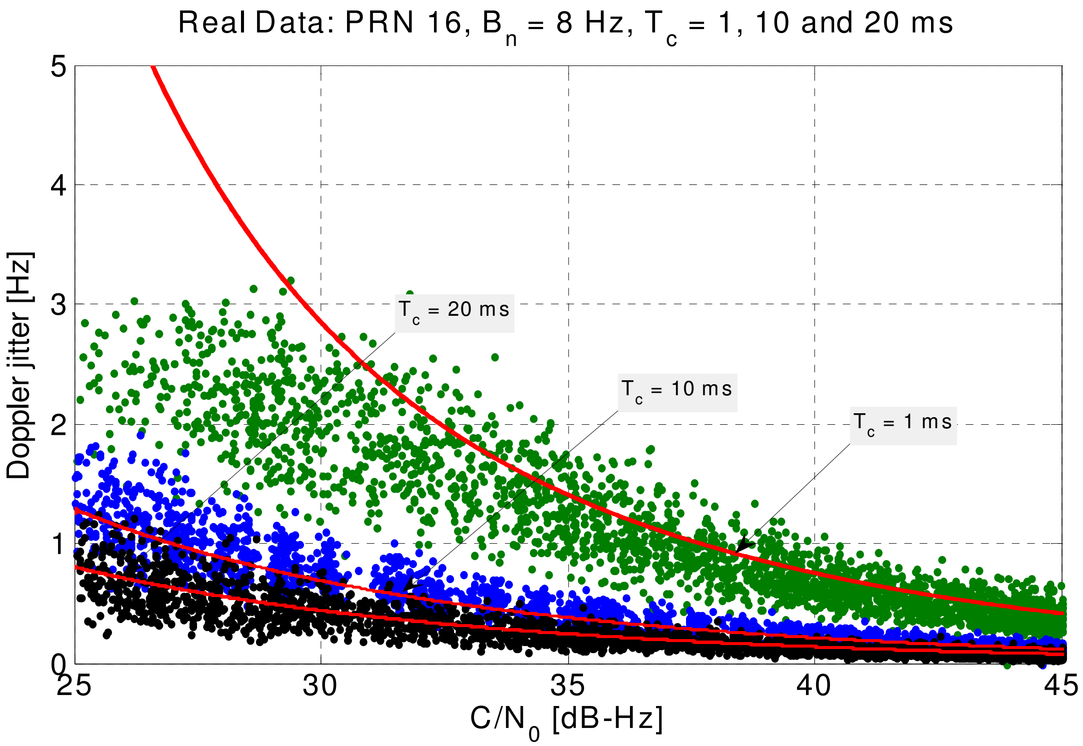

Figure 5-4: Empirical and theoretical Doppler jitter of the raw Doppler measurements as a function of C/N$_0$ and coherent integration time.

The impact of the coherent integration time is illustrated in Fig.5-4 which shows the empirical Doppler jitter as a function of signal attenuation for different coherent integration times. These results show the dependence between Doppler jitter and coherent integration time. The longest coherent integration time used in this test (20 ms) gave the best quality of the Doppler estimates compared to the results obtained using 10 ms and 1 ms periods. This is due to the fact that the longest coherent integration time results in the highest reduction of the noise power, and because of this, the amount of noise transferred to the Doppler estimates is the lowest. Again a good agreement between theoretical and empirical results is found, supporting the validity of the developed theoretical model.

It is important to consider that the Doppler bandwidth is increasing with the extension of the coherent integration time (Table 5-2). However, as it can be seen in Fig.5-4 that the benefit in terms of noise reduction is higher than the increase in Doppler bandwidth. Thus, the total Doppler jitter is reduced. The reason why the Doppler bandwidth increases with the coherent integration time requires further investigation, but is more likely related to the way the tracking loop is designed by fixing the loop bandwidth, B_n.

Table 5-2: Doppler bandwidth and coherent integration time, T_c, for raw Doppler estimation; B_n = 8Hz.

Parameter	Value		
T_c [ms]	1	10	20
B_d [Hz]	0.21	1.79	2.99

The same analysis has been repeated with carrier phase derived Doppler measurements considering the effect of the smoothing filter, $S(z)$. This effect can be observed by comparing the results of Fig. 5-5 with those of Fig. 5-3. Figure 5-5 shows the case of Doppler measurements derived using a Savitsky-Golay filter over an analysis window of

200 ms total duration. The coherent integration time used was 20 ms and three different values of the loop bandwidth B_n = 2, 5 and 8 Hz were considered.

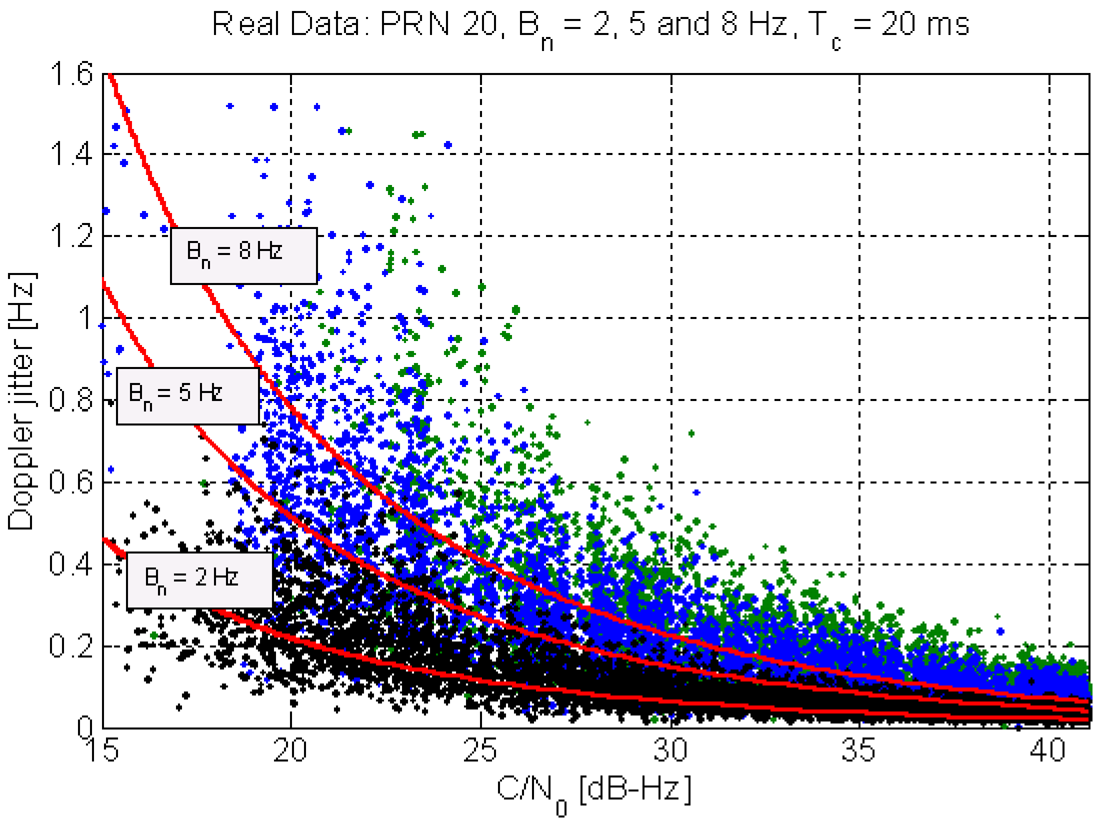

Figure 5-5: Empirical and theoretical Doppler jitter of the carrier phase derived Doppler measurements using a Savitsky-Golay filter as a function of C/N$_0$ and loop bandwidth.

It can be again concluded that a good match between theoretical and empirical results is observed showing the ability of the proposed theoretical model to predict the quality of carrier phase derived Doppler measurements as well.

As described in **Chapter 4** the same approach can be applied for the analysis of memory discriminator based PLLs. Figure 5-6 illustrates the theoretical Doppler tracking jitter estimated using different values of the forgetting factor, α, compared to empirical results. The coherent integration time in this case was 20 ms and the loop bandwidth 2 Hz allowing to use α up to 0.8. It should be noted that $\alpha = 0$ represents the case of a standard tracking loop.

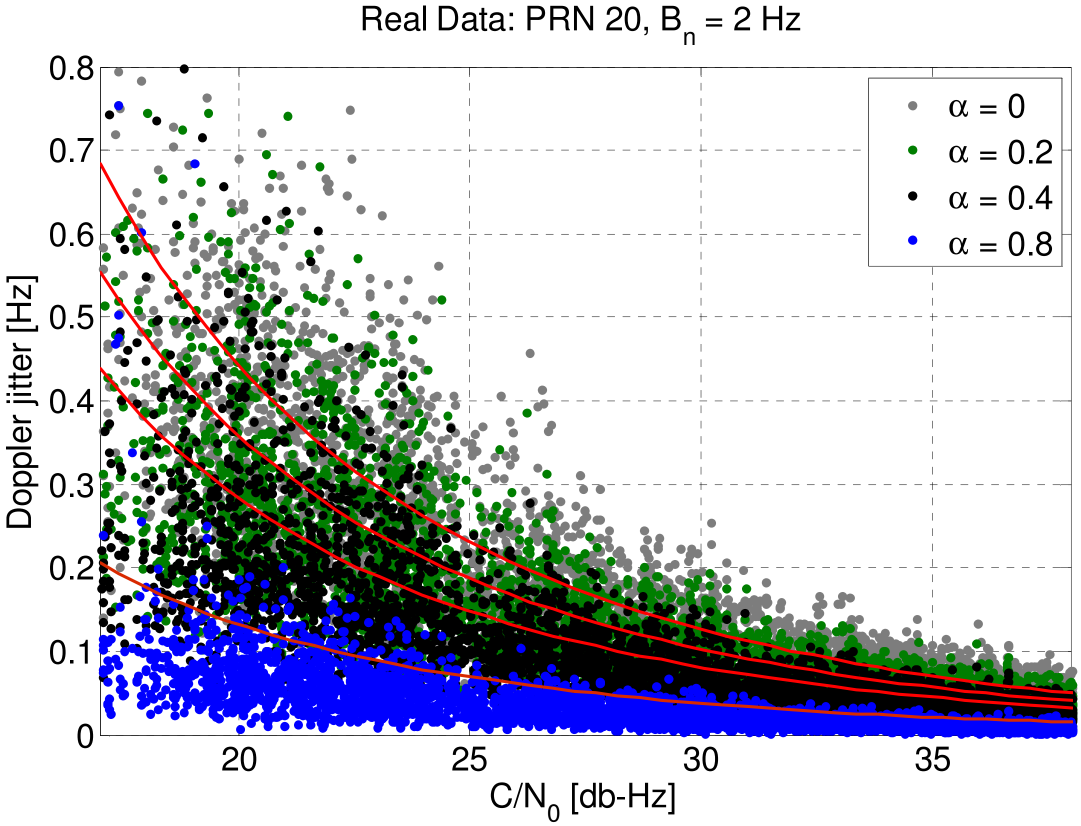

Figure 5-6: Empirical and theoretical Doppler jitter of raw Doppler measurements as a function of C/N$_0$ and forgetting factor, α, obtained using a memory discriminator based tracking loop architecture.

As Fig. 5-6 is showing, memory discriminators improve the quality of Doppler estimates by reducing the variance of the measurements. Using the extended theoretical model including the effect of memory discriminators allows one to effectively predict the quality of Doppler measurements obtained from memory discriminator based tracking loops.

5.1.2 Degraded Environment Tests

Further analysis of the Doppler jitter was performed by studying data collected in more realistic conditions and in the presence of different signal impairments. Several tests were performed in various real world operating environments such as under forest canopy, in urban canyon environment and indoors. Although all the tests were successfully performed, only the two of them, are detailed here in order to avoid repetition of similar results.

Moderate Urban Canyon Environment

The first test has been performed in a moderate urban canyon environment on the University of Calgary campus area. This particular scenario has been chosen because it represents a realistic situation with a steep elevation mask present in moderate urban canyons.

Figure 5-7: Moderate urban canyon data test: environment view.

Buildings obscured the signals on the east and west sides of the location at elevation angles up to 50° and 30°, respectively. In addition, a walled walkway obscured signals arriving from the north below about 25° in elevation (MacGougan 2003). The southern direction was relatively unhindered with some trees contributing to signal masking from the southwest side of the test site. Photos of the test location are shown in Fig. 5-7. Moreover, the buildings surrounding the test location have glass and metallic surfaces that act as signal blockers and reflectors creating strong multipath.

As both the C/N_0 estimates and the Doppler values provided by the GSNRx^{TM} receiver are evaluated from the same correlator outputs, they are both affected by the same impairments. Therefore, such phenomena as multipath and fading which are not accounted for in the theoretical model of the Doppler jitter (Eq. 4.29) are partially compensated by the use of the C/N_0 provided by the receiver.

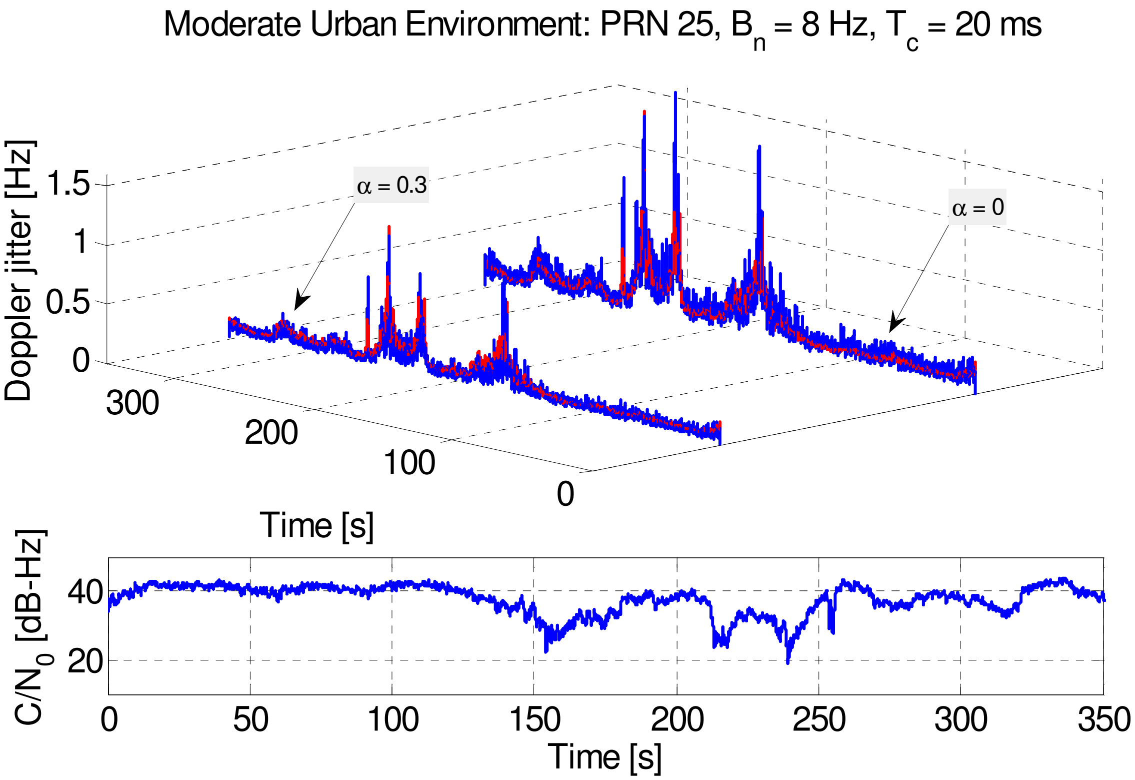

Figure 5-8: Empirical and theoretical Doppler jitter of raw Doppler measurements obtained using memory discriminator based tracking loop architecture.

Figure 5-8 shows the results obtained in this environment from a standard version of the software receiver compared to the ones obtained from the memory discriminator based architecture using α = 0.3. Coherent integration time in this case was set to 20 ms and a fixed value of 8 Hz loop bandwidth was used.

An urban canyon is a type of environment where the measured C/N_0 is significantly affected by slow fades that degrade the signal quality, directly translating the reduced received power into increased Doppler tracking jitter (Lachapelle et al 2004). This trend can be seen in Fig. 5-8. This figure illustrates as well the ability of the memory discriminator based architecture to provide better Doppler estimates in the presence of multipath and fading compared to the standard receiver architecture.

Heavy Indoor Environment

The second test considers a much more challenging environment represented by a heavy indoor area in a corridor where GPS signals are blocked from two sides by heavy walls and strongly attenuated by silvered glass windows (about 20 dB attenuation) in the other directions. Figure 5-9 shows the test location and the view of the environment.

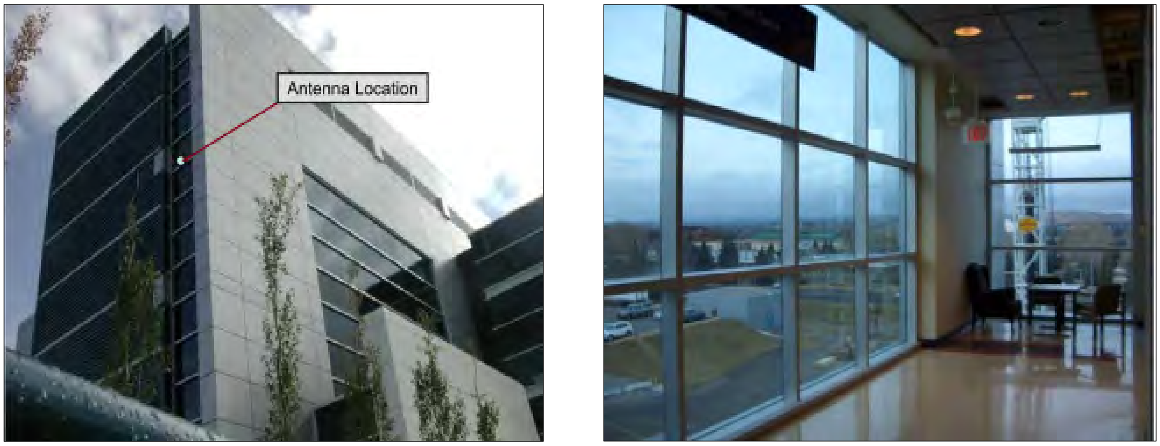

Figure 5-9: Indoor data test: environment view.

In such environments the already attenuated GPS signals are significantly affected by strong multipath and fading. Moreover, as illustrated in Figure 5-10 that shows the Power Spectral Density (PSD) of the received signal, interference has been detected with a particularly strong tone at around 2.98 MHz. It is noted that Figure 5-10 represents the PSD of the downconverted signal where the GPS L1 centre frequency (1575.42 MHz) was mapped to a 3.42 MHz intermediate frequency. The sampling rate used in this case was 12.5 MHz. The highest intensity tone seen in Fig. 5-10 was removed by the implementation of a notch filter.

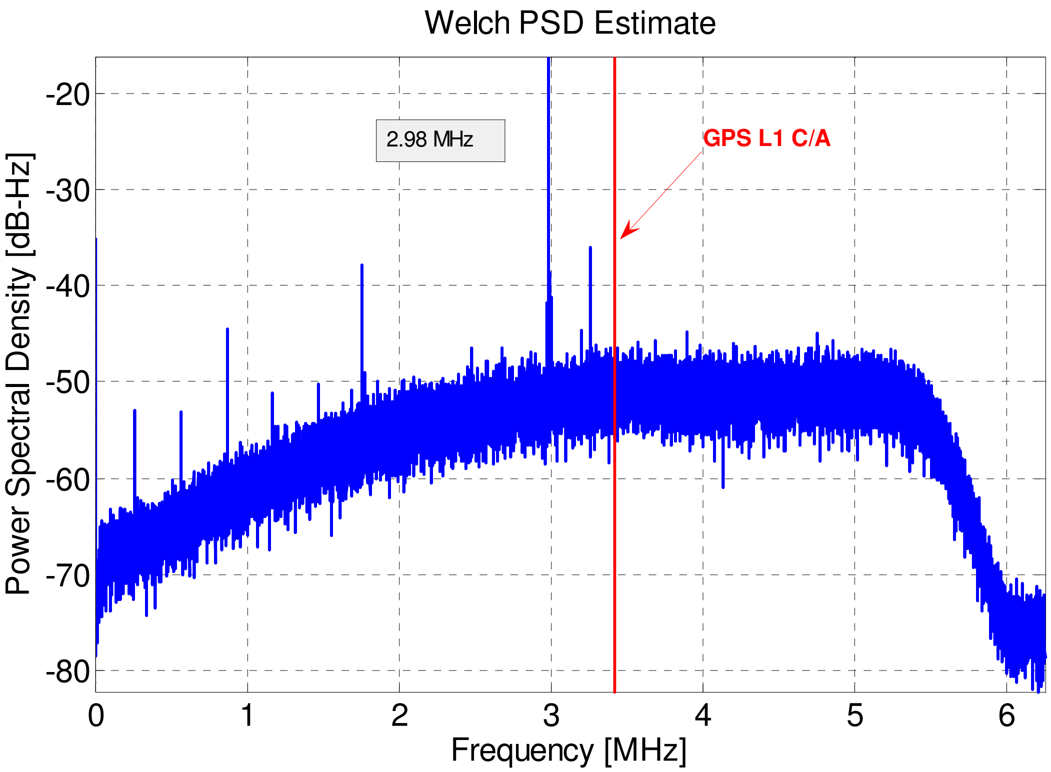

Figure 5-10: PSD of the signal with interference present in the data collected indoors.

As the receiver was not able to determine bit synchronization, the coherent integration time was reduced to 1 ms. And a loop bandwidth of 5 Hz was used so that the receiver would be able to respond to the signal amplitude fluctuations caused by multipath reflections. Figure 5-11 illustrates the results obtained in this environment. Therein the theoretical values of the Doppler jitter are compared with the results obtained empirically. Capability of the memory discriminator based architecture to produce less noisy Doppler measurements compared to the standard tracking loop architecture is also illustrated by comparing the results obtained using standard architecture ($\alpha = 0$) and memory discriminator based architecture with α set equal to 0.5.

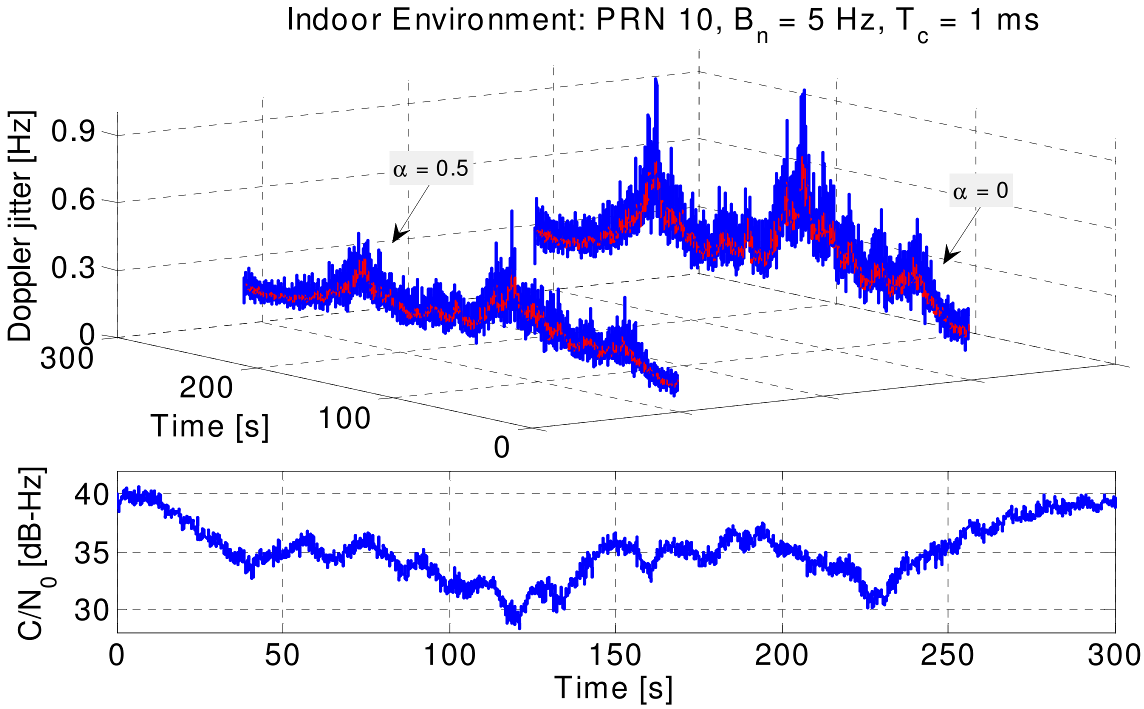

Figure 5-11: A sample of empirical and theoretical Doppler jitter of the raw Doppler measurements obtained using standard GSNRx^{TM} in the indoor environment.

During this test frequent signal fading has been experienced as it can be observed in Fig. 5-11. As mentioned previously, this phenomena is not accounted for in the theoretical model of the Doppler jitter, but is partially compensated by the use of the C/N$_0$ provided by the receiver. For this reason the Doppler jitter values increase in correspondence to the signal fades. Considering Fig. 5-11, it can be concluded again that there is a good match between theoretical and empirical results.

Similar performance to the tests described in this section was also observed in the tests performed under forest canopy, as well as those performed in the previously mentioned environments, but when using carrier phase derived Doppler measurements. All the data sets have also been evaluated for different PRNs and comparable results were obtained. This confirms that the proposed theoretical model can be used to effectively predict the Doppler jitter in various GPS operational environments and for different methods of Doppler derivation.

5.2 Comparative Hardware Receiver Analysis Based on Doppler Bandwidth

The theoretical model for the Doppler tracking jitter analysis presented in **Chapter 4** can be adopted for estimating the Doppler bandwidth, B_d, of different hardware receivers. This allows not only better characterization of the receiver under analysis, but provides a metric for the comparison of different hardware receivers.

Given the Doppler measurements and the C/N_0 estimates from a hardware receiver, the procedure described in Fig. 5-2 can be followed to determine the values of the empirical Doppler jitter, $\hat{\sigma}_f$, Eq.(5.1). It is noted that the Doppler jitter given by Eq. 4.29 can be written in the following form:

$$\sigma_f^2 = B_d \cdot f(C/N_0), \tag{5.2}$$

where B_d is the Doppler bandwidth and

$$f(C/N_0) = \frac{1}{(2\pi T_c)^2} \cdot \frac{1}{(C/N_0)} \cdot \left(1 + \frac{1}{2T_c(C/N_0)}\right), \tag{5.3}$$

is a function of the C/N$_0$ estimated by the receiver. Thus, the Doppler bandwidth and the update rate of the loop, T_c, can be estimated using the procedure described in Figure 5-12.

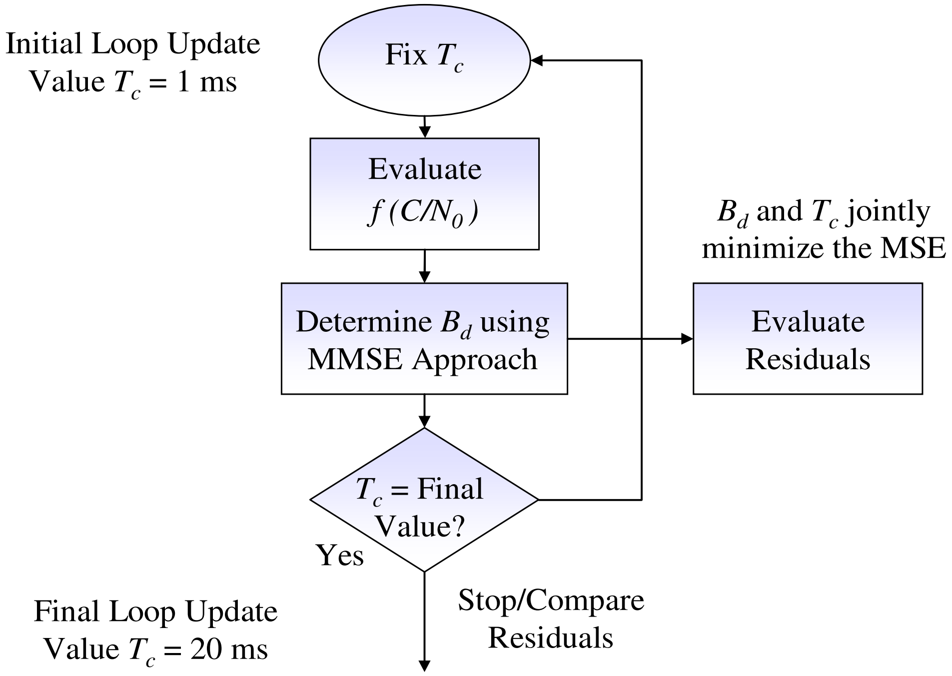

Figure 5-12: Procedure adopted for estimating the Doppler bandwidth and the loop update rate (T_c) using raw Doppler measurements provided by a hardware receiver.

First T_c is fixed so that the Doppler bandwidth, given a specific loop update interval is obtained by minimizing the following:

$$\left|\hat{\sigma}_f^2 - B_d \cdot f(C/N_0)\right|^2 . \tag{5.4}$$

For each value of T_c, a Doppler bandwidth and a residual error are found. Different values of T_c are tried in the range [1 ms, 20 ms] and the final estimates are the values that minimize the residual errors. This interval has been chosen under the assumption that the receivers under consideration are not using any external assistance in order to extend the coherent integration time by removing the effect of the data bits. When the values of the Doppler bandwidth and the coherent integration time for the hardware receiver are found they can be used to perform a similar analysis of the Doppler jitter as described in the previous section.

This approach has been tested using several commercial hardware receivers in various environments. Results obtained from the progressively attenuated LOS GPS data will be used to illustrate the performance of the proposed approach. A similar setup as shown in Fig.5-1 has been used, where the signal at the output of the LNA was splitted between the NI system and several hardware receivers including an OEMV-1 GPS receiver from NovAtel (NovAtel, 2009) and a HSGPS AEK-4T receiver from u-blox (u-blox, 2009). Using the approach described above the values of the Doppler bandwidth and the coherent integration time for each receiver were estimated allowing to determine and plot the theoretical Doppler jitter as a function of C/N_0. The estimated values are summarized in Table 5-3.

Table 5-3: Estimated values of Doppler bandwidth, B_d, and coherent integration time, T_c, for the OEM -V1 and AEK-4T hardware receivers.

Receiver	**T_c [ms]**	**B_d [Hz]**
OEM -V1	20	6.7
AEK-4T	20	62.8

Due to the tracking method used in the u-blox HSGPS receiver the estimated Doppler bandwidth of the u-blox HSGPS receiver is much higher than the one estimated for the OEM-V1 receiver resulting in lower quality observables.

As shown in Table 5-3, it was determined that the final value of the estimated coherent integration time used by the OEMV-1 receiver is 20 ms. Although, it should be considered that the residual error (Eq.(5.4)) for this combination of Doppler bandwidth and coherent integration time is marginal with the residual error obtained using T_c = 10 ms as illustrated in Figure 5-13. According to the algorithm described in Fig. 5-12 it has been specified that the final estimates of T_c and B_d are the ones that produce the smallest residual error. Therefore, in spite of marginal difference in between the residual error values the combination of T_c and B_d presented in Table 5-3 was chosen. This relationship is also illustrated in Figure 5-14, where the empirical values of the Doppler jitter for the OEMV-1 receiver are compared against the theoretical values obtained using the coherent integration time of 1 ms, 10 ms and 20 ms. A verification of this pattern is seen in Fig. 5-14, where the curves for theoretical Doppler jitter obtained using T_c =10 ms and T_c =20 ms are nearly overlaid, while the curve for T_c =1 ms departs from the others.

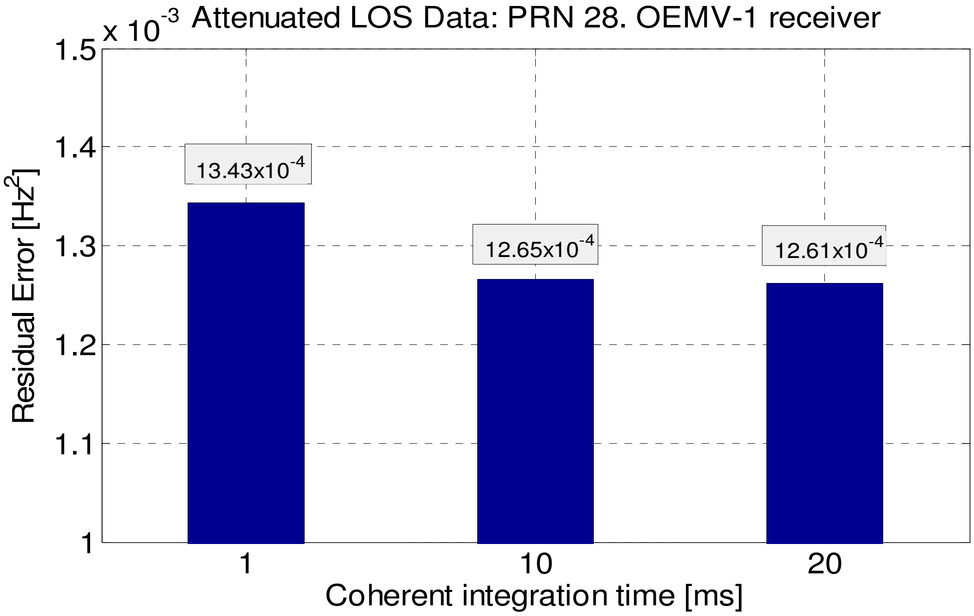

Figure 5-13: Residual error as a function of the coherent integration time, NovAtel OEMV-1 hardware receiver.

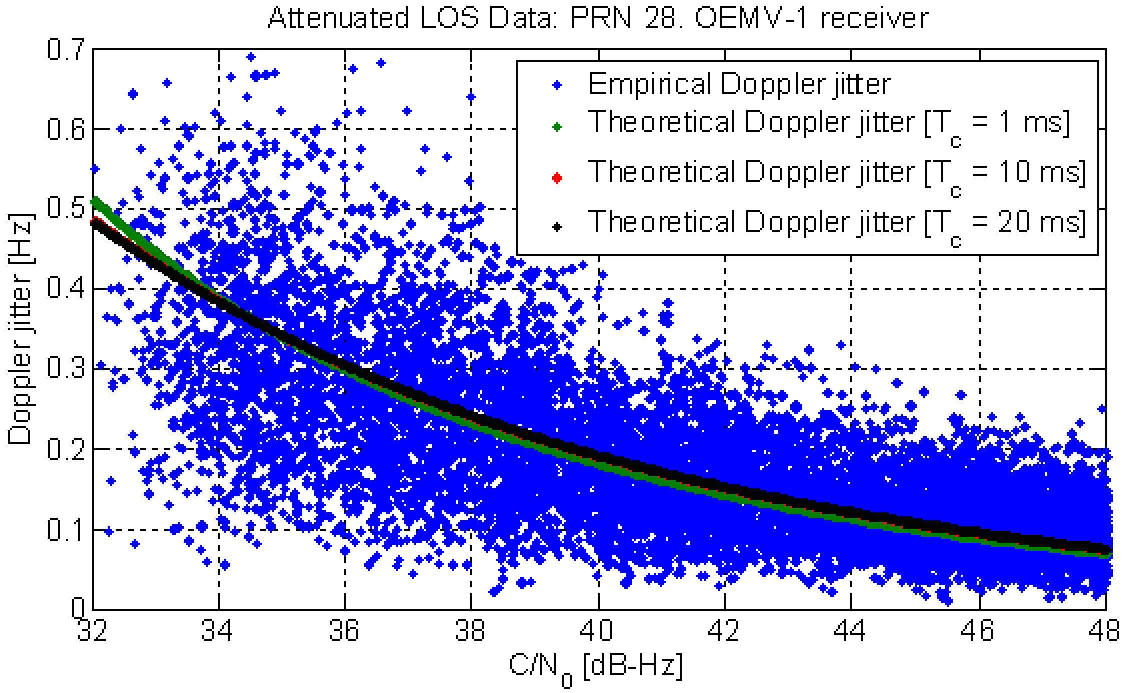

Figure 5-14: Empirical Doppler jitter compared to theoretical Doppler jitter for different values of the coherent integration time, NovAtel OEMV-1 hardware receiver.

Figures 5-15 and 5-16 compare the empirical values of Doppler jitter to the theoretical values determined using the estimated value of the Doppler bandwidth of the OEM-V1 and AEK-4T hardware receivers. The results are compared at the same time to the ones obtained from the standard GSNRx^{TM} software receiver processed using coherent integration time, T_c , equal to 20 ms and loop bandwidth, B_n, 8 Hz.

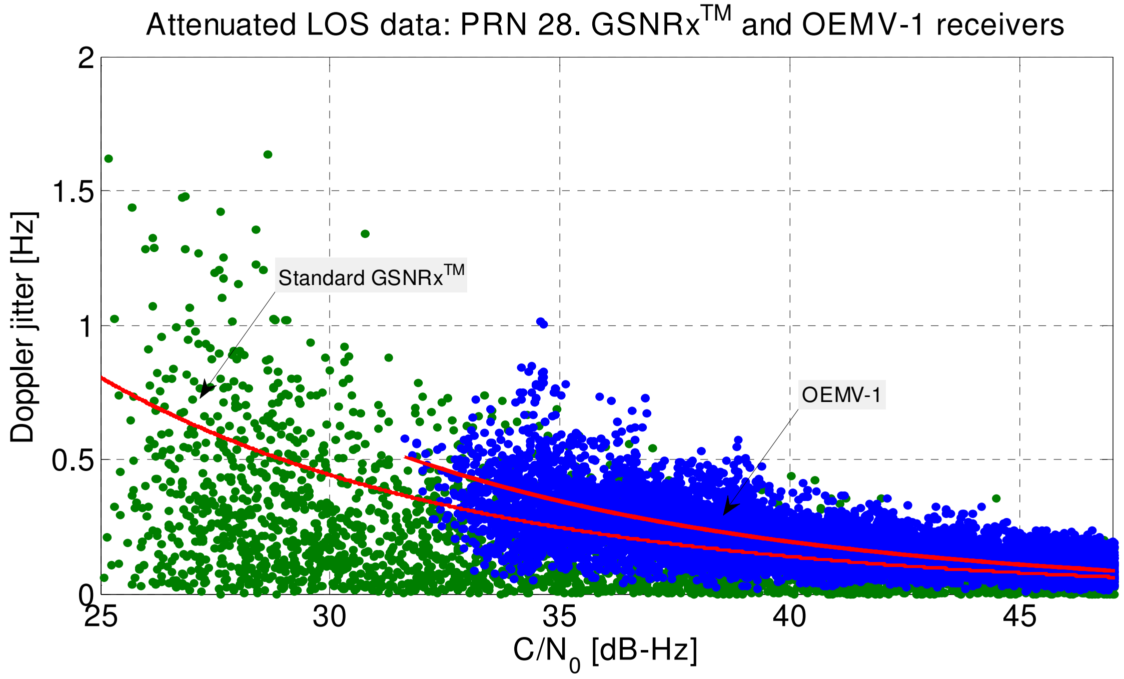

Figure 5-15: Empirical and theoretical Doppler jitter of the raw Doppler measurements obtained using GSNRx^{TM} software (B_n = 8 Hz, T_c = 20 ms) and NovAtel OEMV-1 hardware receivers.

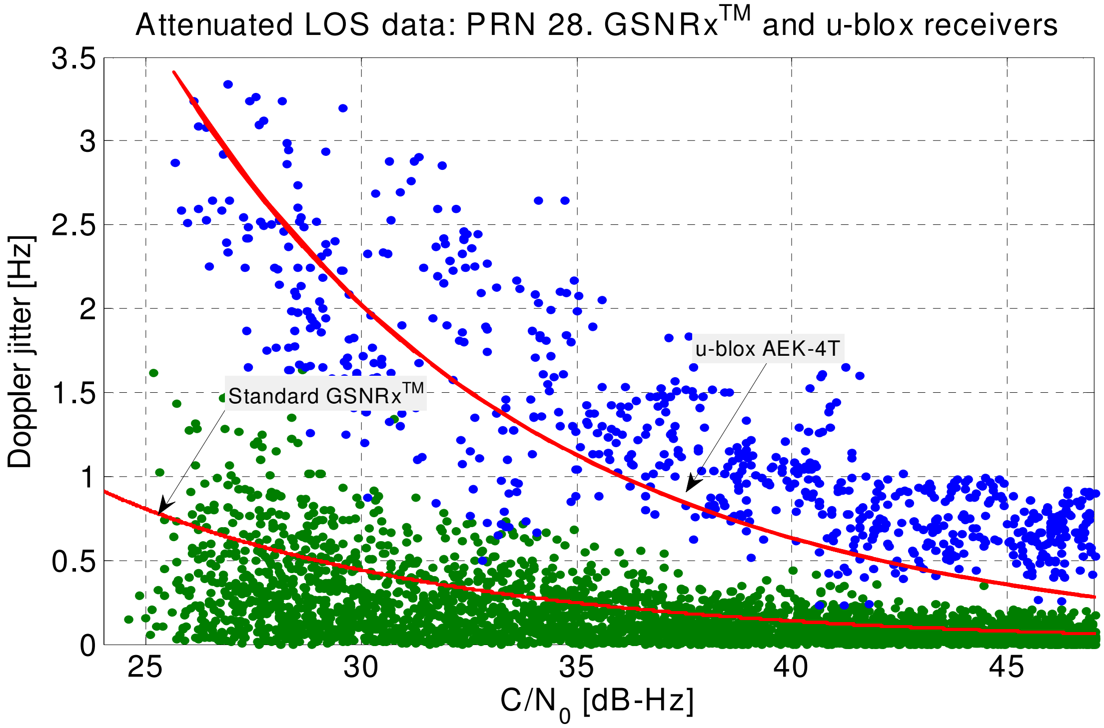

Figure 5-16: Empirical and theoretical Doppler jitter of the raw Doppler measurements obtained using GSNRx™ software (B_n = 8 Hz, T_c = 20 ms) and u-blox AEK-4T hardware receivers.

As it has been explained in **Chapter 4**, the proposed model is general and applies to receivers using standard tracking loops using sequential causal processing. However, although it is conjectured that the u-blox AEK-4T HSGPS receiver uses block processing techniques, the proposed model seems to fit with the empirical observations with the exception of some deviations for high values of C/N$_0$. A more thorough study and extension of the analysis to receivers adopting block processing techniques is required and it is left for future work.

The summarized results indicate that the proposed theoretical model for Doppler jitter analysis can be effectively applied to hardware receivers allowing one to characterize the performance of the receiver in terms of Doppler bandwidth and the resulting quality of Doppler measurements.

CHAPTER 6: EXPERIMENTAL ANALYSIS: DYNAMIC MODE

To perform a complete evaluation of the theoretical framework developed for the Doppler jitter and bias analysis, it was necessary to validate the proposed model also in the presence of dynamics. Therefore, several real world pedestrian-based tests and simulations were performed to complete the evaluation of the developed model.

The first part of this chapter describes the experimental setup adopted for the pedestrian tests and discusses the results comparing the empirical and the theoretical Doppler jitter values determined in various environments using different methods for Doppler measurements derivation and for different combinations of the tracking loop parameters.

The second part of the chapter describes the methodology adopted for the Doppler bias analysis. Impact of different levels of dynamics and of different combinations of tracking loop parameters is studied and discussed. The performance of the memory discriminator based tracking loop architecture introduced in **Chapter 3** is also evaluated under different levels of dynamics and compared against the performance of the standard tracking loop architecture.

6.1 Doppler Jitter Analysis

A number of pedestrian-based tests in various operating environments were performed in order to verify the validity of the theoretical model for the Doppler tracking jitter (Eq. (4.29)). As mentioned previously, no reference solution for the Doppler frequency is required to be able to analyse this parameter. Because of its size and mobility, the SiGe front-end was used for data collection in all the experiments presented in this section. Specifications for the SiGe front-end are reported in Table 6-1.

Table 6-1: Characteristics of the GPS signals collected using the SiGe front-end.

Parameter	**Value**
Sampling frequency	$f_s = 16.367\ MHz$
Intermediate frequency	$f_{IF} = 4.1304\ MHz$
Sampling	Real

The experimental setup used for pedestrian testing is illustrated in Figure 6-1.

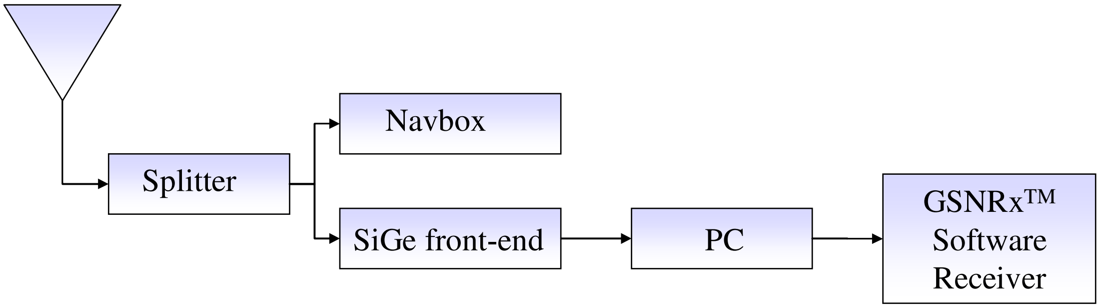

Figure 6-1: Equipment setup adopted for pedestrian-based real world data collections.

The NavBox, a data logging device developed by the PLAN Group, University of Calgary, was used for powering the antenna which was mounted on a rigid backpack for stability, together with the front-end equipment and cabling. Data was logged from the SiGe front-end to a laptop and processed in post mission using two versions of the GSNRx^{TM}, namely the standard and the memory discriminator based versions.

The same methodology for Doppler jitter estimation from empirical data as described in detail in **Chapter 5**, (Fig. 5-2 and Eq. (5.1)), was used. The empirical data was then compared to the theoretical Doppler jitter values determined using the proposed theoretical model (Eq. (4.29)).

For all the experiments considered in this section the length of the moving average filter for the empirical estimation of the Doppler jitter, *K*, (Eq. (5.1)), has been limited to 40 ms in order to preserve the oscillations in the Doppler measurements caused by the pedestrian motion. Long integrations would remove the effects of the user gait from the Doppler mean, leading to biased estimates of the Doppler jitter. This approach was adopted in order to avoid the problems described in Petovello et al (2003).

In this section results from pedestrian tests under forest canopy and in moderate urban environment with a steep elevation mask are discussed. Those two tests are only sample results and several additional experiments have been performed with similar findings.

Foliage Obstructed Environment

The first experiment was performed on a trajectory with a large amount of tall poplar and evergreen trees. The test was initialized in an open-sky area, where the user stayed stationary for one minute. An L-shaped trajectory (portions seen in Figure 6-2) included areas with open-sky at the start and the end of the test, and a forested area in the middle of the trajectory. In total the test lasted for just over six minutes and nine satellites were in view. Results for this test are summarized in Figure 6-2 where the empirical and theoretical Doppler jitter are compared.

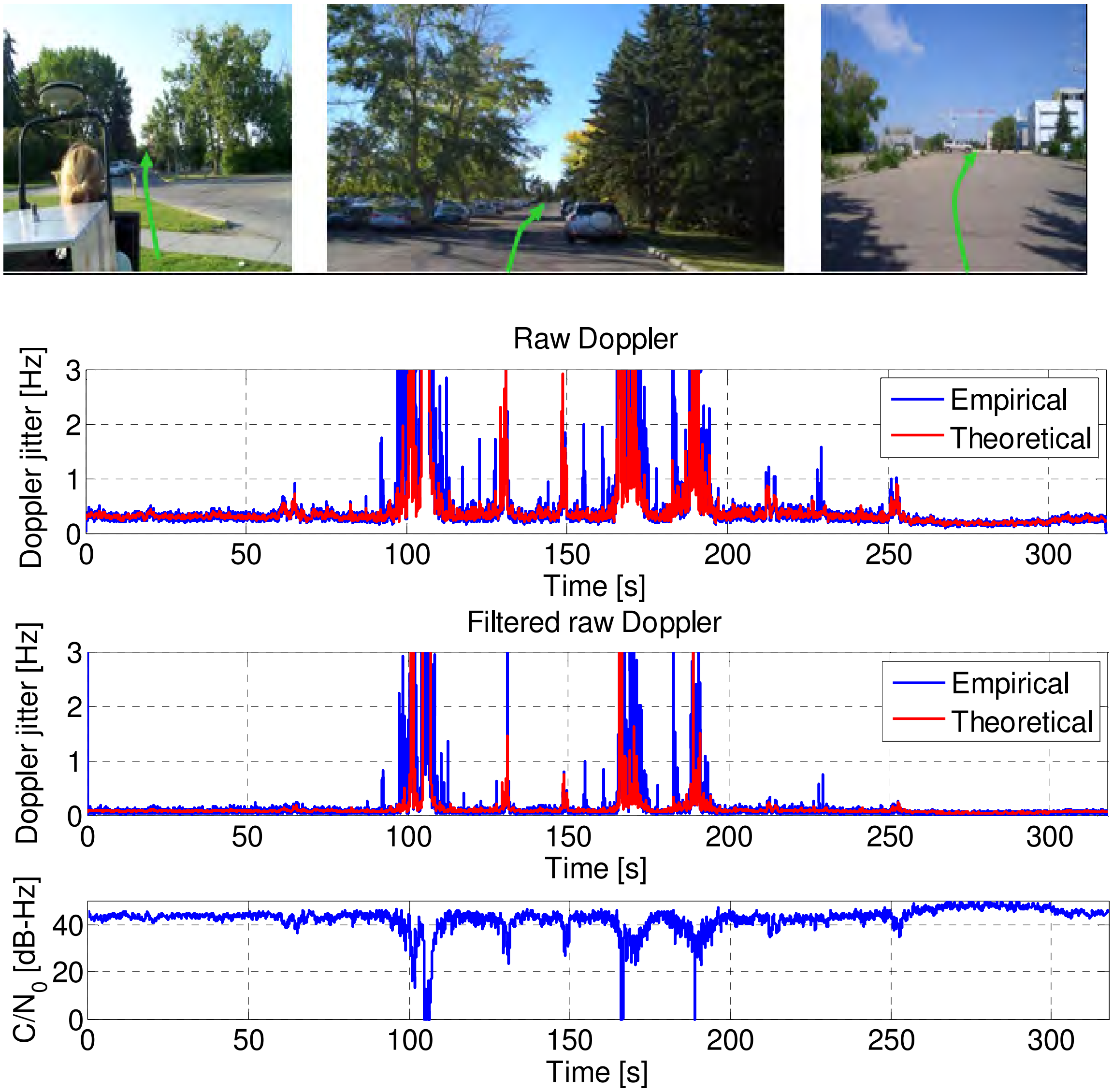

Figure 6-2: Environment view and Doppler jitter analysis in a pedestrian test using a standard tracking loop architecture. Foliage obstructed environment, PRN 28.

Cases of raw Doppler and filtered raw Doppler measurements are considered in Fig.6-2, where the filtered raw Doppler measurements were obtained using a moving average (MA) filter with a 10 ms analysis window size. A loop bandwidth of 8 Hz and 1 ms coherent integration time were used in both cases.

As expected, due to the effect of the smoothing filter, $S(z)$, a MA filter in this case, the Doppler jitter of the filtered raw Doppler measurements is smaller than the Doppler jitter of the raw observations. In both cases a good match between empirical and predicted Doppler jitter is observed.

As it has been discussed in **Chapter 5**, since the C/N_0 estimates are obtained from the same correlator outputs as the Doppler values, they are both affected by the same impairments such as fading and multipath. Because the C/N_0 provided by the GSNRx^{TM} software receiver is used for the estimation of the theoretical Doppler jitter, effects of fading and multipath are partially compensated for. As it can be observed from the C/N_0 plot in Fig.6-2, the signal was severely attenuated during the section of the test trajectory obstructed by foliage. This effect was directly transferred to the Doppler jitter, as is expected by the theory.

Moderate Urban Canyon Environment

Further analysis of the Doppler jitter was performed by studying the data collected in moderate urban canyon environment on the University of Calgary campus area, as detailed in **Section 5.1.2**. There were in total 6 satellites in view during the test. Photos of the test environment are shown in Fig. 6-3 followed by a sky-plot for the duration of the experiment in Fig. 6-4. The same equipment setup (Fig.6.1) adopted in the previous experiment was used. The test was initialized in an open-sky area with a 30 second stationary period, and then a pedestrian walking path illustrated in Figure 6-3 was followed.

Figure 6-3: Moderate urban canyon. Test trajectory and environment view.

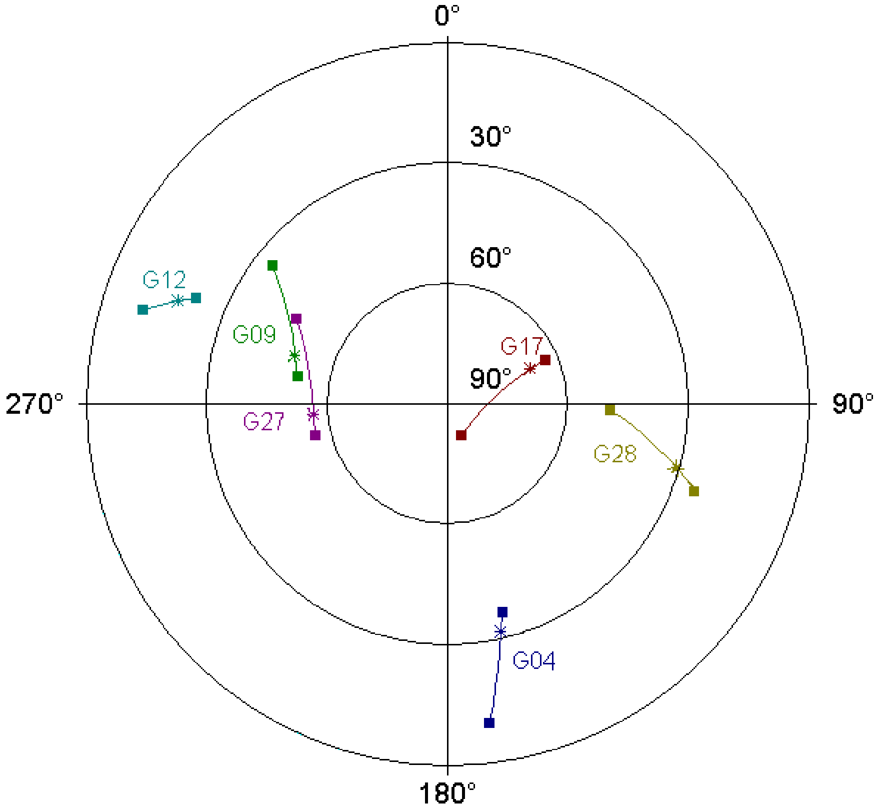

Figure 6-4: Sky-plot for the duration of the test. Moderate urban canyon environment.

Figure 6-4 considers the case of PRN 4, arriving from the South-East side of the test trajectory which has a relatively clear view of the sky. The signal of PRN 4 was characterized by a 45.5 dB-Hz C/N$_0$.

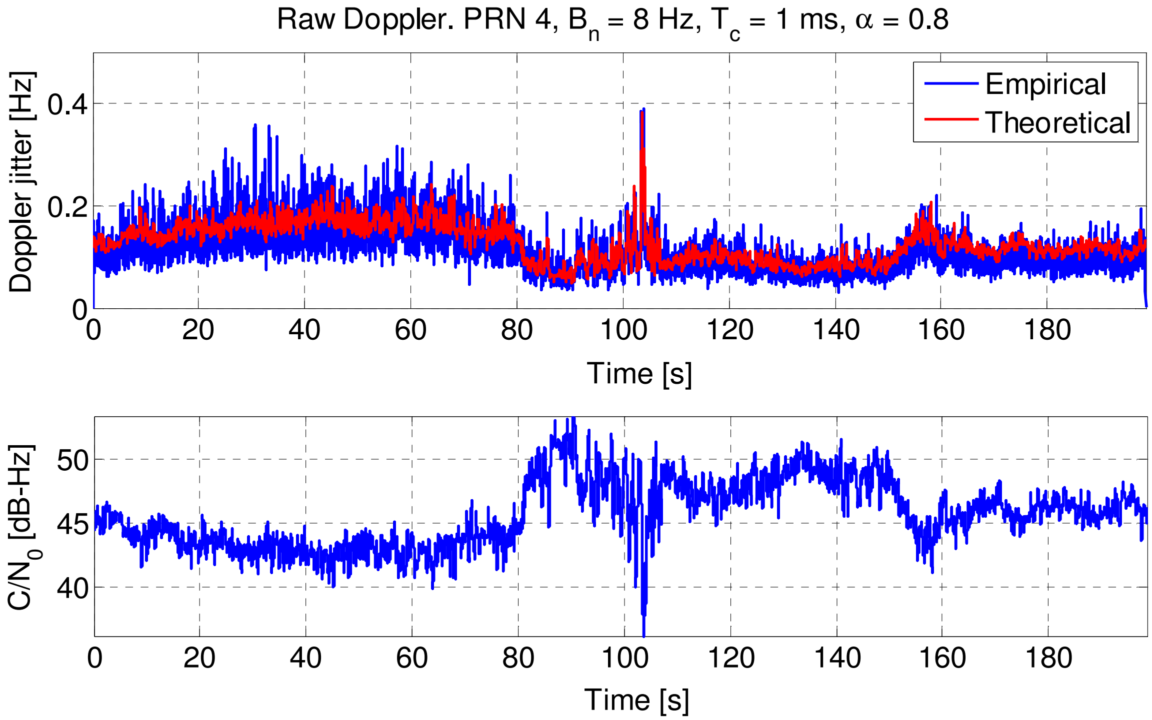

Figure 6-4: Doppler jitter analysis for a pedestrian test in moderate urban environment using the memory discriminator based architecture, PRN 4.

In order for the receiver to maintain phase lock during the duration of the entire test, the memory discriminator based tracking loop architecture was used. The data set was processed using a 0.8 forgetting factor, together with an 8 Hz loop bandwidth and a 1 ms coherent integration time. This combination of tracking loop parameters allowed the receiver to stay in the PLL tracking mode during the entire trajectory resulting in good agreement between the theoretical and the empirical results.

A case with a weaker satellite is considered in Figure 6-5. In this case the satellite (PRN 9) was arriving from the North-West side of the test trajectory which was obstructed by a tall concrete building (Fig.6-3). Memory discriminator based tracking loop architecture was also used in this case with the same tracking loop parameters combination as above (T_c =1 ms, B_n = 8 Hz, α =0.8).

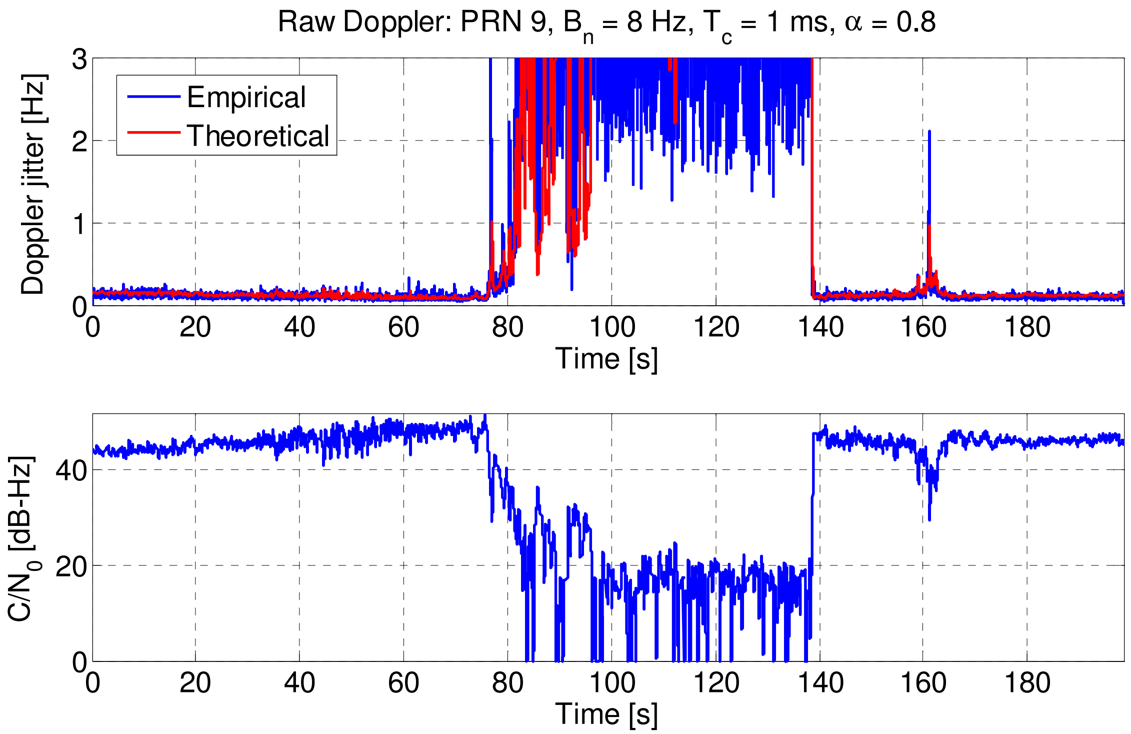

Figure 6-5: Doppler jitter analysis for a pedestrian test in moderate urban environment using the memory discriminator based architecture. PRN 9.

The measured C/N$_0$ is severely affected by signal fading during the section of the test trajectory when the user passes adjacent to the building on the North-West side. Because of this, the receiver lost phase lock during this period as shown in Figure 6-6 which illustrates the tracking state of the receiver during the test.

Since the theoretical model developed in this thesis is valid for PLL only, in the section where the receiver was losing phase lock theoretical values of the Doppler jitter do not match the empirical results.

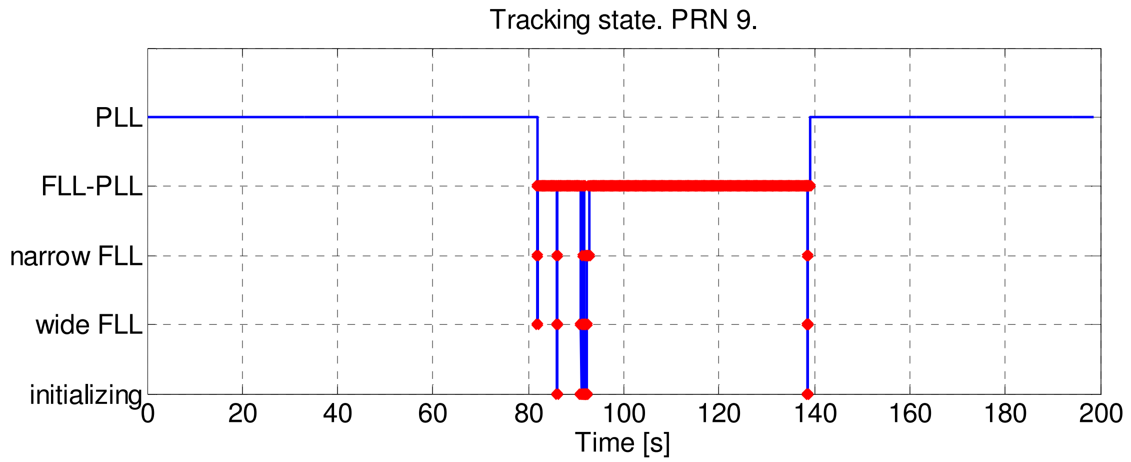

Figure 6-6: Tracking state of the memory discriminator based architecture, pedestrian test in a moderate urban canyon environment, PRN 9.

Table 6-2 lists the tracking modes specified for the GSNRx^{TM} software (Petovello & O'Driscoll 2007) which are valid for both receiver architectures used in this thesis and abbreviations that will be used herein for these modes.

Table 6-2: Abbreviations of tracking modes of the GSNRx^{TM} software receiver.

Abbreviation used herein	GSNRx^{TM} tracking mode
PLL	PLL
FLL-PLL	FLL assisted PLL
narrow FLL	narrow pull-in FLL
wide FLL	wide pull-in FLL
initializing	initializing

Several pedestrian tests have also been performed in indoor environments including the heavy indoor area used for the stationary data collection detailed in **Chapter 5** and a typical North American residential house basement area. Due to the similarity of the obtained results only the latter test is discussed here.

The basement has a concrete wall structure, small windows located at ceiling level and lies underneath one upper level. This environment produced very low power signals with C/N_0 ranging as low as 23 dB-Hz and with the available signals severely affected by multipath. The collected data have been processed using both the standard and memory discriminator based tracking loop architectures for different forgetting factors and for different values of the loop bandwidth and coherent integration time. Unfortunately, both architectures were unable to achieve phase lock during the entire test as shown in Fig.6-7, which illustrates the tracking state of memory discriminator based architecture initialized with T_c =1 ms, B_n = 8 Hz and α =0.8.

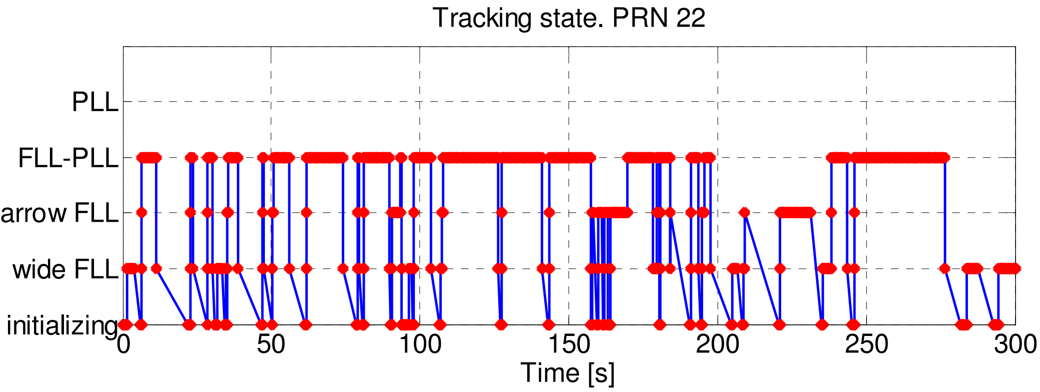

Figure 6-7: Tracking state of the memory discriminator based architecture, pedestrian test in a residential house basement environment, PRN 22.

To be able to predict the Doppler jitter in this case the developed theoretical framework has to be extended to include the FLL model. This requires further studies and is left for future work.

6.2 Doppler Bias Analysis

This section gives a brief overview of the test methodology suggested for the Doppler bias analysis using the model given in Eq. (4.31). As defined previously, Doppler bias is a measure of the systematic error in the Doppler estimates introduced by the transient response of the loop on the changes in the input frequency.

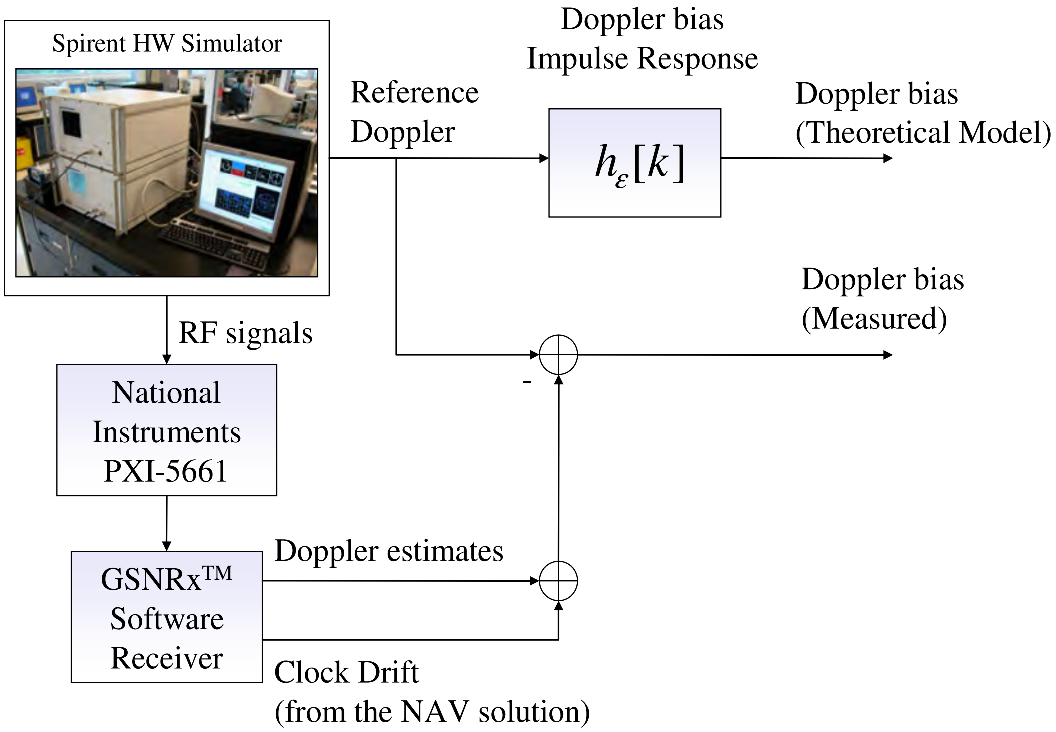

Figure 6-8: Experimental setup adopted for the evaluation of the Doppler bias.

To be able to determine the Doppler bias a reference solution is required. Therefore, a GPS hardware simulator, the GSS 7700 from Spirent capable of providing an accurate reference Doppler solution and generating various scenarios, was used. The adopted setup is shown in Figure 6-8. As Fig. 6-8 illustrates, the Spirent GSS 7700 hardware simulator was used for generating RF signals and reference Doppler values. The RF signals were collected using the NI PXI 5661 front-end settings configured according to the parameters listed in Table 6-3. The collected data was then processed by the GSNRx^{TM} receiver to estimate the Doppler and clock drift and evaluate the Doppler bias.

Table 6-3: NI PXI 5660 front-end settings for the data collection using the GSS 7700 hardware simulator.

Parameter	**Value**
Sampling frequency	$f_s = 5\ MHz$
Intermediate frequency	$f_{IF} = 0.42\ MHz$
Sampling	Complex

The theoretical Doppler bias was obtained by filtering the true Doppler provided by the simulator with the bias impulse response given by Eq.(4.32) and compared against the measured Doppler bias. Two different scenarios were considered. In both scenarios clear-sky conditions were simulated in order to better observe the biases that could have been completely hidden by noise in the presence of strong attenuation. In total, there were 10 satellites in view during the simulation, all with a relative channel power of 10 dB (-150 dBW).

6.2.1 Low dynamics

In the first scenario a case of low dynamics has been considered. The dynamics of the trajectory was set to simulate the dynamics of a pedestrian moving along the square trajectory illustrated in Figure 6-9 with maximum velocity of 1.5 m/s.

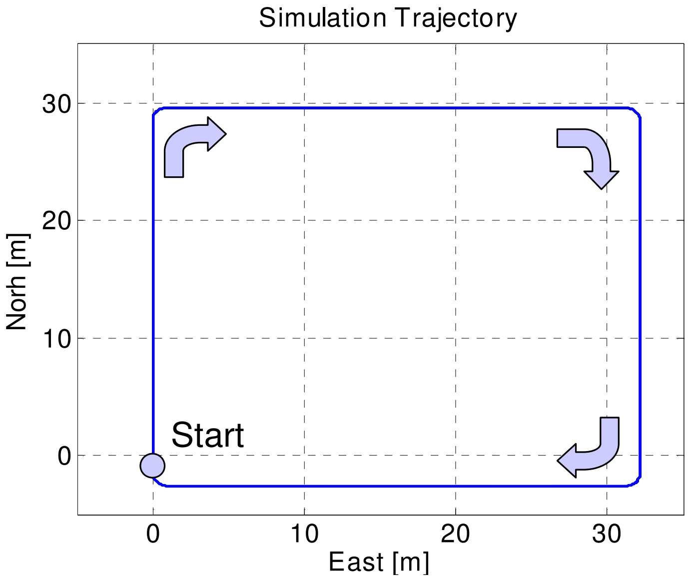

Figure 6- 9: Simulated test trajectory, low dynamics scenario.

As it has been discussed in **Chapter 4**, the PLL is not able to instantaneously follow the variations in Doppler, thereby introducing a bias during the transient time.

At each turn in the trajectory a sudden change in the Doppler frequency was observed, an example of which is shown in Figure 6-10, where the true Doppler generated by the hardware simulator is compared against the Doppler estimates produced by the standard GSNRx^{TM} software receiver after applying the corrections for the clock drift. The satellite considered here is PRN number 16 with a signal characterized by a 48 dB-Hz C/N$_0$. It should be considered that the GSS 7700 hardware simulator is not able to generate a continuous reference Doppler which is approximated by a piece-wise linear function resulting in Doppler frequency values linearly changing over 100 ms intervals.

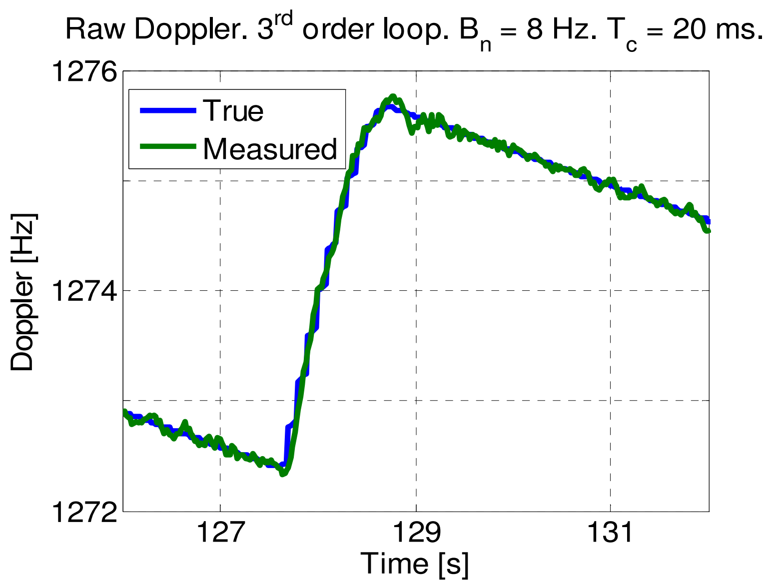

Figure 6-10: Comparison between estimated and true Doppler, low dynamics scenario, PRN 16.

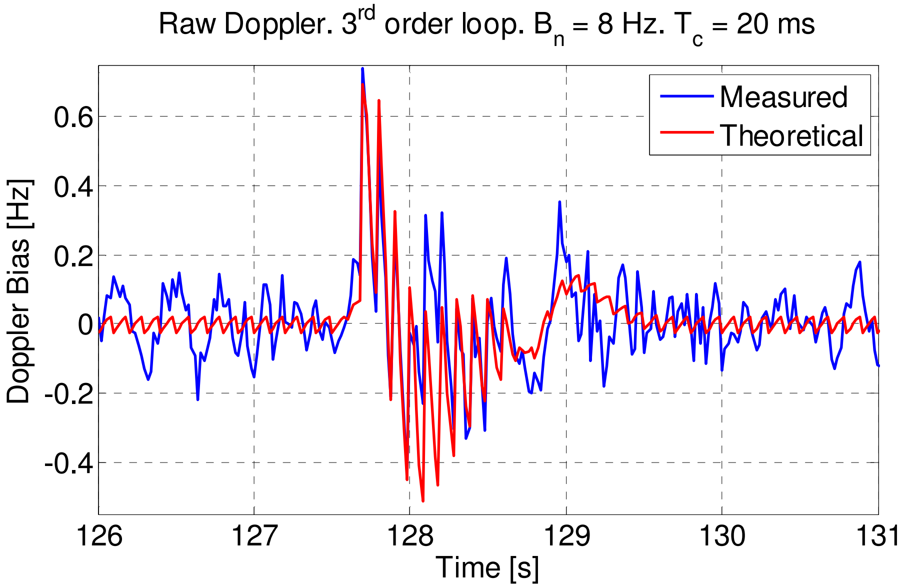

Figure 6-11: Comparison between the observed and predicted Doppler bias, low dynamics scenario, PRN 16.

The observed and the theoretically predicted biases for one of the turns in the simulated trajectory are compared in Figure 6-11. The theoretical Doppler bias was obtained by filtering the true Doppler using the bias filter $h_{\varepsilon}[k]$, Eq.(4.32).

A good agreement between measured and predicted Doppler bias is found showing the validity of the proposed theoretical model in the case of low user dynamics.

As it has been explained above, because of the way the hardware simulator generates the reference Doppler the theoretical Doppler bias looks like a sawtooth wave in the periods with no change in Doppler due to user dynamics. Since the true Doppler is piece-wise linear, its derivative is discontinuous and these discontinuities are reflected in the predicted Doppler bias that assumes a sawtooth shape. It should be noted that this behaviour is observed in all the results presented in this section.

6.2.2 Medium and high dynamics

In order to allow a complete evaluation of the model for the Doppler bias given by Eq. (4.31) a simulation of a trajectory with higher dynamics was performed using the same equipment setup as described in Fig.6-8. The dynamics in this case were set to simulate the dynamics of a road bound vehicle. Figure 6-12 shows the trajectory chosen for this scenario. For this test maximum constant velocity of 17 m/s was simulated. In all, there were seven 90 degrees turns of a trajectory, each turn, starting from the second one, exhibiting increasing magnitudes of acceleration from 0.5 g to 3 g in 0.5 g increments per turn.

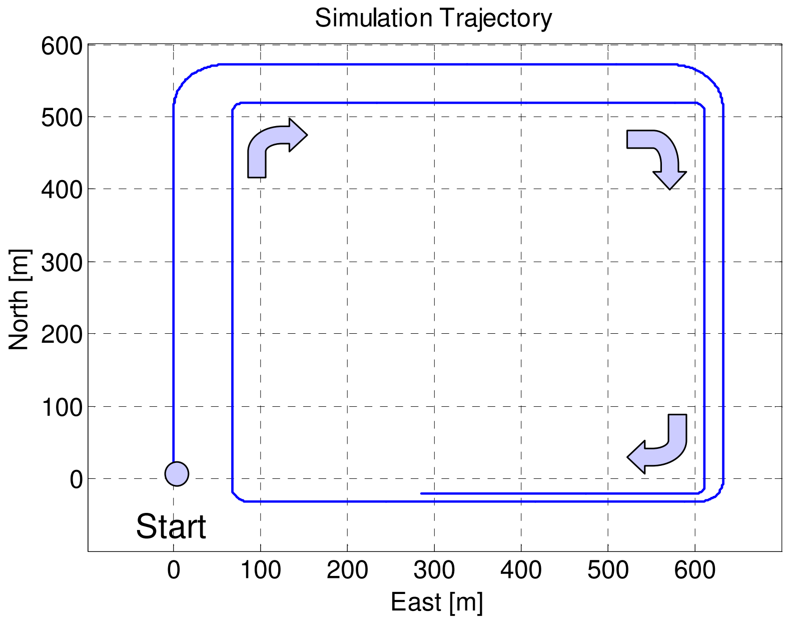

Figure 6-12: Simulated test trajectory, medium and high dynamics scenario.

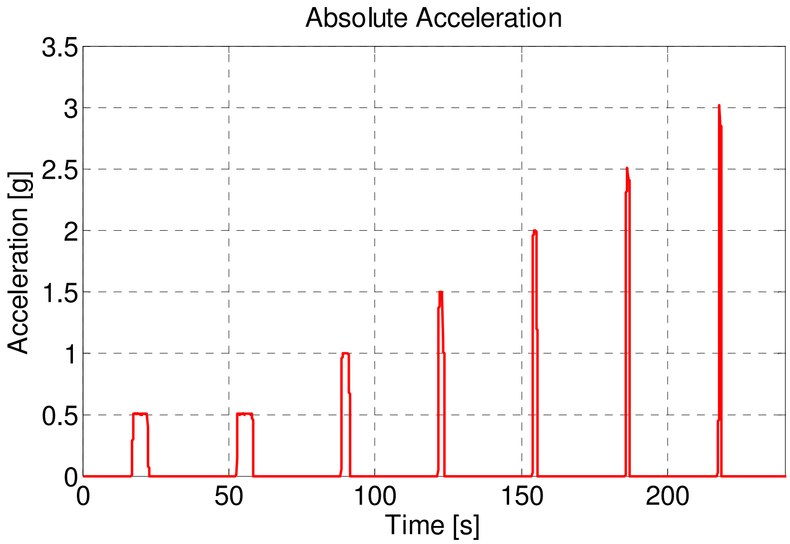

Figure 6-13: Simulated trajectory dynamics experienced by the receiver, medium and high dynamics scenario.

Figure 6-13 shows the dynamics experienced by the receiver during the simulation in terms of the absolute acceleration. The RF signal was processed using both the standard and memory discriminator based tracking loop architectures using different values of tracking loop parameters. The observed and theoretical Doppler biases were then determined for the different tracking loop parameters configurations, where the theoretical Doppler bias was obtained by following the same procedure as described in the previous section.

As it has been shown in **Chapter 3**, the memory discriminator based tracking loop architecture is capable to provide more accurate Doppler estimates by rejecting a larger quantity of noise with respect to the standard tracking loop architecture.

Introduction of a low-pass filter prior to the memory-less discriminator in a PLL (Fig.3-1) reduces the amount of noise transferred to the discriminator, allowing the discriminator to stay in its linear region and the phase loop to maintain lock. This makes the memory discriminator based PLL capable of bearing higher dynamics without loosing phase lock when compared to the standard PLL architecture.

This fact can be illustrated by the results obtained from this simulation. Figures 6-14 and 6-15 show the results obtained using the standard and memory discriminator based tracking loop architectures where the predicted Doppler bias is compared to the measured Doppler bias and the tracking mode indicating which state the given receiver channel is operating.

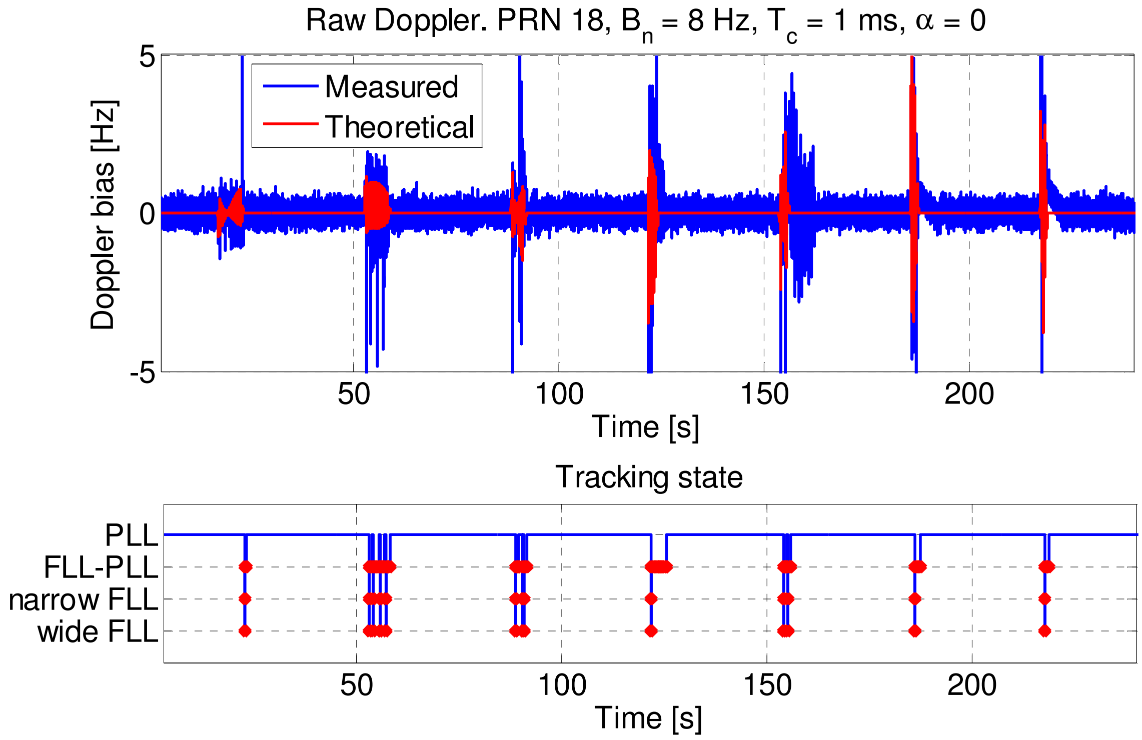

Figure 6-14: Observed and predicted Doppler bias and tracking state of the standard tracking loop architecture, PRN 18.

Results shown in Figures 6-14 and 6-15 were obtained using coherent integration time T_c = 1 ms and loop bandwidth B_n = 8 Hz. In the case with the memory discriminator based architecture (Fig.6-15) forgetting factor α = 0.8 was used.

While the standard receiver was losing phase lock and therefore transiting to the FLL assisted PLL mode during all the turns in the trajectory, the memory discriminator based receiver architecture was capable to maintain phase lock and remain in the PLL-only mode during the first 3 turns (from 0.5 g to 1 g). It should be noted though that for higher values of the loop bandwidth higher level of dynamics can be resisted by both standard and memory discriminator tracking loops architectures, but the same relative improved performance of the memory discriminator based architecture is observed.

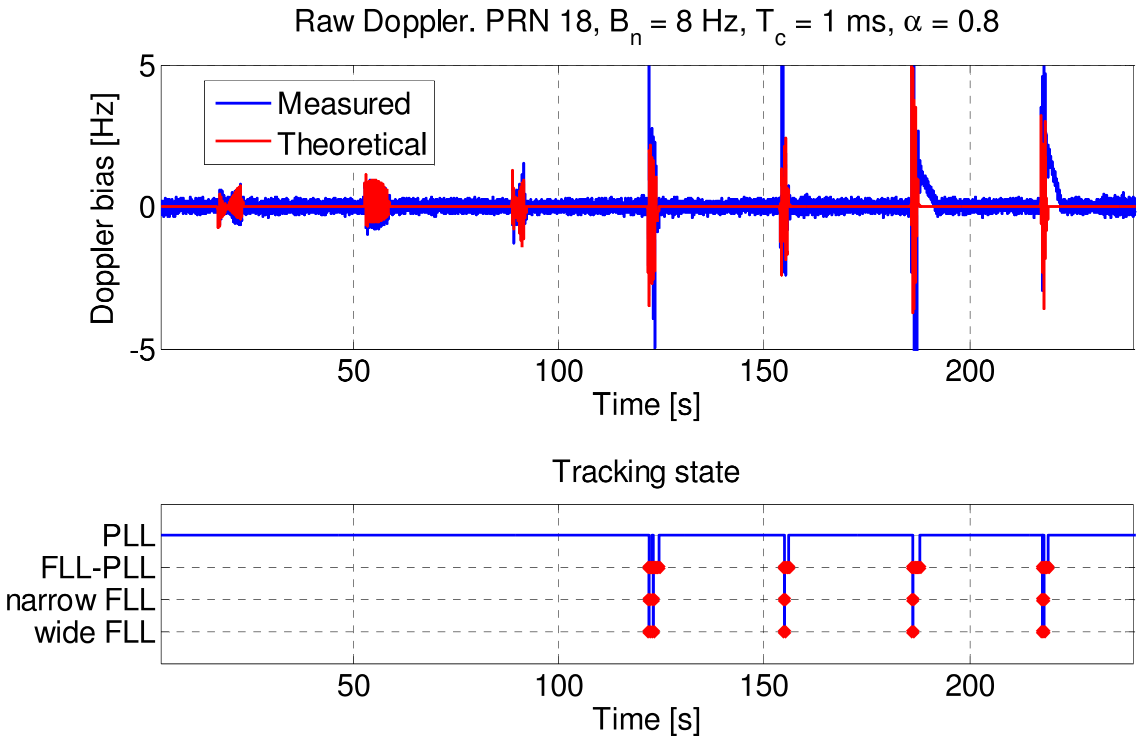

Figure 6-15: Observed and predicted Doppler bias and tracking state of the memory discriminator based tracking loop architecture, PRN 18.

In order to provide a better insight into the relative performance between the standard and memory discriminator based tracking loop architectures, a case considering a section of the trajectory with a 1 g turn is studied. Figure 6-16 shows the dynamics (acceleration and jerk) during this section of the simulation.

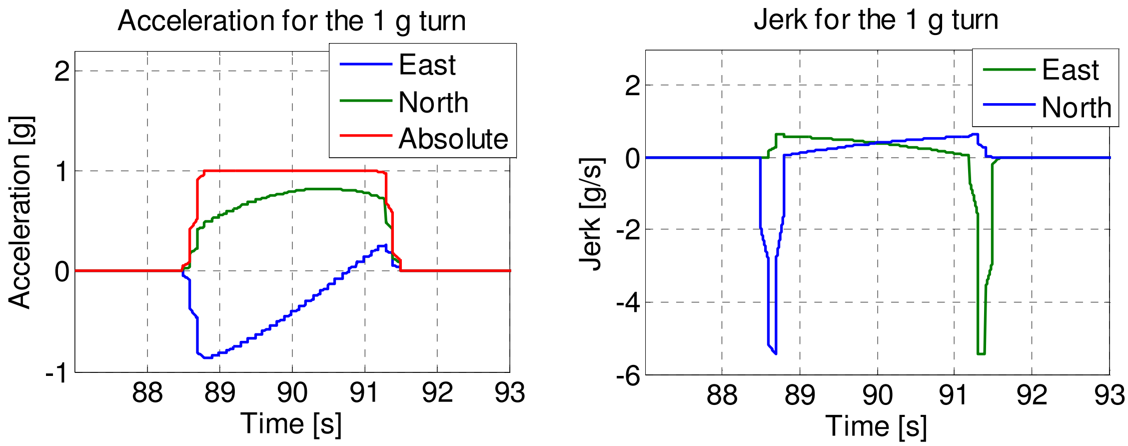

Figure 6-16: Acceleration and jerk experienced by the receiver during a 1 g turn.

For this 1 g turn, as with the other consecutive turns, there are a sharp north and east jerk values at the start and end of the turn. As a result of this rapid change in dynamics the standard PLL was losing phase lock and as the tracking state plot in Fig.6-17 (b) shows, the receiver was transitioning to other tracking modes. Results shown in Fig.6-17 (b) were obtained using a 1 ms coherent integration time and an 8 Hz loop bandwidth. Results presented in Fig.6-17 (a) were obtained using the memory discriminator based tracking loop architecture. The value of the forgetting factor, α, used in this particular case was 0.8, while the values of the coherent integration time and loop bandwidth were set equal to 1 ms and 8 Hz respectively to match the combination of parameters used with the standard tracking loop architecture. As indicated by the tracking states of the receiver plotted in Fig.6-17 (a), the memory discriminator based PLL was capable to maintain phase lock during the entire turn. Consistent with the results obtained from the previous simulation, results presented in Fig.6-17 (a) also demonstrate a good match between empirical and predicted Doppler bias, showing the validity of the proposed theoretical model. It should be noted that the theoretical model developed in this thesis is valid for PLL-only tracking, and therefore, as it can be observed from the results presented in Fig.6-17 (b), when the receiver loses phase lock and exits the PLL mode, the theoretical model is no longer valid and there is no agreement between predicted and empirical results.

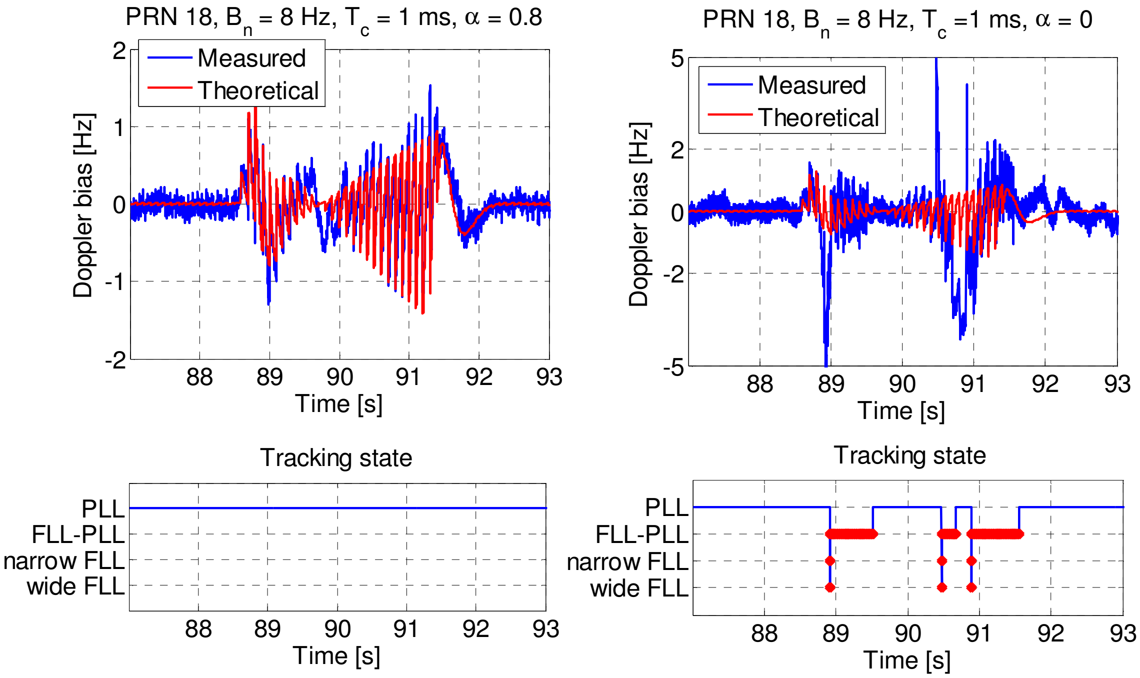

(a) **(b)**

Figure 6-17: Observed and predicted Doppler bias and tracking state of the receiver, 1 g turn.

a) Obtained using the memory discriminator based tracking loop architecture.

b) Obtained using the standard tracking loop architecture.

To give a better overview of how the developed model for Doppler bias analysis performs under a higher level of dynamics, analysis of the results for a section of the same trajectory with accelerations up to 3 g are presented in the following.

Figures 6-18 and 6-19 show the acceleration experienced during a higher dynamics section of the simulated trajectory (3 g turn) and compare the measured and predicted values of the Doppler bias.

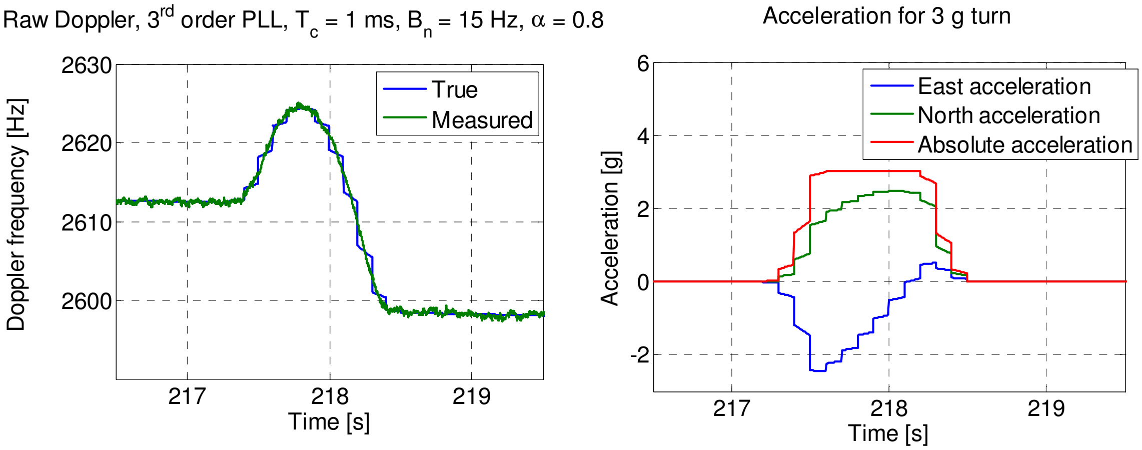

Figure 6-18: Estimated and true Doppler frequency for PRN 18, and acceleration experienced by the receiver during the 3 g turn.

To assure that the receiver maintains phase lock during this high dynamic section the memory discriminator based architecture was used. A 0.8 forgetting factor was used and the coherent integration time and the loop bandwidth set to 1 ms and 15 Hz respectively. Also in this case, with a higher level of dynamics, the proposed theoretical model was able to effectively predict the Doppler bias introduced by a third order loop.

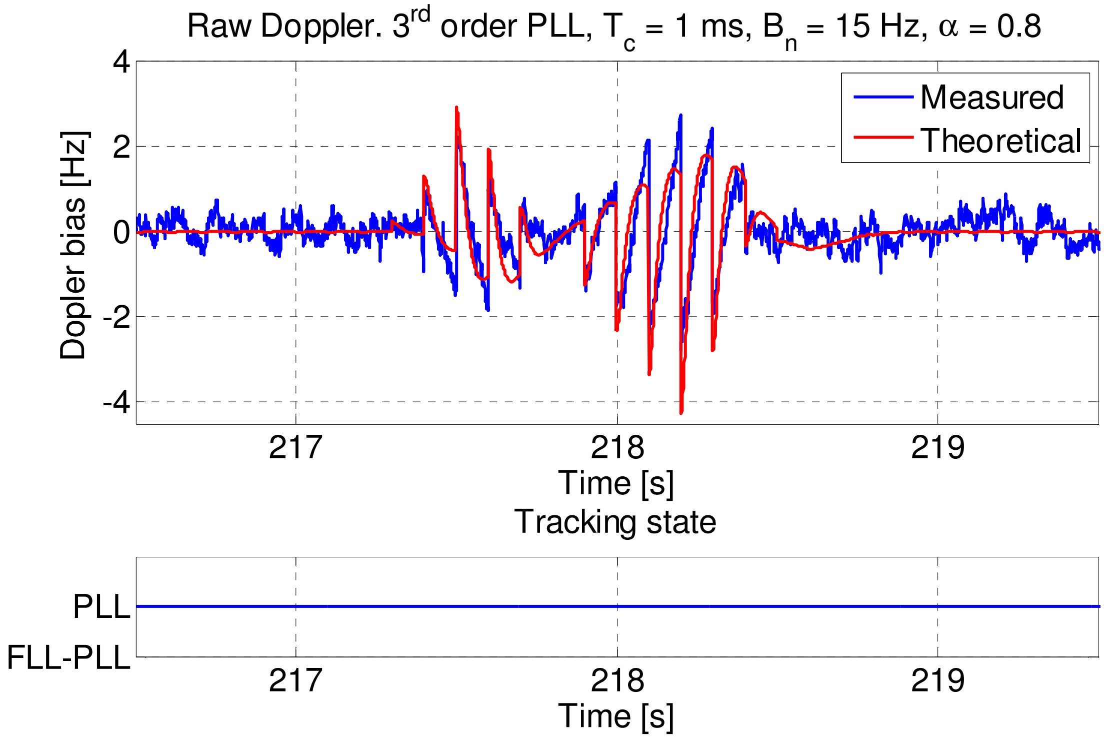

Figure 6-19: Observed and predicted Doppler bias and tracking state of the memory discriminator based tracking loop architecture for a 3 g turn.

Results presented in this subsection indicate that the proposed theoretical model (Eq. (4.31)), is able to effectively predict the Doppler bias caused by changes in the input Doppler frequency. The developed model can be used for quantifying the effect of dynamics on the Doppler estimates for standard and memory discriminator based loops and can also include the effect of the smoothing filter, $S(z)$. The model has been evaluated for different levels of dynamics and in all cases a good agreement between the measured and predicted Doppler bias was observed.

CHAPTER 7: CONCLUSIONS AND FUTURE WORK

The major contribution of this thesis is the development of a complete theoretical framework for the analysis of the process of velocity estimation in a GNSS receiver. The provided analysis allows one to study and characterize the impact of PLL parameters such as the PLL bandwidth and integration time, as well as the C/N_0 and the user dynamics on the accuracy of Doppler and velocity measurements. In this regard the quality of Doppler measurements was theoretically evaluated by extending the PLL linear analysis and characterizing the noise propagation process from the input signal to the Doppler estimate. In particular, the concept of Doppler bandwidth was introduced and theoretical formulas for the Doppler variance and Doppler jitter were provided for the cases of both the raw and the carrier-phase derived Doppler. To model the error propagation from the Doppler frequency measurements to the velocity estimates, the concept of Dilution of Precision was used.

The developed theoretical framework also includes the evaluation of the Doppler bias introduced by the transient response of the PLL during changes in the input frequency. The validity of the developed theoretical framework has been proven using live GPS data collected in various GPS operating environments in both static and dynamic modes. Moreover, a number of simulations were carried out to test the model under a wider range of dynamics. A thorough analysis and comparison of empirical and theoretical results for Doppler jitter and Doppler bias obtained using different tracking loop parameters and methods for Doppler derivation has been performed.

The developed theoretical model was expanded to include the effect of the memory discriminator for use with the memory discriminator based type of High-Sensitivity tracking loop architecture. Performance of this novel tracking loop architecture has then been evaluated using the proposed theory in static and dynamic modes under various GPS operating environments.

The following sections outline the major conclusions found in the course of this work and recommend possible improvements.

7.1 Conclusions

The following conclusions have been made from the research presented throughout this thesis:

1. The concept of Doppler bandwidth was introduced to quantify the amount of noise transferred from the input of the tracking loop to the final frequency estimate. This concept represents a counterpart of the loop bandwidth for frequency estimation and summarizes in a single parameter the ability of a tracking loop to produce smooth frequency estimates, including the effects of the loop components and the smoothing filter, $S(z)$. This quality makes it an effective metric for comparing different receivers.
2. The developed theoretical model of the Doppler jitter (Eq.(4.29)) can be effectively used for the assessment of the Doppler measurement quality as a function of the input C/N$_0$, the coherent integration time and the Doppler

bandwidth, B_d . The validity of the model has been thoroughly verified and in all cases a good agreement between empirical and theoretical results was observed.

3. The developed theoretical framework is general and applies to different methods for the derivation of Doppler measurements such as raw Doppler, carrier phase derived and filtered raw Doppler measurements. The relationship between raw and carrier phase derived Doppler measurements was investigated. In this regard, it has been shown that carrier phase derived measurements can be reconstructed by filtering raw Doppler observations, showing the equivalence of the two methods.
4. The theoretical model for the Doppler jitter analysis (Eq.(4.29)), can also be used to characterize hardware GPS receivers. The developed model allows one to estimate the value of the Doppler bandwidth, B_d, and an approximate value of the coherent integration time of the hardware receiver under consideration. This allows for the application of the analytical model for predicting the Doppler jitter also to hardware receivers based on a standard tracking loop architecture. This approach has been illustrated using a NovAtel OEMV-1 hardware receiver.
5. The proposed model for the Doppler bias analysis (Eq.(4.31)) is able to effectively predict the errors caused by changes in the input Doppler frequency and the transient response of the PLL. The developed model can be used for quantifying the effect of dynamics on the Doppler estimates for standard and memory discriminator based loops, including the effect of the smoothing filter, $S(z)$. The model has been evaluated for different levels of dynamics

(acceleration levels up to 3 g) and in all cases a good agreement between measured and predicted Doppler bias was observed.

6. Exponential filter in the memory discriminator based tracking loop architecture introduces an extra pole to the system. Location of this pole is controlled by forgetting factor, α, and impacts strongly the loop stability. Therefore, the threshold values of the forgetting factor for different bandwidths were studied and quantified.
7. The memory discriminator based tracking loop architecture has shown superior performance in all the experiments performed for this research when compared to the standard tracking loop architecture. Because of its increased noise rejection capability this type of tracking loop architecture is able to provide a faster lock-in time and more accurate Doppler estimates. In particular, in degraded signal environments in the presence of strong fading, in the case when the receiver is not able to determine the bit boundaries and a short coherent integration time has to be used, memory discriminators allow non-coherent integration that in turn provides better Doppler estimates. Moreover, as the simulation results have shown, the memory discriminator based tracking loop architecture is capable to bear higher dynamics without loosing phase lock when compared to the standard PLL architecture.

7.2 Future Work

Based on the results and conclusions of this research, the following recommendations can be made:

1. Theoretical framework developed in this thesis is valid for PLLs only. To allow prediction of the Doppler jitter and Doppler bias in the cases when the receiver is losing phase lock, it is desirable to extend the theoretical framework presented in this thesis to Frequency Lock Loops (FLLs) and FLL assisted PLLs.

2. In this thesis, only the case of standard tracking loops using sequential causal processing has been considered. The developed framework should be extended to include analysis of block processing architectures.

3. Further studies are required to include the effects of errors in the satellite ephemeris and in the user position when investigating the Doppler variance propagation process into the final velocity estimates.

References

Antoniou, A. (1993) *Digital Filters: Analysis, Design and Applications*, New York: McGraw-Hill Inc

Bancroft, J.B., G. Lachapelle, M.E. Cannon and M.G. Petovello (2008) "Twin IMU-HSGPS Integration for Pedestrian Navigation," in *Proceedings of GNSS08*, Savannah, GA, 16-19 Sep, The Institute of Navigation

Borio, D. (2009) *Velocity Estimates from Digital Tracking Loop*, Notes, 3 March, Calgary

Borio, D. (2008) FFT Sign Search with Secondary Code Constraints, IEEE VTC2008 Fall Conference, Calgary, 22-25 September

Borio, D., C. O'Driscoll (2008) *Discriminator based approaches for increasing the Integration Time in Digital Tracking Loops*, Progress report presentation. 9 July, Calgary

Borio, D., and G. Lachapelle (2009) "A Non-Coherent Architecture for GNSS Digital Tracking Loops," *Annals of Telecommunications*, *Springer*, in press

Borio, D., N. Sokolova, G. Lachapelle (2009a) “Memory Discriminators for Non-Coherent Integration in GNSS Tracking Loops,” accepted to *European Navigation Conference*, May 3- 6, Naples

Borio, D., N. Sokolova and G. Lachapelle (2009b) “Doppler Measurements and Velocity Estimation: a Theoretical Framework with Software Receiver Implementation,” *Proceedings of GNSS09*, Savannah, GA, 22-25 Sep, The Institute of Navigation, in preparation

Bruton, A.M. (2000) *Improving the Accuracy and Resolution of SINS/DGPS Airborne Gravimetry.* Ph.D. Thesis, Report No. 20145, Department of Geomatics Engineering, University of Calgary

Bruton A.M., Glennie C.L. and Schwarz K.P. (1999) “Differentiation for High-Precision GPS Velocity and Acceleration Determination.” *GPS solutions* 2(4), pp. 7-21

Cannon, M.E., G. Lachapelle, M. Szarmes, J. Hebert, J. Keith and S. Jokerst (1997) “DGPS Kinematic Carrier Phase Signal Simulation Analysis for Precise Velocity and Position Determination,” in *Proceedings of National Technical Meeting*, Santa Monica, January 14-16, The Institute of Navigation, Alexandria, VA., 335-350

Cheney, W. and D. Kincaid (1985) “Numerical Mathematics and Computing,” 2nd Edition, Brooks/Cole Publishing: Pacific Grove, CA

Enge, Per and Pratap Misra (2001) "Global Positioning System: Signals, Measurements, and Performance", Ganga-Jamuna Press

FCC. *Fact sheet: FCC wireless 911 requirements*, Available at: http://www.fcc.gov/pshs/services/911-services/enhanced911/ , last accessed in June 2008

Gaggero, P. and D. Borio (2008) "Ultra-stable Oscillators: Limits of GNSS Coherent Integration," in *Proceedings of GNSS08*, Savannah, GA, 16-19 Sep, the Institute of Navigation

Gardner F. M., (2005) *Phaselock Techniques*, 3rd ed. Wiley-Interscience

Gelb, A. (1974) *Applied Optimal Estimation*, The Massachusetts Institute of Technology Press, USA

Hebert, J. (1997) "High Accuracy GPS Velocity Using the Carrier Phase Observable," in *Proceedings of International Symposium on Kinematic Systems in Geodesy*, Geomatics and Navigation (KIS97), Banff, Canada, June 3-6, pp. 265-269

Hebert, J., J. Keith, S. Ryan, M. Szarmes, G. Lachapelle and M.E. Cannon (1997) "GPS Carrier Phase Signal Simulation Analysis for Aircraft Velocity Determination," in *Proc. of 53rd Annual Meeting of the Institute of Navigation,* Albuquereque, N.M., June 30 - July 2, pp. 607-617

Julien, O. (2008) *GNSS Receiver Design*, ENGO 638 Lecture Notes, Department of Geomatics Engineering, University of Calgary, Canada

Kaplan E. D. and C. J. Hegarty (2005), Eds., Understanding *GPS: Principles and Applications*, 2nd ed. Norwood, MA, USA: Artech House Publishers

Kazemi P. L. and C. O'Driscoll (2008) "Comparison of Assisted and Stand-Alone Methods for Increasing Coherent Integration Time for Weak GPS Signal Tracking," in *Proc. of ION/GNSS'08*, Savannah, GA

Lachapelle, G. (2008) *Advanced GNSS Theory*, ENGO 625 Lecture Notes. Department of Geomatics Engineering, University of Calgary, Chapter 6

Lachapelle, G., H. Kuusniemi, D. Dao, G. MacGougan and M.E. Cannon (2004) "HSGPS Signal Analysis and Performance Under Various Indoor Conditions", Navigation, U.S. Institute of Navigation, 51, 1, 29-43

Lindsey W. and C. M. Chie (1981) "A survey of digital phase-locked loops," Proc. IEEE, vol. 69, no. 4, pp. 410–431, Apr. 1981

MacGougan, G. (2003) *High Sensitivity GPS Performance Analysis in Degraded Signal Environments*, MSc Thesis, published as UCGE Report No. 20176, Department of Geomatics Engineering, University of Calgary, Canada

Moafipoor, S., Grejner-Brzezinska, D.A. and Toth, C.K. (2004) "Tightly coupled GPS/INS integration based on GPS carrier phase velocity update," *ION NTM 2004*, San Diego CA, pp. 1094-1102

O'Driscoll, C. (2007) *Performance analysis of the parallel acquisition of weak GPS signals*, Ph.D. dissertation, National University of Ireland, Cork

NovAtel: *OEMV Family Installation and Operation User Manual*, http://www.novatel.com/Documents/Manuals/om-20000093.pdf, last accessed September 3, 2009

Pany, T., J.-H. Won, G. Hein (2006) "GNSS Software Defined Radio: Real Receiver or Just a Tool for Experts?" InsideGNSS, vol. 1, no. 5, Gibbons Media&Research

Parkinson B.W., J.J. Spiker, Jr., P. Axelrad and P. Enge (1996) "Global Positioning System: Theory and Applications," AIAA, Washington, DC

Peterson, B., D. Bruckner, and S. Heye (1997) "Measuring GPS Signals Indoors," in *Proceedings of ION GPS 1997*, September 16-19, Kansas City, Missouri, pp. 615–624, Institute of Navigation, Alexandria, VA, USA

Petovello, M.G. and C. O'Driscoll (2007) *GSNRx™ Algorithm Design Document,* Position, Location And Navigation (PLAN) Group, Department of Geomatics

Engineering, University of Calgary, Canada

Petovello, M.G., C. O. Driscoll, and G. Lachapelle (2008) “Weak signal carrier tracking using extended coherent integration with an ultra-tight GNSS/IMU receiver,” in *Proc. of the European Navigation Conference*, Apr. Toulouse, France

Petovello, M.G., C. O’Driscoll, G. Lachapelle, D. Borio, and H. Murtaza (2008), “Architecture and Benefits of an Advanced GNSS Software Receiver,” in *Proc. of International Symposium on GPS/GNSS*, Tokyo, Japan

Petovello, M.G., O. Mezentsev, G. Lachapelle and M.E. Cannon (2003) “High Sensitivity GPS Velocity Updates For Personal Indoor Navigation Using Inertial Navigation Systems,” in *Proceedings of GPS2003*, Session F6, Portland, OR, 9-12 September, The Institute of Navigation

Proakis J.G., P.R. Drouilhet, Jr., and R. Price (1964) “Performance of Coherent Detection Systems Using Decision-Directed Channel Measurement”, *IEEE Transactions on Communication Systems*, vol. CS-12, pp.54-63

Raquet, J. (1998) *Development of a Method for Kinematic GPS Carrier-Phase Ambiguity Resolution Using Multiple Reference Receivers*, Ph.D. Thesis, UCGE Report No. 20116, Department of Geomatics Engineering, University of Calgary

Ryan, S., G. Lachapelle, and M.E. Cannon (1997) "DGPS Kinematic Carrier Phase Simulation Analysis in the Measurement and Position Domain," in *Proceedings of GPS97*, Session D3, The Institute of Navigation, Kansas City, 16-19 September, pp. 1035-1045

Savitzky A. and Marcel J.E. Golay (1964) "Smoothing and Differentiation of Data by Simplified Least Squares Procedures," Analytical Chemistry, 36: 1627–1639

Serrano, L., D. Kim, R. B. Langley, K. Itani and M. Ueno (2004) "A GPS Velocity Sensor: How Accurate Can It Be? - A First Look," in *Proceedings of ION NTM 2004*, San Diego, California, USA, pp. 875-885

Soloviev A., S. Gunawardena, and F. van Graas (2004) "Deeply Integrated GPS/Low-Cost IMU for Low CNR Signal Processing: Flight Test Results and Real Time Implementation," in *Proc. of ION/GNSS*, Long Beach, CA, pp. 1598 – 1608

Soloviev, A., F. Van Grass and S. Gunawardena (2008) "Decoding Navigation Data Messages from Weak GPS Signals," *IEEE Transactions on Aerospace and Electronic Systems*, Accepted for publication

Stephens S.A. and J. Thomas (1995) "Controlled root formulation for digital phase-locked loops," *IEEE Trans. Aerosp. Electron. Syst.*, vol. 31, no. 1, pp. 78 – 95

Strässle C., D. Megnet, H. Mathis, and C. Bürgi (2007) “The squaring loss paradox,” in *Proc. of ION/GNSS*, FortWorth, TX, pp. 2715 – 2722

Szarmes, M., S. Ryan, G. Lachapelle and P. Fenton (1997) “GPS High Accuracy Aircraft Velocity Determination Using Doppler Measurements,” in *Proceedings of International Symposium on Kinematic Systems in Geodesy*, Geomatics and Navigation - KIS97, Banff, June 3-6, Dept of Geomatics Engineering, the University of Calgary, 167-174

Turunen, S. (2007) “Network Assistance: What Will New GNSS Signals Bring to It?” *Inside GNSS*, pp. 35–41

u-blox: *AEK-4P-4H-4T Product Summary*, http://www.amtechs.co.jp/2_gps/download/catalog/u-blox/ **,** last accessed June 20, 2009

Van Dierendonck A. J. (1996) “GPS Receivers,” in Global Positioning System: Theory and Applications, B. W. Parkinson and J. J. Spilker Jr, Eds., Vol. 1. American Institute of Aeronautics and Astronautics (AIAA), 1996

Van Diggelen F. (2001) “Global Locate Indoor GPS Chipset & Services,” in *Proceedings of the ION GPS*, Salt Lake City

Van Graas, F., A. Soloviev (2004) “Precise Velocity Estimation Using a Stand-Alone GPS Receiver,” Navigation, *Journal of the Institute of Navigation*, Vol. 51 No. 4

Ward P.W., J.W.Betz and C.J.Hegarty (2005) “Satellite Signal Acquisition, Tracking, and Data Demodulation,” [Chapter 5] in Kaplan E. D. and C. J. Hegarty (2005), Eds., *Understanding GPS: Principles and Applications*, *2nd ed*. Norwood, MA, USA: Artech House Publishers

Watson, R., G. Lachapelle, R. Klukas, S. Turunen, S. Pietilä and I. Halivaara (2006) “Investigating GPS Signals Indoors with Extreme High-Sensitivity Detection Techniques,” *NAVIGATION*, 52(4), pp. 199-213

Wendel, J., Meister, O., Moenikes, R. and G.F. Trommer, (2006) “Time-differenced carrier phase measurements for tightly coupled GPS/INS integration,” *PLANS 2006*, San Diego CA, pp. 54-60

Zhang J., K. Zhang, R. Grenfell, Y. Li and R. Deakin, (2005) “Real-time doppler/doppler rate derivation for dynamic applications,” Journal of Global Positioning System (JGPS), vol. 4, no. 1, pp. 95–105

2.7 GHz RF Vector Signal Analyzer with Digital Downconversion, National Instruments, http://www.ni.com/pdf/products/us/catvectorsignalanalyzer.pdf, 2006